

Magnetic Moments of Leptons, Charged Lepton Flavor Violations and Dark Matter Phenomenology of a Minimal Radiative Dirac Neutrino Mass Model

Bibhabasu De,^{*} Debottam Das,[†] and Manimala Mitra[‡]

Institute of Physics, Sachivalaya Marg, Bhubaneswar, 751 005, India and

Homi Bhabha National Institute, Training School Complex, Anushakti Nagar, Mumbai 400 094, India

Nirakar Sahoo[§]

Center of Excellence, High Energy and Condensed Matter Physics,

Department of Physics, Utkal University, Bhubaneswar- 751004, India

In a simple extension of the standard model (SM), a pair of vector like lepton doublets (L_1 and L_2) and a $SU(2)_L$ scalar doublet (η) have been introduced to help in accommodating the discrepancy in determination of the anomalous magnetic moments of the light leptons, namely, e and μ . Moreover, to make our scenario friendly to a Dirac like neutrino and also for a consistent dark matter phenomenology, we specifically add a singlet scalar (S) and a singlet fermion (ψ) in the set-up. However, the singlet states also induce a meaningful contribution in other charged lepton processes. A discrete symmetry $\mathcal{Z}_2 \times \mathcal{Z}'_2$ has been imposed under which all the SM particles are even while the new particles may be assumed to have odd charges. In a bottom-up approach, with a minimal particle content, we systematically explore the available parameter space in terms of couplings and masses of the new particles. Here a number of observables associated with the SM leptons have been considered, e.g., masses and mixings of neutrinos, $(g-2)$ anomalies of e , μ , charged lepton flavor violating (cLFV) observables and the dark matter (DM) phenomenology of a singlet-doublet dark matter. Neutrinos, promoted as the Dirac type states, acquire mass at one loop level after the discrete \mathcal{Z}'_2 symmetry gets softly broken, while the unbroken \mathcal{Z}_2 keeps the dark matter stable. The mixing between the singlet ψ and the doublet vector lepton can be constrained to satisfy the electroweak precision observables and the spin independent (SI) direct detection (DD) cross section of the dark matter. In this analysis, potentially important LHC bounds have also been discussed.

^{*} bibhabasu.d@iopb.res.in

[†] debottam@iopb.res.in

[‡] manimala@iopb.res.in

[§] nirakar.pintu.sahoo@gmail.com

I. INTRODUCTION

The standard model (SM) of particle physics has been quite successful in explaining the interactions of elementary particles [1]. The recent discovery of a Higgs boson with a mass of 125 GeV at the Large Hadron Collider [2, 3] has been showing good agreements with the SM expectations [4, 5]. However, there exists a few experimental and theoretical issues, which cannot be explained in the SM paradigm, thus, hint towards a more complete theory — beyond SM physics (BSM) at the TeV scale. Among these signatures, the precise measurement of the dark matter (DM) abundance and the non-zero values of the neutrino masses and mixings are of particular interests to us. Here, one may broadly recall the issues at hand. (i) Assuming the origin of the dark matter is related to a new kind of particle, the simplest and most compelling candidate has been considered as a weakly interacting massive particle (WIMP). The experiments like PLANCK [6] and WMAP [7] have already provided precise measurements of DM relic density. WIMPs with masses ~ 1 TeV can lead to the correct relic density through its annihilations to SM particles. Such a mass scale can be probed at the high-energy collider experiments like the LHC and also at the dark matter direct detection experiments. (ii) Non-zero neutrino masses and substantial mixing among the three light neutrino states require specific extensions of the SM. In the simplest case, one may introduce right handed neutrinos ν_R and assumes a Dirac mass term m_D for the neutrinos. But, then the neutrino Yukawa couplings are assumed to be $\simeq 10^{-11}$ to generate a neutrino mass ~ 0.1 eV. However, being a singlet under the SM gauge group, ν_R can also accommodate a large Majorana mass parameter M which violates the lepton number by 2 units. Such a mass term leads to an attractive possibility — called “seesaw mechanism” where the light neutrinos ν_L obtain an effective small Majorana mass term [8–10]. The tiny mass of neutrinos can be explained naturally without requiring a tiny Yukawa coupling. Though seesaw mechanism is more favoured, experimentally, the searches to probe the Majorana nature of neutrinos through neutrinoless double beta decay experiments have not yet lead to any conclusive evidence. So the simple idea of considering neutrino as a Dirac particle has been still quite popular.

There have already been many proposals which may incorporate new particles and appropriate mixings, thus, explains the masses for neutrinos and the dark matter abundance in the extensions of the SM. However, it is more natural to consider that there exists a tie-up between these two important pieces which may lead to a somewhat economical and an attractive extension of the SM to deal with. Driven by the same pursuit, here we will also furnish a connection between these two important issues assuming neutrino as a Dirac particle. Interestingly and more importantly, we will observe that the precision observables like anomalous magnetic moments of μ ($a_\mu = \frac{(g-2)_\mu}{2}$) and e ($a_e = \frac{(g-2)_e}{2}$) can be accommodated along with

the experimental constraints related to the charged lepton flavor violations.

The idea of neutrino as a Dirac particle has revived in the recent past when the main theoretical objection of having a very tiny tree level Yukawa coupling has been addressed through the radiative generation of neutrino masses [11–24] (for a review see [25]). The main idea is simple and can be realized through an additional $\mathcal{Z}_2 \times \mathcal{Z}'_2$ symmetry in the SM set up : (1) one may assume a discrete symmetry (here \mathcal{Z}'_2) to forbid a tree-level Dirac neutrino masses. This symmetry would be finally broken softly to generate a tiny neutrino mass through a radiative mechanism. (2) New fields may be introduced; in the simplest case, an inert scalar doublet $(\eta^+ \quad \eta^0)^T$ and neutral singlet fermions can be considered (see below) to radiatively induce neutrino masses in the loop. The new fields may transform odd under the another \mathcal{Z}_2 symmetry to prohibit their couplings with the other SM fermions, thus, offers an interesting possibility where the lightest state (a new \mathcal{Z}_2 odd fermion or a neutral scalar) may become the cold dark matter (CDM) of the universe. This class of models where neutrinos acquire masses through dark matter in the loop, thereby connects the two important BSM aspects of the particle physics has been dubbed as “scotogenic” model [26]. In the original idea, the neutrino masses have been assumed to be of Majorana type. However, one may employ the same idea to generate the masses for the neutrinos radiatively considering them as the Dirac particle, if a symmetry like global or gauge $U(1)$ symmetry is assumed to prohibit the Majorana mass term in the Lagrangian [14].

Assuming the lepton number as a good symmetry of the Lagrangian at the backdrop of our work we start our discussion with a simple realization¹. We consider new leptons/scalars at the electroweak (EW) scale in addition to the usual right handed neutrinos ν_R : singlet Dirac fermion(s) (N), two scalars — an inert scalar doublet η and a real singlet scalar S in the particle content of the SM. A perturbative value of the coupling $Y_\ell \bar{N}_R \ell \eta$ ($\ell \in e, \mu, \tau$) may help to realize tiny nature of the neutrino Yukawa couplings radiatively, if the other interaction terms $Y_R \bar{N} S \nu_R$ and $\mu' \eta^\dagger H S$ are included in the interacting Lagrangian. Here the last term μ' can be regarded as the soft symmetry breaking parameter. As in the case of a “scotogenic” model, with proper charge assignments under $\mathcal{Z}_2 \times \mathcal{Z}'_2$ symmetry, Dirac masses for the SM neutrinos, proportional to the soft breaking scale μ' , would be generated radiatively through a $N - \eta - S$ loop. Similarly, observable abundance of the dark matter N would follow naturally. However, this simple model fall short to account for the BSM contributions in the measurement of the anomalous magnetic moment of muon a_μ [33], though can help to acclimatize the measurement of a_e . Primarily, the non-SM contribution, controlled by the $N - \eta^\pm$ loop, comes out to be negative while the discrepancy in the muon anomalous magnetic moment Δa_μ requires a positive boost, thus, disfavours this simple set-up (for a

¹ for some recent works, see [19, 27–32].

generic discussion on the new physics contributions to a_μ , see [34–36]).

We next consider the vector like (VL) leptons in place of singlet Dirac like state N in the SM set-up, without changing the basic structure of the model. For a color singlet VL, left and right handed components transform similarly under the SM gauge symmetries, and one may observe that Δa_μ can be accommodated through the mixings with the SM leptons [37–41]. However, addressing a_e along with a_μ invites a further modification. We, thus introduce a pair of $SU(2)$ vector like leptons $L_1 \equiv (L_1^0 \ L_1^-)^T$, $L_2 \equiv (L_2^0 \ L_2^-)^T$ with same hypercharge (but charged differently under $\mathcal{Z}_2 \times \mathcal{Z}_2'$ symmetry) which can be found to be suitable when coupled to new states; e.g., an inert Higgs doublet η , a real singlet scalar S and a SM singlet fermion ψ in the present context. As in the previous case, S acts to realize the soft breaking of \mathcal{Z}_2' symmetry; thus to generate Dirac masses for the neutrinos while ψ has its role to realize the proper dark matter abundance. In fact, L_1 and ψ can enjoy the same transformation properties under the $\mathcal{Z}_2 \times \mathcal{Z}_2'$ symmetry; thus the neutral L_1^0 and ψ can mix to provide with a suitable candidate for dark matter (χ_0) and to accommodate $(g-2)_e$ anomaly through neutral fermions and charged scalars running in the loop. The charged components of the new leptons help to explain the other anomaly in $(g-2)_\mu$. Naturally, neutrino mass as well as cLFV processes receive contributions from the diagrams that involve both of the VL leptons in the loops. In [40], authors find that a vector like lepton doublet in presence of a right handed neutrino and inert Higgs doublet may indeed be helpful in explaining $(g-2)_\mu$ deviation while the tiny Majorana masses for the neutrinos can also be generated in a “scotogenic” model. Here we will try to find if the both anomalous $(g-2)_\mu$ and $(g-2)_e$ can be accommodated with the said particle contents while neutrinos acquire Dirac masses through dark matter χ_0 in the loop.

In dark matter phenomenology, singlet-doublet DM χ_0 comprised of L_1^0 and singlet ψ , could just be able to produce the correct relic abundance [42–50]. Admitting only VL doublet lepton L_1^0 , one finds a large DM-nucleon elastic cross-section through Z mediated processes, thus has essentially been ruled out by the experiments such as XENON1T [51] or LUX [52]. As a natural deviation, one finds that a singlet-doublet fermion dark matter, through its SM singlet component may escape the stringent direct detection bounds. For practical purposes, the dark matter particle has to be essentially dominated by the singlet component, while only a very small doublet part can be allowed. For the same reason, we purposefully introduce ψ in the particle content.

We organise our paper as follows. In sec II, we explain the details of our model including the new particles and their charges under the complete gauge group which would be considered. After electroweak symmetry breaking (EWSB), our model predicts additional neutral and charged leptons. Consequently, relevant interactions of the new particles with the SM particles can be realized. Theoretical and experimental

bounds on their couplings and masses have been summarized in III. These include (i) anomalous magnetic moments and different charged lepton flavor violating decays of the SM leptons, (ii) vacuum stability of the tree level scalar potential, (iii) Electroweak precision observables (EWPO) and (iv) collider physics constraints. In the results sections, we present radiative generation of the neutrino masses and mixing angles in sec IV. As discussed, one of the motivations is to show that our model can accommodate anomalous magnetic moments of the lighter charged leptons. We depict the parameter space of our model in sec V, where discrepancies in $a_{\mu/e}$ can simultaneously be satisfied. Subsequently, we probe our model parameters with different charged lepton flavor violating (cLFV) observables, namely $\ell_\alpha \rightarrow \ell_\beta \gamma$, $\ell_\alpha \rightarrow 3\ell_\beta$ and flavor violating decays of Z boson. DM phenomenology including the relic density and the direct detection of a singlet-doublet fermionic DM have been covered in sec VI. Finally, we conclude this work in sec VII.

II. THE MODEL: RELEVANT LAGRANGIAN AND SCALAR POTENTIAL AT THE TREE LEVEL

As stated, the proposed model is a simple extension of the Standard Model where we augment two scalars, namely a real singlet (S) and a $SU(2)_L$ doublet $\eta \equiv (\eta^+ \quad \eta^0)^T$, two vector like lepton doublets $L_1 \equiv (L_1^0 \quad L_1^-)^T$, $L_2 \equiv (L_2^0 \quad L_2^-)^T$, a singlet fermion ψ and the usual SM singlet right handed neutrinos ν_R . All the new states are charged under an additional $\mathcal{Z}_2 \times \mathcal{Z}'_2$ symmetry (see Table I).

The allowed interactions of the new fields and the SM fields can be read from the following Lagrangian :

$$\mathcal{L} = \mathcal{L}_{SM} + \mathcal{L}_{new} , \quad (1)$$

where \mathcal{L}_{new} , the new physics Lagrangian is given by,

$$\begin{aligned} \mathcal{L}_{new} = & i\bar{L}_1 \not{D} L_1 - M_{L_1} \bar{L}_1 L_1 + i\bar{L}_2 \not{D} L_2 - M_{L_2} \bar{L}_2 L_2 + i\bar{\psi} \not{D} \psi - M_\psi \bar{\psi} \psi - \\ & \left[Y_{1(1i)} \bar{L}_{1L} \eta \ell_{Ri} + Y_{2(1i)} \bar{L}_{2L} \tilde{\eta} \nu_{Ri} + Y_{3(i1)} \bar{\ell}_i L_{2S} + Y_{4(i1)} \bar{\ell}_i \tilde{\eta} \psi + Y_5 \bar{L}_1 \tilde{H} \psi + Y_{6(1i)} S \bar{\psi}_L \nu_{Ri} + h.c. \right] + \\ & + (\partial^\mu S)^\dagger (\partial_\mu S) + (D^\mu \eta)^\dagger (D_\mu \eta) - V(\eta, H, S). \end{aligned} \quad (2)$$

Here, D_μ is the $SU(2)_L \times U(1)_Y$ covariant derivative and $V(\eta, H, S)$ is the scalar potential. We define field $\tilde{\Phi}$ as $i\tau_2 \Phi^*$. We are following the convention $Q_{EM} = T_3 + Y$. For clarity, we refrain from explicit showing of $SU(2)$ contractions. Except for the right handed neutrinos, single generation of all the other new states would suffice for our purpose (see Table I for details). Here we note that, L_1 and L_2 are assumed to have different charges under $\mathcal{Z}_2 \times \mathcal{Z}'_2$ symmetry. Interacting Lagrangian is realized through the new Yukawa couplings $Y_1 \cdots Y_6$ where in the parenthesis, number of the fermion generations that are involved, are

presented. All the Yukawa couplings are assumed to be real. The new fermion states L_1 , L_2 , ψ and also the RH neutrino ν_R have one unit of lepton number to preserve the lepton number conservation. Moreover, in this work, VLs can only couple to the SM leptons through the new scalar states which do not acquire any vacuum expectation values (VEV); thus the masses and mixings of the SM charged leptons would remain unaffected. In Eq. (2), the interaction between L_1 and SM singlet ψ is felicitated through the SM Higgs H which drives the DM phenomenology.

Finally, we may express the scalar potential $V(\eta, H, S)$ in Eq. (2) which adheres the proposed symmetry as follows:

$$V(\eta, H, S) = \mu_H^2 H^\dagger H + \mu_\eta^2 \eta^\dagger \eta + \mu_S^2 S^\dagger S + \lambda_H (H^\dagger H)^2 + \lambda_\eta (\eta^\dagger \eta)^2 + \lambda_S (S^\dagger S)^2 + \lambda_{\eta H} (\eta^\dagger \eta) (H^\dagger H) + \lambda'_{\eta H} (\eta^\dagger H) (H^\dagger \eta) + \frac{\lambda''_{\eta H}}{2} [(\eta^\dagger H)^2 + h.c.] + \lambda_{HS} (H^\dagger H) (S^\dagger S) + \lambda_{\eta S} (\eta^\dagger \eta) (S^\dagger S). \quad (3)$$

There can be a few additional terms like which are allowed by gauge and Lorentz invariance, but due to the imposed $\mathcal{Z}_2 \times \mathcal{Z}'_2$ symmetry these terms transform non-trivially and hence are forbidden (see e.g., last four terms in Table I(b)). This in turn ensures that the new scalars S, η do not acquire any induced VEV. As usual μ_H^2 can take negative values. As stated, to generate the mass terms for the SM neutrinos, \mathcal{Z}'_2 symmetry can be broken explicitly by introducing a soft breaking term at the scalar potential,

$$\mathcal{L}_{SB} = \mu' \eta^\dagger H S. \quad (4)$$

Since μ' breaks the \mathcal{Z}'_2 , it may be argued to be very small, thus may be helpful in fitting neutrino masses. Similarly, $\bar{L}_1 L_2$ can also accommodate a soft beraking term. The mass term can also be generated at the two loops ($\propto \mu'$) which we assume to be small for further consideration. If the VL states would be considered to transform identically under \mathcal{Z}'_2 , then we will have a restricted class of the Yukawa terms and consequently accommodating the anomalous magnetic momemts of μ and e simultaneously cannot be realized in this proposed model with the given particle content. However, we may consider a global $U(1)$ symmetry (the charge assignments could read as $L_1, S, \Psi, \eta=1$ while $L_2=-1$ with all the SM particles including ν_R assume zero charges), then our model and its phenomenology would be completely unchanged. Infact, it will make the dark matter stable thus \mathcal{Z}_2 can be assumed to be replaced.

Before discussing the phenomenology, let us briefly outline the role of different discrete symmetries in the present analysis. We assume \mathcal{Z}_2 to be an exact symmetry which always ensures that (i) a tree level Dirac like neutrino mass term, e.g., $\bar{\ell} \tilde{H} \psi$ would be absent and (ii) χ_0 , the singlet like admixture of L_1^0 and ψ , a state odd under \mathcal{Z}_2 may become stable to form the cold dark matter. On the other hand \mathcal{Z}'_2 forbids the usual tree level Yukawa interaction $\bar{\ell} \tilde{H} \nu_R$, but it needs to be broken softly to generate neutrino

masses through radiative corrections. Additionally, there are a few other couplings among the new fields and the SM fields which fail to qualify as the valid interactions. For a better understanding, we list them in Table I along with their transformations under the proposed symmetry group. Here \checkmark and \times refer to the occasions when a particular interaction term turns out to be even or odd under a symmetry operation respectively.

| Fields | Generation | $SU(2)_L \times U(1)_Y$ | \mathcal{Z}_2 | \mathcal{Z}'_2 |
|---------------------------------------|------------|-------------------------|-----------------|------------------|
| $\ell = (\nu_L \ e_L)^T$ | 3 | 2, -1/2 | +1 | +1 |
| $\ell_R = (e_R, \mu_R, \tau_R)$ | 3 | 1, -1 | +1 | +1 |
| $Q_L = (u_L \ d_L)^T$ | 3 | 2, 1/6 | +1 | +1 |
| $U_R = (u_R, c_R, t_R)$ | 3 | 1, 2/3 | +1 | +1 |
| $D_R = (d_R, s_R, b_R)$ | 3 | 1, -1/3 | +1 | +1 |
| $H = (0 \ \frac{1}{\sqrt{2}}(v+h))^T$ | 1 | 2, 1/2 | +1 | +1 |
| ν_R | 3 | 1, 0 | +1 | -1 |
| ψ | 1 | 1, 0 | -1 | +1 |
| $L_1 = (L_1^0 \ L_1^-)^T$ | 1 | 2, -1/2 | -1 | +1 |
| $L_2 = (L_2^0 \ L_2^-)^T$ | 1 | 2, -1/2 | -1 | -1 |
| $\eta = (\eta^+ \ \eta^0)^T$ | 1 | 2, 1/2 | -1 | +1 |
| S | 1 | 1, 0 | -1 | -1 |

(a)

| Forbidden terms | $SU(2)_L$ | $U(1)_Y$ | \mathcal{Z}_2 | \mathcal{Z}'_2 |
|---|--------------|-------------------------|-----------------|------------------|
| $\bar{\ell} H \psi_R \ (\bar{\ell} \tilde{H} \psi_R)$ | \checkmark | $\times \ (\checkmark)$ | \times | \checkmark |
| $\bar{\ell} H \nu_R \ (\bar{\ell} \tilde{H} \nu_R)$ | \checkmark | $\times \ (\checkmark)$ | \checkmark | \times |
| $\bar{\ell} \eta \nu_R \ (\bar{\ell} \tilde{\eta} \nu_R)$ | \checkmark | $\times \ (\checkmark)$ | \times | \times |
| $\bar{\ell}_R S \psi$ | \checkmark | \times | \checkmark | \times |
| $\bar{L}_2 H \psi \ (\bar{L}_2 \tilde{H} \psi)$ | \checkmark | $\times \ (\checkmark)$ | \checkmark | \times |
| $\bar{\ell} L_1 S$ | \checkmark | \checkmark | \checkmark | \times |
| $\bar{L}_2 \eta \ell_R \ (\bar{L}_2 \tilde{\eta} \ell_R)$ | \checkmark | $\checkmark \ (\times)$ | \checkmark | \times |
| $\bar{L}_1 \eta \nu_R \ (\bar{L}_1 \tilde{\eta} \nu_R)$ | \checkmark | $\times \ (\checkmark)$ | \checkmark | \times |
| $\bar{L}_1 L_2 S$ | \checkmark | \checkmark | \times | \checkmark |
| $\lambda_{\eta H S S} (\eta^\dagger H) (S^\dagger S)$ | \checkmark | \checkmark | \times | \checkmark |
| $\lambda (\eta^\dagger H)$ | \checkmark | \checkmark | \times | \checkmark |
| $\lambda_{S S S} (S^\dagger S) S$ | \checkmark | \checkmark | \times | \times |
| $\lambda_3 S$ | \checkmark | \checkmark | \times | \times |

(b)

TABLE I. (a) Particles and their transformations under $SU(2)_L \times U(1)_Y \times \mathcal{Z}_2 \times \mathcal{Z}'_2$. (b) Forbidden interaction terms and their transformations under different gauge and discrete symmetries.

Possible completion of the model at the GUT scale : Here we discuss a possibility to embed our low energy model to a larger gauge group e.g., $SO(10)$. Specific gauge breaking chains may include, e.g., left-right (LR) symmetric phase at the intermediate scale [53–57],

$$SO(10) \xrightarrow{M_{GUT}} SU(3)_C \times SU(2)_L \times SU(2)_R \times U(1)_{B-L} \xrightarrow{M_{LR}} \text{SM} \quad (5)$$

with M_{GUT} denoting the breaking scale of $SO(10)$ gauge group which is subsequently broken to the SM at $M_{LR} < M_{GUT}$. There are a few reasons for considering the LR models: (i) the particle content contains automatically the right-handed neutrino, (ii) a TeV scale LR symmetric intermediate phase may be obtained within a class of renormalizable $SO(10)$ GUTs with a perfect gauge coupling unification [58].

Here one has to account for a few copies of one or two types of extra fields; e.g., additional triplet and/or doublet scalars under $SU(2)_R$. However, for different possibilities, we refer the reader to Ref. [58]. Of course, the new scalars can effect the low energy phenomenology e.g., $(g-2)_\mu$ through a gauge invariant interaction at the LR scale. The matter content of the model along with their possible transformations at each intermediate stage is given in table II. Here Q , Q^c , L and L^c (we follow the notation in [56]) are the quark and lepton families with the addition of (three) right-handed neutrino(s) ν_R . The SM Higgs and the inert doublet can be included as bidoublets under $SU(2)_L \times SU(2)_R$. More than a single bidoublet is required for a correct Yukawa Lagrangian at the low scale [58]. Similarly, transformations of the VL states $L_{1,2}$ and the SM singlet states are noted. The electric charges of particles are calculated through the eigenvalues of the left (T_{3L}) and right (T_{3R}) generators of the $SU(2)_L$ and $SU(2)_R$ groups, respectively, as $Q_{EM} = T_{3L} + T_{3R} + (B - L)/2$. The index c refers to the equivalent SM field which transforms under

| Fields | Generation | $3_c 2_L 2_R 1_{B-L}$ | $SO(10)$ |
|-----------------|------------|-------------------------|------------|
| Q | 3 | $(3, 2, 1, 1/3)$ | 16 |
| Q^c | 3 | $(\bar{3}, 1, 2, -1/3)$ | 16 |
| L | 3 | $(1, 2, 1, -1)$ | 16 |
| L^c | 3 | $(1, 1, 2, 1)$ | 16 |
| Φ | 2 | $(1, 2, 2, 0)$ | 10 |
| $L_{1,2}$ | 2 | $(1, 2, 1, -1)$ | 16 |
| $\hat{L}_{1,2}$ | 2 | $(1, 2, 1, 1)$ | $\bar{16}$ |
| ψ | 1 | $(1, 1, 2, -1)$ | $\bar{16}$ |
| $\hat{\psi}$ | 1 | $(1, 1, 2, 1)$ | 16 |
| S | 1 | $(1, 1, 1, 0)$ | 1 |

TABLE II. One of the Possible completion of the particle content under $SO(10)$.

$SU(2)_R$. All the interaction terms in Eq. (2) can now be cast under the enlarged gauge symmetry. For example, $Y_{1(1i)} \bar{L}_{1L} \eta \ell_{Ri}$ can be cast as $L_1^T \Phi L^c$ which, under, $SO(10)$ goes as $\mathbf{16} \times \mathbf{10} \times \mathbf{16}$. Similarly, $Y_{6(1i)} S \bar{\psi}_L \nu_{Ri}$ can be cast as $S \psi L^c$ which, under, $SO(10)$ goes as $\mathbf{1} \times \bar{\mathbf{16}} \times \mathbf{16}$. Though the particle contents can easily be accommodated under a unified gauge group, one has to admit a minor change, e.g., ψ in Eq. (2) should refer to the neutral component of $SU(2)_R$ doublet in Table II. Alternatively, one may also consider the symmetry breaking chain as $SO(10) \rightarrow SU(5) \times U(1)_X \rightarrow SU(3)_C \times SU(2)_L \times U(1)_Y \times U(1)_X$ which was earlier considered in Ref. [40, 59].

Mixings and couplings of the VL states with bosons and fermions: As can be seen from Eq. (2) that lepton phenomenology is primarily governed by the new Yukawa couplings $Y_i (i = 1 \dots 6)$. Apparently,

the first four couplings are more important for the phenomenology in the lepton sector, while Y_5 primarily controls the DM physics. The Yukawa interactions involving the singlet states may contribute to neutrino masses and also the dark matter relic abundance. For a generic study, we keep all the couplings with $Y_i (i = 1 \dots 6)$ in the flavor space.

Let us first start our discussion with the interactions mediated by Y_5 in Eq. (2). The Yukawa interaction, $Y_5 \bar{L}_1 \tilde{H} \psi$ generates a mass matrix,

$$\mathcal{M} = \begin{pmatrix} M_\psi & \frac{Y_5 v}{\sqrt{2}} \\ \frac{Y_5 v}{\sqrt{2}} & M_{L_1} \end{pmatrix}, \quad (6)$$

in the basis of (ψ, L_1^0) . We can rotate this to the mass basis with the help of (2×2) orthogonal matrix, such that $\mathcal{M}_D = U^\dagger \mathcal{M} U$, where,

$$U = \begin{pmatrix} \cos\theta & -\sin\theta \\ \sin\theta & \cos\theta \end{pmatrix}. \quad (7)$$

The two mass eigenstates can be defined as,

$$\chi_0 = \cos\theta \psi + \sin\theta L_1^0, \quad (8)$$

$$\chi_1 = -\sin\theta \psi + \cos\theta L_1^0, \quad (9)$$

with the masses are given by,

$$M_{\chi_0} = M_{L_1} \sin^2\theta + M_\psi \cos^2\theta + \frac{Y_5 v}{\sqrt{2}} \sin 2\theta, \quad (10)$$

$$M_{\chi_1} = M_{L_1} \cos^2\theta + M_\psi \sin^2\theta - \frac{Y_5 v}{\sqrt{2}} \sin 2\theta. \quad (11)$$

The mixing angle is defined as,

$$\tan 2\theta = \frac{\sqrt{2}(Y_5 v)}{M_\psi - M_{L_1}}. \quad (12)$$

If we assume a small mixing angle i.e., $\theta \ll 1$ then χ_1 is dominantly doublet-like with a small admixture of singlet ψ , while χ_0 is mostly singlet-like. Since the direct detection experiments require DM to be mostly singlet dominated, we can propose χ_0 as the DM candidate with the condition that $M_{\chi_0} < M_{\chi_1}$, which is further ensured by the choice $M_\psi < M_{L_1}$. The Yukawa coupling Y_5 , now being a dependent parameter, can be expressed in terms of M_{χ_1} , M_{χ_0} and θ through the following relation,

$$Y_5 = -\frac{(M_{\chi_1} - M_{\chi_0}) \sin 2\theta}{v\sqrt{2}}. \quad (13)$$

At this point we can recast the Yukawa terms in Eq. (2) in this new basis of (χ_0, χ_1) as:

$$\begin{aligned} \mathcal{L}_{new} \supset & Y_{1(1i)} \left[\cos\theta \bar{\chi}_1 \eta^+ \ell_{Ri} + \sin\theta \bar{\chi}_0 \eta^+ \ell_{Ri} + \bar{L}_1^- \eta^0 \ell_{Ri} \right] + Y_{2(1i)} \left[\bar{L}_2^0 \eta^0 - \bar{L}_2^- \eta^- \right] \nu_{Ri} \\ & + Y_{3(i1)} \left[\bar{\nu}_{li} L_2^0 S + \bar{e}_{li} L_2^- S \right] + Y_{4(i1)} \left[\bar{\nu}_{li} \eta^0 (\cos\theta \chi_0 - \sin\theta \chi_1) - \bar{e}_{li} \eta^- (\cos\theta \chi_0 - \sin\theta \chi_1) \right] \\ & + Y_{6(1i)} \left[\cos\theta S \bar{\chi}_0 \nu_{Ri} - \sin\theta S \bar{\chi}_1 \nu_{Ri} \right] + h.c. + \frac{Y_5}{\sqrt{2}} h \left[(\bar{\chi}_0 \chi_0 - \bar{\chi}_1 \chi_1) \sin 2\theta + (\bar{\chi}_1 \chi_0 + \bar{\chi}_0 \chi_1) \cos 2\theta \right]. \end{aligned} \quad (14)$$

All the Yukawa couplings appearing above need to satisfy a generic condition $|Y| \leq 4\pi$ so to remain perturbative at the TeV scale. Similarly, the terms appearing in the covariant derivative can be collected to write down the couplings with the gauge bosons. Using $D_\mu = \partial_\mu - i \frac{g}{\cos\theta_W} (T^3 - \sin^2\theta_W Q) Z_\mu - ieQ A_\mu$, one finds that,

$$\begin{aligned} \mathcal{L}_{new} \supset & \frac{g}{\sqrt{2}} \left[\cos\theta \bar{\chi}_1 \gamma^\mu L_1^- + \sin\theta \bar{\chi}_0 \gamma^\mu L_1^- + \bar{L}_2^0 \gamma^\mu L_2^- \right] W_\mu^+ + h.c. \\ & + \frac{g}{2 \cos\theta_W} \left[\cos^2\theta \bar{\chi}_1 \gamma^\mu \chi_1 + \sin^2\theta \bar{\chi}_0 \gamma^\mu \chi_0 + \frac{1}{2} \sin 2\theta (\bar{\chi}_1 \gamma^\mu \chi_0 + \bar{\chi}_0 \gamma^\mu \chi_1) + \bar{L}_2^0 \gamma^\mu L_2^0 \right] Z_\mu \\ & + \frac{g}{\cos\theta_W} \left(-\frac{1}{2} + \sin^2\theta_W \right) \left[\bar{L}_1^- \gamma^\mu L_1^- + \bar{L}_2^- \gamma^\mu L_2^- \right] Z_\mu - e \left[\bar{L}_1^- \gamma^\mu L_1^- + \bar{L}_2^- \gamma^\mu L_2^- \right] A_\mu. \end{aligned} \quad (15)$$

Note that, all the other terms in Eq. (2) will not be affected by this basis change.

III. BOUNDS RELATED TO DIFFERENT EXPERIMENTS AND THEORIES

Here we review different bounds related to experimental searches and theories. We will use the limits in delineating the parameter space consistent with the anomalous magnetic moments of leptons, charged lepton flavor violations and the dark matter abundance.

A. Anomalous magnetic moment and different LFV decays

Bounds on anomalous magnetic moment: From the first precision measurement of the magnetic dipole moment of the muon a_μ at BNL (Brookhaven National Laboratory), the persistent discrepancy in its determination compared to its SM prediction has been undoubtedly one of the most promising hints towards a new physics signal at the TeV scale. The discrepancy can be expressed through its experimental measurements ($\equiv a_\mu^{exp}$) and the SM prediction ($\equiv a_\mu^{SM}$). The difference in the two values can be seen to be driven by the BSM contributions ($\equiv \Delta a_\mu$). For the last many years, the experimental data produced a roughly 3.7σ deviation from the standard model (SM) value [60–63]. For a better understanding of the known physics, it was imperative to resolve the tension related to the hadronic vacuum polarization

(HVP) of a_μ^{SM} [64–71] (see also [63] and references therein). The tension lies in the fact that a recent lattice-QCD [64] estimation of the HVP may bring the SM prediction of a_μ into agreement with experiments which seems to be in contradiction with $e^+e^- \rightarrow \text{hadrons}$ cross section data and global fits to electroweak precision observables [69, 71]. The Fermilab-based Muon g-2 experiment has just reported a new result [72, 73] which, if combined with the BNL result reads 4.2σ deviation from the SM value².

$$\Delta a_\mu = (25.1 \pm 5.9) \times 10^{-10}. \quad (16)$$

Thus, as stated earlier, from Eq. (16) it is clearly visible that one needs a positive BSM contribution to satisfy the experimental constraint on Δa_μ . In the context of a_e , the experimental value has been updated in 2018 [90] from a precision measurement of the fine-structure constant [91] that relies on the caesium recoil measurements. This measurement also shows a possible disagreement between the experimental observation and theory prediction, though with a less significance $\sim 3\sigma$.

$$\Delta a_e = -(8.7 \pm 3.6) \times 10^{-13}. \quad (17)$$

More importantly, here the measured value is lower than the corresponding SM prediction. Following the improved estimates, specially in the evaluation of a_e , attempts have been made to link the both discrepancies with a common new physics origin [92–109]. Here we note that a very recent determination of the fine structure constant [110], obtained from the measurement of the recoil velocity on rubidium atoms, result into a positive discrepancy of about 1.6σ . Clearly the discrepancy in the measurement of a_e can only be settled in the future. This work focuses on caesium recoil measurements, thus, Eq. (17) in the subsequent sections.

Bounds on charged lepton flavor violating decays: Charged lepton flavor violating processes, specifically $\ell_\alpha \rightarrow \ell_\beta \gamma$ or $\ell_\alpha \rightarrow 3\ell_\beta$ through photon penguins may be influenced by the same dipole operators which provides the BSM contributions to $a_{\mu/e}$. Non observations of any cLFV processes so far, can potentially constrain the new physics parameters. Currently, the radiative decay of $\ell_\alpha \rightarrow \ell_\beta \gamma$, specifically $\mu \rightarrow e \gamma$, is the leading candidate among the cLFV observables to put a stringent constraint on the parameter space. In the future upgrades, the MEG collaboration can reach a sensitivity of about 6×10^{-14} after 3 years of acquisition time [111]. Similarly, in the near future, $\mu \rightarrow 3e$ can be probed by the Mu3e experiment [112, 113] with a branching ratio sensitivity of 10^{-16} . A significant improvement is expected compared to the present limit, set by the SINDRUM experiment [114]. An impressive improvement on most of the LFV modes of the rare τ decays can be expected from searches in B factories [115, 116].

² Recent measurement at the Fermilab has drawn some interests to our community [74–89].

Table III includes the present and future sensitivities of the important cLFV processes which would be considered in this work.

| LFV Process | Present Bound | Future Sensitivity |
|--|-----------------------------|-------------------------------|
| $Br(\mu \rightarrow e\gamma)$ | 4.2×10^{-13} [117] | 6×10^{-14} [111] |
| $Br(\tau \rightarrow e\gamma)$ | 3.3×10^{-8} [118] | $\sim 3 \times 10^{-9}$ [115] |
| $Br(\tau \rightarrow \mu\gamma)$ | 4.4×10^{-8} [118] | $\sim 3 \times 10^{-9}$ [118] |
| $Br(\mu \rightarrow 3e)$ | 1.0×10^{-12} [114] | $\sim 10^{-16}$ [112] |
| $Br(\tau \rightarrow 3e)$ | 2.7×10^{-8} [119] | $\sim 10^{-9}$ [115] |
| $Br(\tau \rightarrow 3\mu)$ | 3.3×10^{-8} [119] | $\sim 10^{-9}$ [115] |
| $Br(\tau^- \rightarrow e^- \mu^+ \mu^-)$ | 2.7×10^{-8} [119] | $\sim 10^{-9}$ [115] |
| $Br(\tau^- \rightarrow \mu^- e^+ e^-)$ | 1.8×10^{-8} [119] | $\sim 10^{-9}$ [115] |
| $Br(\tau^- \rightarrow e^+ \mu^- \mu^-)$ | 1.7×10^{-8} [119] | $\sim 10^{-9}$ [115] |
| $Br(\tau^- \rightarrow \mu^+ e^- e^-)$ | 1.5×10^{-8} [119] | $\sim 10^{-9}$ [115] |

TABLE III. Current Experimental bounds and future sensitivities for the LFV processes.

B. Condition of Vacuum stability and the masses of scalars

The scalar potential must be bounded from below i.e., it does not acquire negative infinite value in any of the field directions for large field values. This physical requirement puts certain constraints on the scalar couplings. Considering the tree level scalar potential, these conditions are listed below [120].

$$\begin{aligned}
\lambda_H, \lambda_\eta, \lambda_S &> 0, \\
\lambda_{\eta H} + 2\sqrt{\lambda_\eta \lambda_H} &> 0, \\
\lambda_{\eta H} + \lambda'_{\eta H} - |\lambda''_{\eta H}| + 2\sqrt{\lambda_\eta \lambda_H} &> 0, \\
\lambda_{HS} + 2\sqrt{\lambda_H \lambda_S} &> 0, \\
\lambda_{\eta S} + 2\sqrt{\lambda_\eta \lambda_S} &> 0.
\end{aligned} \tag{18}$$

After the electroweak symmetry breaking only H field gets a VEV, $v \simeq 246$ GeV. Thus, scalar fields can be expressed as :

$$H = \begin{pmatrix} 0 \\ \frac{1}{\sqrt{2}}(v + h) \end{pmatrix}, \quad \eta = \begin{pmatrix} \eta^+ \\ \frac{1}{\sqrt{2}}(\eta_R + i\eta_I) \end{pmatrix}, \quad S = S. \tag{19}$$

Substituting H and η in Eq. (3) one finds

$$\begin{aligned}
M_h^2 &= 2\lambda_H v^2, \\
M_{\eta_R}^2 &= \mu_\eta^2 + \frac{1}{2}(\lambda_{\eta H} + \lambda'_{\eta H} + \lambda''_{\eta H})v^2, \\
M_{\eta_I}^2 &= \mu_\eta^2 + \frac{1}{2}(\lambda_{\eta H} + \lambda'_{\eta H} - \lambda''_{\eta H})v^2, \\
M_{\eta^\pm}^2 &= \mu_\eta^2 + \frac{1}{2}\lambda_{\eta H}v^2, \\
M_S^2 &= \mu_S^2 + \frac{1}{2}\lambda_{HS}v^2.
\end{aligned} \tag{20}$$

We identify h as our SM like Higgs scalar with mass $M_h \simeq 125$ GeV. Again for simplicity we assume that the new scalars are heavier to forbid the constraints coming from the invisible Z and h decays. Similarly the mass splitting between the charged and the neutral components of the doublet η are considered to be negligible, i.e., $M_{\eta_I} = M_{\eta_R} = M_{\eta^\pm} \equiv M_\eta$. This is indeed possible (see Eq. (20)), if the couplings $\lambda'_{\eta H}$ and $\lambda''_{\eta H}$ can be assumed to be very small. In fact, $\lambda''_{\eta H}$ is absent under a global or gauge $U(1)$ symmetry. However, such a mass splitting may play a significant role for its discovery at the LHC (see e.g., [121]).

C. Electroweak precision observables (EWPO)

In the presence of two BSM scalars (η , S), two vector like lepton doublets (L_1 , L_2) and a singlet fermion (ψ), our model may introduce corrections to the gauge boson vacuum polarization amplitudes or electroweak precision observables (EWPO). These observables were initially discussed by Peskin and Takeuchi as S, T and U parameters in Ref. [122]. Later Barbieri et al. introduced \hat{S} , \hat{T} , W , Y [123] as the most general parameterization of the new physics effects. \hat{S} and \hat{T} are related to the original S and T parameters through the simple relations: $\hat{S} = \frac{\alpha S}{4s_W^2}$ and $\hat{T} = \alpha T$, where α is the fine structure constant and $s_W = \sin \theta_W$. Among the generalized Peskin-Takeuchi parameters, W and Y are important at LEP2 energy scale [123, 124], thus will not be considered here. Usually for any generic model, one can find from the global analysis that the electroweak precision parameters are much smaller (at the level of 10^{-3}) and this does not depend on the mass of the Higgs scalar. Our calculations of the precision observables are based upon Refs. [124, 125].

The current experimental constraints are [62, 123],

$$\hat{S} = (0.0 \pm 1.3) \times 10^{-3}, \tag{21}$$

$$\hat{T} = (0.1 \pm 0.9) \times 10^{-3}. \tag{22}$$

Inert doublet η may particularly effect T or \hat{T} parameter through $\lambda'_{\eta H}$ and $\lambda''_{\eta H}$ [125]. But in the limit, $M_{\eta_I} = M_{\eta_R} = M_{\eta^\pm} \equiv M_\eta$, which we assume in the subsequent analysis, the electroweak parameters seem to be unaffected by the presence of new scalars. Hence the correction is completely due to the effect of vector like fermions (VLF), i.e., in our model $\Delta(\hat{S}, \hat{T}) = (\hat{S}, \hat{T})_{VLF}$. Therefore, the correction in \hat{T} parameter appearing due to the mixing between L_1 and ψ for $q^2 \rightarrow 0$ limit can be expressed as [124],

$$\hat{T} = \frac{g^2}{16\pi^2 M_W^2} \left[\tilde{\Pi}(M_{L_1}, M_{L_1}, 0) + \cos^4 \theta \tilde{\Pi}(M_{\chi_1}, M_{\chi_1}, 0) + \sin^4 \theta \tilde{\Pi}(M_{\chi_0}, M_{\chi_0}, 0) \right. \\ \left. + 2 \sin^2 \theta \cos^2 \theta \tilde{\Pi}(M_{\chi_0}, M_{\chi_1}, 0) - 2 \cos^2 \theta \tilde{\Pi}(M_{L_1}, M_{\chi_1}, 0) - 2 \sin^2 \theta \tilde{\Pi}(M_{L_1}, M_{\chi_0}, 0) \right], \quad (23)$$

where M_{L_1} is the mass term for L_1^- , g is the $SU(2)_L$ coupling constant, θ is the mixing angle between L_1^0 and ψ as discussed earlier, M_W stands for the mass of W boson and

$$\tilde{\Pi}(m_a, m_b, 0) = -\frac{1}{2}(m_a^2 + m_b^2) \left[Div + \ln \left(\frac{\mu^2}{m_a m_b} \right) \right] - \frac{1}{4}(m_a^2 + m_b^2) - \frac{(m_a^4 + m_b^4)}{4(m_a^2 - m_b^2)} \ln \left(\frac{m_b^2}{m_a^2} \right) \\ + m_a m_b \left[Div + \ln \left(\frac{\mu^2}{m_a m_b} \right) + 1 + \frac{(m_a^2 + m_b^2)}{2(m_a^2 - m_b^2)} \ln \left(\frac{m_b^2}{m_a^2} \right) \right], \quad (24)$$

is the correction to gauge boson propagators in presence of the new VLF's. $Div = \frac{1}{\epsilon} + \ln(4\pi) - \gamma$ is the usual divergent piece appearing in the dimensional regularisation and μ denotes the renormalization scale. One can easily see that for $m_a = m_b$, Eq. (24) vanishes. Hence Eq. (23) simplifies to

$$\hat{T} = \frac{g^2}{16\pi^2 M_W^2} \left[2 \sin^2 \theta \cos^2 \theta \tilde{\Pi}(M_{\chi_0}, M_{\chi_1}, 0) - 2 \cos^2 \theta \tilde{\Pi}(M_{L_1}, M_{\chi_1}, 0) - 2 \sin^2 \theta \tilde{\Pi}(M_{L_1}, M_{\chi_0}, 0) \right]. \quad (25)$$

It can be noted that the divergent part of the first term of Eq. (25) is cancelled by the divergences encapsulated in the last two terms. Moreover in the limit, when the mass splitting between M_{L_1} and M_{χ_1} vanishes, (i.e., $\sin \theta \rightarrow 0$) one finds $\hat{T} \rightarrow 0$.

In our model, the correction in \hat{S} can be parameterized as,

$$\hat{S} = \frac{g^2}{16\pi^2} \left[\tilde{\Pi}'(M_{L_1}, M_{L_1}, 0) - \cos^4 \theta \tilde{\Pi}'(M_{\chi_1}, M_{\chi_1}, 0) - \sin^4 \theta \tilde{\Pi}'(M_{\chi_0}, M_{\chi_0}, 0) \right. \\ \left. - 2 \sin^2 \theta \cos^2 \theta \tilde{\Pi}'(M_{\chi_0}, M_{\chi_1}, 0) \right], \quad (26)$$

where the ' \prime ' signifies derivative with respect to q^2 . The general expression for $\tilde{\Pi}'(m_a, m_b, 0)$ is given

as [124, 126],

$$\begin{aligned} \tilde{\Pi}'(m_a, m_b, 0) = \frac{1}{3} \left[Div + \ln \left(\frac{\mu^2}{m_a m_b} \right) \right] + \frac{m_a^4 - 8m_a^2 m_b^2 + m_b^4}{9(m_a^2 - m_b^2)^2} + \frac{(m_a^2 + m_b^2)(m_a^4 - 4m_a^2 m_b^2 + m_b^4)}{6(m_a^2 - m_b^2)^3} \ln \left(\frac{m_b^2}{m_a^2} \right) \\ + m_a m_b \left[\frac{(m_a^2 + m_b^2)}{2(m_a^2 - m_b^2)^2} + \frac{m_a^2 m_b^2}{(m_a^2 - m_b^2)^3} \ln \left(\frac{m_b^2}{m_a^2} \right) \right]. \end{aligned} \quad (27)$$

For $m_a = m_b$ the above expression reduces to

$$\tilde{\Pi}'(m_a, m_a, 0) = \frac{1}{3} \left[Div + \ln \left(\frac{\mu^2}{m_a^2} \right) \right]. \quad (28)$$

It can be directly verified that the divergent parts along with the scaling factor μ get cancelled when Eq. (27) or Eq. (28) is substituted in Eq. (26).

Numerically, since the oblique parameters are sensitive to the mass splitting $\Delta M = (M_{\chi_1} - M_{L_1})$, we depict its variation with M_{χ_1} in Fig. 1(a) and Fig. 1(b) for three different values of $\sin \theta = 0.01, 0.1$ and 0.3 keeping DM mass $M_{\chi_0} = 120$ GeV. Clearly, electroweak precision constraints on \hat{S} is much relaxed compared to the oblique parameter \hat{T} to the new fermions. For moderate or smaller values of χ_1 mass, one finds that $\Delta M \leq \mathcal{O}(20)$ GeV is allowed by the oblique parameter \hat{T} , which sets an upper bound on $\sin \theta$ ($\simeq 0.1$).

The bounds can be used to constrain the bare masses of the new fermions. For example, one may always cast the bare masses M_{L_1} and M_ψ in terms of M_{χ_0} , M_{χ_1} and mixing angle θ .

$$M_{L_1} = M_{\chi_1} \cos^2 \theta + M_{\chi_0} \sin^2 \theta, \quad (29)$$

$$M_\psi = M_{\chi_1} \sin^2 \theta + M_{\chi_0} \cos^2 \theta. \quad (30)$$

Notably, the change in ΔM is negligible to the variation with M_{χ_0} for a small mixing angle ($\sin \theta \leq 0.1$) (see Fig. 1(c) and (d)). In other words, the EWPOs are insensitive to the lightest neutral fermion mass M_{χ_0} as long as the mixing angle is not much high. In the subsequent section, we consider $\sin \theta \leq 0.01$, thus, in this regime, the mass of the charged component of the VL, M_{L_1} can easily be fixed through M_{χ_1} while satisfying all the bounds coming from EWPOs.

D. Constraints from the collider observables

For vector like quarks, the LHC pair production cross section is determined from QCD, so model independent bounds can be placed in the parameter space. However, for the vector like leptons, the pair-production cross section is mediated by the s-channel electroweak vector boson exchanges, thus depends

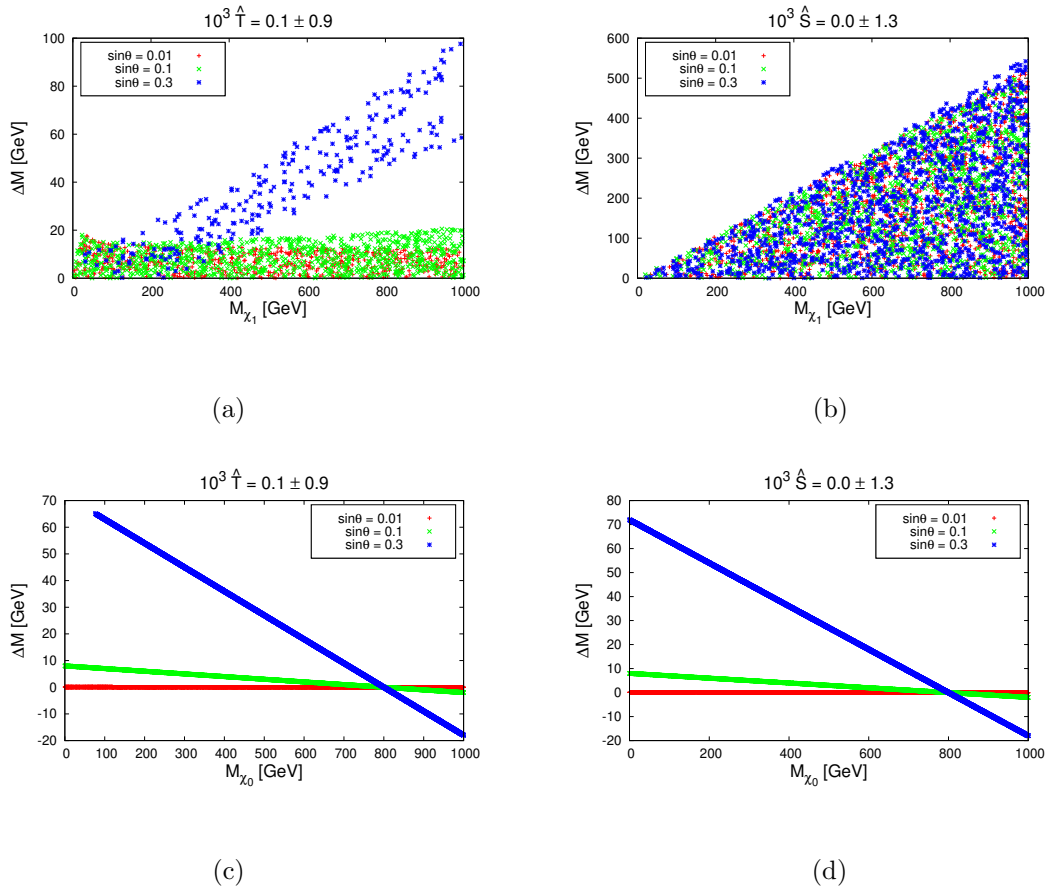


FIG. 1. Constraints on $\Delta M = (M_{\chi_1} - M_{L_1})$ coming from the EWPO (a) \hat{T} and (b) \hat{S} with respect to M_{χ_1} for three different values of $\sin\theta = 0.01, 0.1$ and 0.3 when both M_{χ_1} and M_{L_1} are varied randomly. Here $M_{\chi_0} = 120$ GeV is assumed. (c) and (d) shows the variation of ΔM as a function of M_{χ_0} , when $M_{\chi_1} = 800$ GeV and M_{L_1} is given by Eq. (29).

on the respective $SU(2)_L$ and $U(1)_Y$ couplings of the new states. As the cross section would reside on the lower side, much weaker bounds can be expected. There are several searches by the LHC collaborations [127–129] at $\sqrt{s} = 8$ and 13 TeV run at the LHC. As expected, the constraint is much more stringent for a pure $SU(2)_L$ VL pair that mixes with and decays to SM leptons. For example, heavy lepton mass values in the range 114 – 176 GeV are excluded through decay into Z boson and e, μ . In some recent analysis, the CMS collaboration has published [128, 129] the results of dedicated searches for doublet-like VLs, based on 41.4 fb^{-1} and 77.4 fb^{-1} data samples at $\sqrt{s} = 13$ TeV. The bounds can exclude a VL heavy τ' lepton in the mass range of 130 – 690 GeV or $120 < \tau' < 790$ GeV following its decays to tau leptons. The mass of the VL is the only free parameter both in the production cross section and in the branching fraction calculations, thus in the estimation of the bound. In a recent analysis [130], using a CMS search based on

77.4 fb^{-1} at 13 TeV LHC a bound on doublet-like vector leptons has been presented ($\sim 800 \text{ GeV}$) mainly focusing on 4ℓ final states. Unlike most of the studies presented above, in this model, direct couplings of L_1, L_2 with SM leptons are not allowed. Similarly, a recent analysis [131], using ATLAS search based on 139 fb^{-1} at 13 TeV LHC presents the exclusion limits on simplified SUSY models for a direct slepton production. Here slepton-pair production masses up to 700 GeV are excluded assuming three generations of mass-degenerate sleptons, considering sleptons decaying into final states with two leptons and missing transverse energy. However, such exclusion limits depend much on the masses of the lightest neutralino and it has been observed that even a lighter smuon mass is also allowed depending on the value of $m_{\tilde{\chi}_1^0}$ (e.g. $m_{\tilde{\mu}} \sim 200 \text{ GeV}$ is allowed for $m_{\tilde{\chi}_1^0} \sim 120 \text{ GeV}$).

In the framework that we considered, we shall place $M_{L_1}(M_{\chi_1})$ at 800 GeV , but the other VL L_2 has to be set at a lower value (e.g. $\sim 200 \text{ GeV}$) in order to satisfy $(g-2)_\mu$ constraints. Here we may note a few observations which would be detailed in the next sections. First of all, we will find that, the potentially important contribution in the evaluation of Δa_μ would be driven by the interaction involving coupling $Y_{3\mu}$ and in the perturbative unitarity regime (will be discussed in Sec. V) $Y_{3\mu}$ can only take $\sim O(1)$ values. We will further observe that all other Yukawa couplings of L_2 would be orders of magnitude suppressed either from the neutrino masses and mixings or from $(g-2)_e$ and cLFV observables. Thus, the dominant decay of L_2 can be considered as $L_2 \rightarrow \mu S$ followed by $S \rightarrow \chi_0 \nu$ ($M_{L_1}(M_{\chi_1}) > M_{L_2} > M_S > M_{\chi_0}$ would be followed throughout this analysis). So, naturally, $PP \rightarrow (L_2^\pm L_2^\mp) \rightarrow 2\mu + \cancel{E}_T$ through Z boson exchange can be considered as the most useful constraint for the present analysis. Here we may borrow the limits from Ref. [131] as direct production of sleptons or VL states would have same cross-section. Thus, based upon our previous discussion, we would consider $M_{L_2} = 190 \text{ GeV}$ and $m_{\tilde{\chi}_1^0} = 120 \text{ GeV}$ respectively for the calculation of different observables in the leptonic sector.

In our model, η couples to leptons, so can only be produced through electroweak gauge bosons at the LHC. Also, recall that η does not acquire any VEV, thus do not take part in electroweak symmetry breaking. In a model specific study, one would expect dilepton $+\cancel{E}_T$ [121, 132] through charged η pair production, or mono-lepton $+\cancel{E}_T$ through charged and neutral η productions via Z boson or W boson exchanges. An observable signal may be expected during high luminosity run of LHC through multilepton searches for $M_\eta \leq 250 \text{ GeV}$ [121]. Here, assuming all the charged and neutral components of η are of similar masses, we consider $M_\eta > 100 \text{ GeV}$ which is closely based on the exclusions at LEP [133]. However, our result does not depend much on M_η .

IV. RADIATIVE DIRAC NEUTRINO MASS

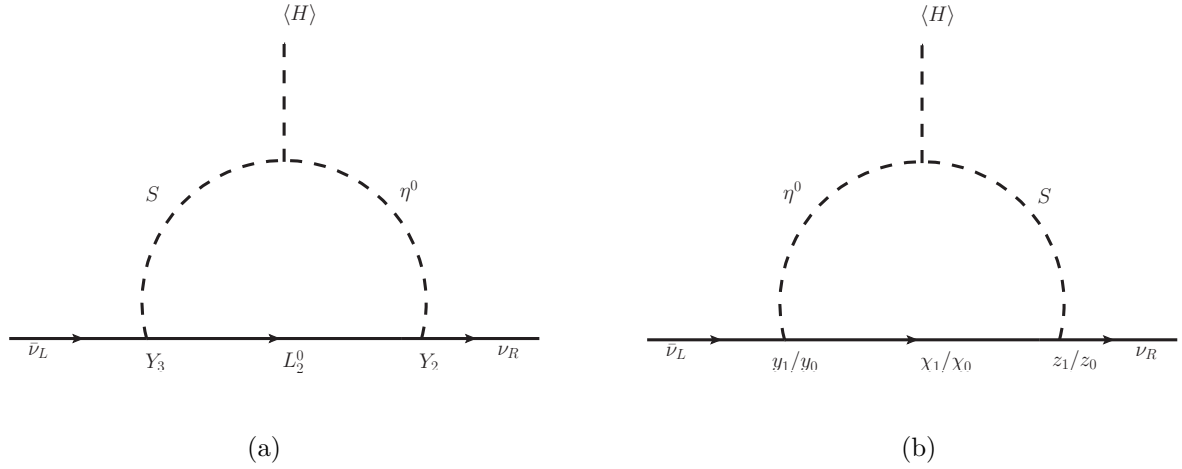


FIG. 2. Radiative mass generation for the neutrinos that adheres lepton number conservation. In the second diagram, neutral fermions are considered where $y_1, z_1 = -(Y_{4(i1)}, Y_{6(1i)})\sin\theta$, $y_0, z_0 = (Y_{4(i1)}, Y_{6(1i)})\cos\theta$ have been used.

As discussed, here neutrinos are massless at the tree level due to the imposed $\mathcal{Z}_2 \times \mathcal{Z}'_2$ symmetry while they may receive appropriate radiative corrections through the symmetry breaking term in Eq. (4). Thus one may develop a Dirac mass term for the SM neutrinos at one loop order after the Higgs field acquires a VEV. Additionally, the neutrino loops contain a stable particle χ_0 that could be treated as the cold DM of the universe [see Fig. 2(b)]. This intrinsically sets up a bridge between the phenomenology of light neutrinos and the other sectors like dark matter. The (3×3) neutrino mass matrix can be read as:

$$M_{\nu ij} = \sum_{f=L_2, \chi_1, \chi_0} \frac{y^f_{i1} M_f z^f_{1j} r_1^f}{16\pi^2 M_S^2 (r_1^f - 1)} \epsilon \left[\frac{\ln(r_1^f/r_2)}{r_1^f - r_2} - \frac{\ln r_2}{r_1^f (r_2 - 1)} \right]. \quad (31)$$

Similarly, $r_1^f = \left(\frac{M_f}{M_S}\right)^2$, $r_2 = \left(\frac{M_\eta}{M_S}\right)^2$ and $\epsilon = \mu' \langle H \rangle$ is the symmetry breaking term, with a mass dimension of 2. For each element in $f \in (L_2, \chi_1, \chi_0)$, the vertices y and z take (3×1) and (1×3) elements respectively which can be read as $y^f = (Y_3, -Y_4 \sin\theta, Y_4 \cos\theta)$ and $z^f = (Y_2, -Y_6 \sin\theta, Y_6 \cos\theta)$. Just as a measure of simplification, we can consider $M_{L_2} \sim M_{\chi_1} \sim M_{\chi_0} \equiv M_f$, so that Eq. (31) becomes,

$$M_{\nu ij} = M_f (Y_{3i1} Y_{21j} + Y_{4i1} Y_{61j}) \frac{r_1}{16\pi^2 M_S^2 (r_1 - 1)} \epsilon \left[\frac{\ln(r_1/r_2)}{r_1 - r_2} - \frac{\ln r_2}{r_1 (r_2 - 1)} \right]. \quad (32)$$

In the above, ϵ defines the order of the neutrino masses. Thus all the new Yukawa couplings can be assumed to take $\mathcal{O}(1)$ values. The diagonal mass terms $\text{diag}[m_i]$ which refer to the masses for the physical neutrino

states are related to the flavor states $M_{\nu ij}$ by the following equation,

$$M_{\nu ij} = U_{PMNS}(\text{diag}[m_i])U_{PMNS}^\dagger; \quad (33)$$

where the PMNS matrix can be parameterized as [1]:

$$U_{PMNS} = \begin{pmatrix} c_{12}c_{13} & s_{12}c_{13} & s_{13}e^{-i\delta} \\ -s_{12}c_{23} - c_{12}s_{23}s_{13}e^{i\delta} & c_{12}c_{23} - s_{12}s_{23}s_{13}e^{i\delta} & s_{23}c_{13} \\ s_{12}s_{23} - c_{12}c_{23}s_{13}e^{i\delta} & -c_{12}s_{23} - s_{12}c_{23}s_{13}e^{i\delta} & c_{23}c_{13} \end{pmatrix} \\ \times \text{diag}(1, e^{i\alpha_{21}/2}, e^{i\alpha_{31}/2}), \quad (34)$$

in which $s_{ij} \equiv \sin \theta_{ij}$, $c_{ij} \equiv \cos \theta_{ij}$; δ is the Dirac CP violating phase, and $\alpha_{21,31}$ are Majorana CP violating phases. Note that, using the global fit based on the current neutrino data, one may compute $|M_{\nu ij}|$ in terms of the different mass hierarchies, namely, normal hierarchy $\Delta m_{32}^2 > 0$ (NH) and inverted hierarchy $\Delta m_{32}^2 < 0$ (IH) as [134] ($\Delta m_{ij}^2 \equiv m_i^2 - m_j^2$). Taking $m_{1(3)} = 0$ for NH (IH), and zero values for the Majorana

| parameter | best fit $\pm 3\sigma$ range |
|---|------------------------------|
| $\Delta m_{21}^2 [10^{-5}\text{eV}^2]$ | 7.05–8.14 |
| $ \Delta m_{31}^2 [10^{-3}\text{eV}^2]$ (NH) | 2.41–2.60 |
| $ \Delta m_{31}^2 [10^{-3}\text{eV}^2]$ (IH) | 2.31–2.51 |
| $\sin^2 \theta_{12}$ | 0.273–0.379 |
| $\sin^2 \theta_{23}$ (NH) | 0.445–0.599 |
| $\sin^2 \theta_{23}$ (IH) | 0.453–0.598 |
| $\sin^2 \theta_{13}$ (NH) | 0.0196–0.0241 |
| $\sin^2 \theta_{13}$ (IH) | 0.0199–0.0244 |
| δ/π (NH) | 0.87–1.94 |
| δ/π (IH) | 1.12–1.94 |

TABLE IV. Neutrino oscillation parameters summary determined from the global analysis [134].

phases ($\alpha_{21(31)} = 0$) and the 3σ uncertainties, the magnitudes of the neutrino mass matrix elements in

units of eV for NH and IH can be estimated as:

$$\begin{aligned}
|M_{\nu ij}| &\simeq \begin{pmatrix} 0.11 - 0.45 & 0.12 - 0.82 & 0.12 - 0.82 \\ 0.12 - 0.82 & 2.4 - 3.3 & 2.0 - 2.2 \\ 0.12 - 0.82 & 2.0 - 2.2 & 2.2 - 3.1 \end{pmatrix} \times 10^{-2}, \\
|M_{\nu ij}| &\simeq \begin{pmatrix} 4.8 - 5.0 & 0.41 - 0.65 & 0.39 - 0.62 \\ 0.41 - 0.65 & 1.9 - 2.8 & 2.4 - 2.6 \\ 0.39 - 0.62 & 2.4 - 2.6 & 2.2 - 3.1 \end{pmatrix} \times 10^{-2}.
\end{aligned} \tag{35}$$

Here, following Eqs. (35) and (31) we may note a few observations related to the neutrino masses and mixings. In fact Eq. (31) can be cast as $M_{\nu ij} = \sum_{f=L_2, \chi_1, \chi_0} y_{i1} \Lambda^f z_{1j}$ and with all the BSM particles $\sim \mathcal{O}(10^2 - 10^3)$ GeV, one may find that $\Lambda^f \simeq \mathcal{O}(10^{-1} - 10^{-2})$ eV. Thus, the involved Yukawa couplings may take $\mathcal{O}(1)$ values to produce the correct values of the neutrino mass matrix as obtained in Eq. (35). Interestingly, out of the four Yukawas, only $Y_{3(i1)}$ and $Y_{4(i1)}$ ($i \in 1...3$) appear in most of the low energy phenomenology which are of interest to us. This includes neutrino masses and their mixings, precision observables like the anomalous magnetic moment of leptons or the cLFV processes and also the DM phenomenology. On the other hand, the other two Yukawa couplings $Y_{2(1i)}$ and $Y_{6(1i)}$ (six in total) related to the singlet state ν_{Ri} can control the neutrino masses and mixings. Thus, one may always use the freedom of choosing the free parameters Y_2 and Y_6 to satisfy the observed mass square differences and mixing angles while Y_3 and Y_4 may be tuned to satisfy the observables related to low energy lepton phenomenology.

To clarify it further numerically, we fix $M_S = 130$ GeV, $M_f = 800$ GeV and $M_\eta = 300$ GeV and use Eq. (32) to delineate the domain for $Y_{2(1i)}$ and $Y_{6(1i)}$ that may produce correct values for $|M_{\nu ij}|$ in Eq. (35) in the NH scenario. For simplicity, we recast the parameter as $Y_{2(1i)} = Y_{2i}$ and $Y_{6(1i)} = Y_{6i}$ (see also the discussion in Sec.V). We also fix $\{Y_3, Y_4\}$ at the given values (see Table V) which would be allowed by $(g-2)_\ell$ and cLFV constraints. We would further detail it in Sec. V. The lower and upper limits in Table V would refer to the minimum and maximum value of the $|M_{\nu ij}|$ in Eq. (35).

| $\{Y_{3i}, Y_{4i}\}$ | $\{Y_{2i}, Y_{6i}\}$ |
|-------------------------------------|--|
| $Y_{3e} = 0, Y_{4e} = 0.2$ | $0.001 \leq Y_{2e} \leq 0.01, 0.018 \leq Y_{6e} \leq 0.04$ |
| $Y_{3\mu} = 2.3, Y_{4\mu} = 0$ | $0.034 \leq Y_{2\mu} \leq 0.048, 0.11 \leq Y_{6\mu} \leq 0.12$ |
| $Y_{3\tau} = 0.01, Y_{4\tau} = 0.6$ | $0.029 \leq Y_{2\tau} \leq 0.032, 0.12 \leq Y_{6\tau} \leq 0.14$ |

TABLE V. Allowed range of $\{Y_{2i}, Y_{6i}\}$ as obtained from Eq. (32) (for $M_S = 130$ GeV, $M_f = 800$ GeV and $M_\eta = 300$ GeV) within which the magnitudes of the neutrino mass matrix elements for NH [Eq. (35)] can be satisfied.

V. LEPTON $g-2$, CLFV PROCESSES AND OTHER CONSTRAINTS

In the lepton phenomenology, apart from tuning the μ and e anomaly, new scalars η , S , charged fermions L_2^\pm, L_1^\pm and neutral leptons χ_1 and χ_0 may lead to observable signatures to lepton flavor violating processes such as $\ell_\alpha \rightarrow \ell_\beta \gamma$, or $\ell_\alpha \rightarrow 3\ell_\beta$ through the Yukawa couplings Y_1 , Y_3 and Y_4 that tie the SM leptons to BSM particles. The free parameters can be listed as:

$$M_{\chi_1}, M_{\chi_0}, M_S, M_\eta, M_{L_2}, Y_{1(i1)}, Y_{3(i1)}, Y_{4(i1)} \ (i \in e, \mu, \tau), \sin \theta. \quad (36)$$

The other charged lepton mass M_{L_1} can be expressed in terms of M_{χ_0} , M_{χ_1} and θ via Eq. (29). Unless otherwise stated, the mixing parameter in the neutral lepton sector $\sin \theta = 0.01$ is being fixed in our analysis. For the sake of clarity, we recast the new Yukawa couplings of Eq. (2) (and hence Eq. (36)) as Y_{ij} where i assumes different types of the couplings e.g., 1, 2, 3, 4, 6 and j takes the different flavors e, μ, τ . As an example, $Y_{1(1e)}$ in the Eq. (2) is simply denoted as Y_{1e} . In this set-up i.e., with the minimal contents of new states, first we survey if the discrepancy between the theoretical and experimental values of the magnetic moments of muon and electron can be explained. Then we will consider the charged lepton flavor violating processes. All the radiatively induced processes could be tested in the present and future generation of experiments; thus a domain for flavor specific Yukawa couplings can be derived.

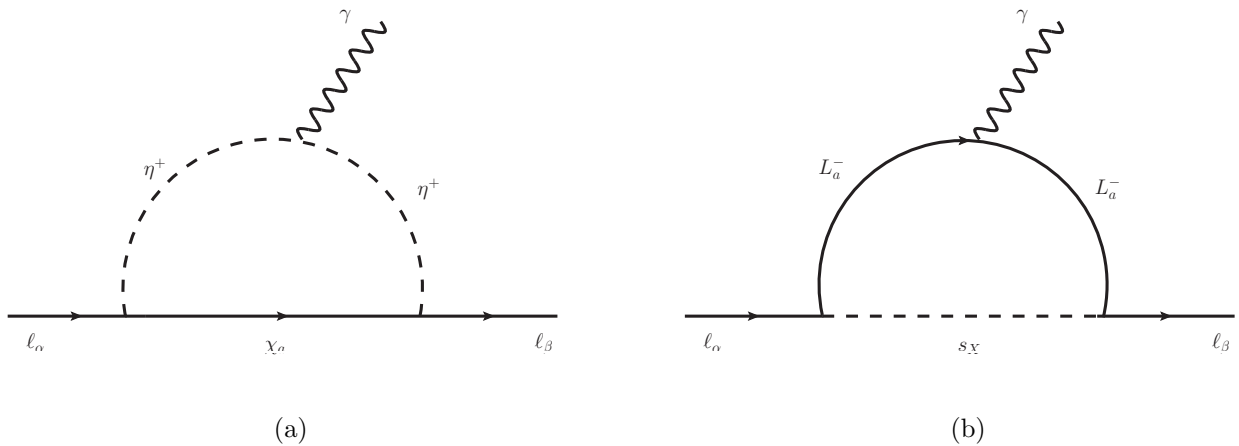


FIG. 3. Diagrams contributing to lepton $(g-2)$ and $\ell_\alpha \rightarrow \ell_\beta \gamma$ processes.

A. Lepton $g-2$

In our model, we would be able to explain $\Delta a_{\mu/e}$ simultaneously through the loop diagrams, shown in Fig. 3. ℓ_α and ℓ_β are general notations for the SM leptons. The total contribution for lepton $g-2$ process

can be given as ($\ell_\alpha = \ell_\beta = \ell$):

$$\Delta a_\ell = \Delta a_\ell^{(c)} + \Delta a_{1\ell}^{(n)} + \Delta a_{2\ell}^{(n)}, \quad (37)$$

where, the superscripts ‘n’ and ‘c’ correspond to the neutral and the charged lepton contributions in Fig. 3(a) and Fig. 3(b) respectively. The three individual contributions of Eq. (37) can be expressed as,

$$\Delta a_\ell^{(c)} = \frac{1}{16\pi^2} \left[|Y_{3\ell}|^2 \left(\frac{m_\ell}{M_S} \right)^2 F_3 \left(\frac{M_{L_2}^2}{M_S^2} \right) + |Y_{1\ell}|^2 \left(\frac{m_\ell}{M_\eta} \right)^2 F_3 \left(\frac{M_{L_1}^2}{M_\eta^2} \right) \right], \quad (38)$$

$$\begin{aligned} \Delta a_{1\ell}^{(n)} = \frac{1}{16\pi^2} \left[-|Y_{1\ell}|^2 \cos^2 \theta \left(\frac{m_\ell}{M_\eta} \right)^2 F_2 \left(\frac{M_{\chi_1}^2}{M_\eta^2} \right) - 2(Y_{4\ell})(Y_{1\ell}) \cos \theta \sin \theta \frac{(m_\ell M_{\chi_1})}{M_\eta^2} F_1 \left(\frac{M_{\chi_1}^2}{M_\eta^2} \right) \right. \\ \left. - |Y_{4\ell}|^2 \sin^2 \theta \left(\frac{m_\ell}{M_\eta} \right)^2 F_2 \left(\frac{M_{\chi_1}^2}{M_\eta^2} \right) \right], \end{aligned} \quad (39)$$

$$\Delta a_{2\ell}^{(n)} = \Delta a_{1\ell}^{(n)} (\cos \theta \rightarrow -\sin \theta, \sin \theta \rightarrow \cos \theta, M_{\chi_1} \rightarrow M_{\chi_0}). \quad (40)$$

The Form factors are defined in Appendix B. It is instructive to identify the positive and negative contributions of Δa_ℓ ($\ell \in e, \mu$) in Eq. (38)-(40).

$$\begin{aligned} \Delta a_\ell^{(+)} = \frac{1}{16\pi^2} \left[|Y_{3\ell}|^2 \left(\frac{m_\ell}{M_S} \right)^2 F_3 \left(\frac{M_{L_2}^2}{M_S^2} \right) + |Y_{1\ell}|^2 \left(\frac{m_\ell}{M_\eta} \right)^2 F_3 \left(\frac{M_{L_1}^2}{M_\eta^2} \right) + \right. \\ \left. (Y_{4\ell})(Y_{1\ell}) \sin 2\theta \frac{(m_\ell M_{\chi_0})}{M_\eta^2} F_1 \left(\frac{M_{\chi_0}^2}{M_\eta^2} \right) \right]. \end{aligned} \quad (41)$$

$$\begin{aligned} \Delta a_\ell^{(-)} = -\frac{1}{16\pi^2} \left[|Y_{1\ell}|^2 \left(\frac{m_\ell}{M_\eta} \right)^2 F_2 \left(\frac{M_{\chi_1}^2}{M_\eta^2} \right) + |Y_{4\ell}|^2 \left(\frac{m_\ell}{M_\eta} \right)^2 F_2 \left(\frac{M_{\chi_0}^2}{M_\eta^2} \right) + \right. \\ \left. (Y_{4\ell})(Y_{1\ell}) \sin 2\theta \frac{(m_\ell M_{\chi_1})}{M_\eta^2} F_1 \left(\frac{M_{\chi_1}^2}{M_\eta^2} \right) \right]. \end{aligned} \quad (42)$$

In the above, $\sin^2 \theta \rightarrow 0$ has been taken for illustration. Additionally, we consider that all the couplings are real and positive. In Eq. (41), the first two terms arise from the diagram with a charged fermion and a neutral scalar in the loop. The third term involves a neutral fermion and a charged scalar in the loop. Here the DM state χ_0 may provide with a positive contribution in Δa_μ , owing to the mixing between L_1^0 and ψ . The negative parts in Δa_ℓ (see Eq. (42)) involves only a neutral fermion and a charged scalar in the loop which is shown in Fig. 3(a). Thus, considering the opposite signs of Δa_μ and Δa_e in mind, one can easily expect that Δa_μ should have a major contribution from Eq. (41) while Eq. (42) may play the dominant role in determining Δa_e . In terms of the controlling parameters, Δa_μ (Δa_e) are managed by a set of new coupling parameters $Y_{4\ell}$, $Y_{3\ell}$, $Y_{1\ell}$ ($\ell \in e, \mu$) and also by the masses of new scalars and mixing of the neutral leptons. Electroweak precision observables restrict the mixing in the neutral leptons

: $\cos \theta \sim 1$, and, thus, $M_{L_1} \simeq M_{\chi_1}$ may be used for illustration (see Eq. (29)). For the scalar mass parameters, M_S is kept fixed at 130 GeV, while $M_\eta = 300$ and 1200 GeV are considered. Keeping this in mind, the variation of the flavor dependent couplings $Y_{i\mu}$ or Y_{ie} ($i \in 1, 3, 4$) with the mass of new scalars or fermions have been depicted through scattered plots where points consistent with Δa_i ($i \in e, \mu$) within the 2σ allowance in Eq. (16) and Eq. (17) are only shown. For a better understanding of interplay of the

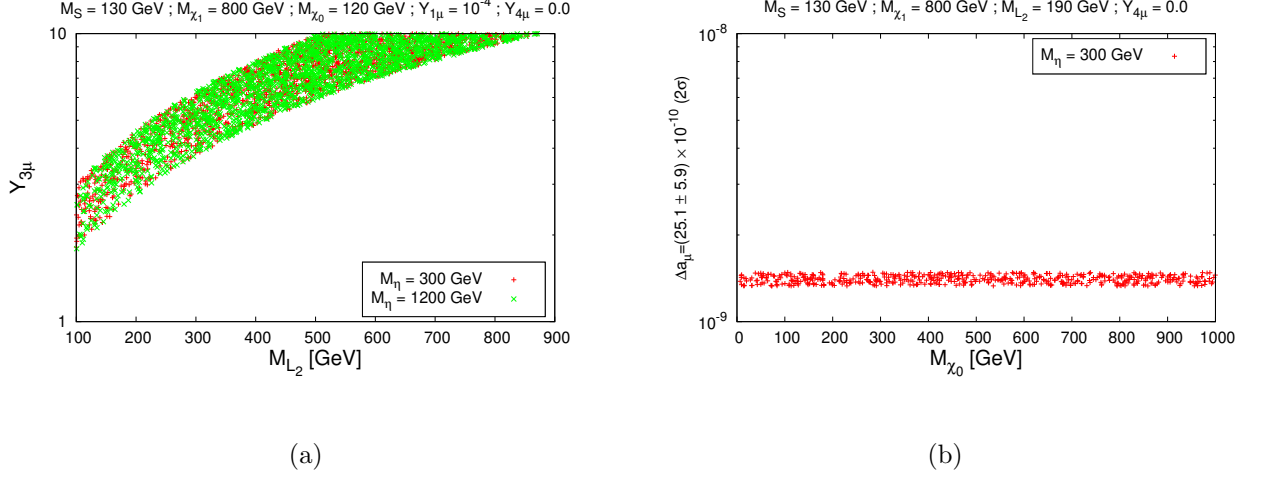


FIG. 4. Allowed parameter space satisfying Δa_μ within 2σ bound. Here $\sin \theta = 0.01$ is assumed. Here, red and green dots represent the scenarios corresponding to $M_\eta = 300$ GeV and 1200 GeV respectively.

different couplings and masses on the $\Delta a_{\mu(e)}$, we recast the Eq. (41) and Eq. (42) in a more convenient form: $\Delta a_{\mu(e)} = \Delta a_{\mu(e)}^{Y_{3\mu(e)}} + \Delta a_{\mu(e)}^{Y_{1\mu(e)}} + \Delta a_{\mu(e)}^{Y_{4\mu(e)}} + \Delta a_{\mu(e)}^{Y_{4\mu(e)}Y_{1\mu(e)}}$, where,

$$\Delta a_{\mu(e)}^{Y_{3\mu(e)}} = \frac{1}{16\pi^2} \left[|Y_{3\mu(e)}|^2 \left(\frac{m_{\mu(e)}}{M_S} \right)^2 F_3 \left(\frac{M_{L_2}^2}{M_S^2} \right) \right], \quad (43)$$

$$\Delta a_{\mu(e)}^{Y_{1\mu(e)}} = \frac{1}{16\pi^2} \left[|Y_{1\mu(e)}|^2 \left(\frac{m_{\mu(e)}}{M_\eta} \right)^2 \left\{ F_3 \left(\frac{M_{L_1}^2}{M_\eta^2} \right) - F_2 \left(\frac{M_{\chi_1}^2}{M_\eta^2} \right) \right\} \right], \quad (44)$$

$$\Delta a_{\mu(e)}^{Y_{4\mu(e)}} = \frac{1}{16\pi^2} \left[-|Y_{4\mu(e)}|^2 \left(\frac{m_{\mu(e)}}{M_\eta} \right)^2 \left\{ F_2 \left(\frac{M_{\chi_0}^2}{M_\eta^2} \right) \right\} \right], \quad (45)$$

$$\Delta a_{\mu(e)}^{Y_{4\mu(e)}Y_{1\mu(e)}} = \frac{1}{16\pi^2} \left[Y_{1\mu(e)}Y_{4\mu(e)} \sin 2\theta \frac{m_{\mu(e)}}{M_\eta^2} \left\{ M_{\chi_0} F_1 \left(\frac{M_{\chi_0}^2}{M_\eta^2} \right) - M_{\chi_1} F_1 \left(\frac{M_{\chi_1}^2}{M_\eta^2} \right) \right\} \right]. \quad (46)$$

We begin our discussion with μ -specific couplings $Y_{i\mu}$ and the relevant mass parameters M_S , M_η , M_{L_2} to probe their limits in controlling Δa_μ . Here the role of $Y_{4\mu}$ is somewhat tricky and depends on the choice of other parameters. For example, it can provide an unhelpful contribution through Eq. (45). Similarly, unless $Y_{1\mu} \ll Y_{4\mu}$, Eq. (46) dominates over the $\Delta a_\mu^{Y_{4\mu}}$. However, the contribution in Eq. (46) can take both

positive and negative values which can be controlled by the ratio M_{χ_0}/M_{χ_1} . Truly, a specific ratio of the neutral fermions, i.e., M_{χ_0}/M_{χ_1} can boost Δa_μ through an overall positive contribution, driven by $Y_{4\mu}$. However, at the same time it becomes unfriendly to obtain a correct Δa_e (since the same bracketed term in Eq. (46) potentially contributes to e magnetic moment). For a practical choice, we set $Y_{4\mu} = 0$ as we will see that $\Delta a_e^{Y_{4e}Y_{1e}}$ term would have to be properly tuned to fit Δa_e . In other words, M_{χ_0}/M_{χ_1} will be chosen to have a negative contribution from $\Delta a_e^{Y_{4e}Y_{1e}}$ to have a consistent Δa_e .

Thus assuming $Y_{4\mu} = 0$, one finds $\Delta a_\mu = \Delta a_\mu^{Y_{3\mu}} + \Delta a_\mu^{Y_{1\mu}}$. A prominent cancellation between the two terms in $\Delta a_\mu^{Y_{1\mu}}$ can always be observed irrespective of the value of $Y_{1\mu}$, and, thus, one finds $\Delta a_\mu \simeq \Delta a_\mu^{Y_{3\mu}}$. Thus, naturally, we may choose $Y_{1\mu}$ at any value within its perturbative limit while satisfying the experimental bounds on Δa_μ . We will see that a smaller $Y_{1\mu}$ (which will be chosen in the subsequent analysis) would be highly desired to satisfy $\mu \rightarrow e\gamma$ constraint.

Fig. 4(a) shows the variation of $Y_{3\mu}$ as a function of M_{L_2} when $M_S = 130$ GeV, $M_\eta = 300$ GeV and $M_\eta = 1200$ GeV. The other input parameters are $M_{\chi_1} = 800$ GeV, $M_{\chi_0} = 120$ GeV, $Y_{1\mu} = 10^{-4}$ while $Y_{4\mu}$ is fixed at zero. Clearly, the doublet scalar does not have any influence to the result. As said earlier, only $L_2 - S$ loop can manage to attune Δa_μ , and thus, one requires somewhat larger values for $Y_{3\mu}$. This can be further verified through Fig. 4(a). Note that, here mass of the singlet M_S needs to be smaller to make $Y_{3\mu}$ within the perturbative bound, and this can only be realized if our model considers light dark matter (since $M_{\chi_0} < M_S$ needs to be satisfied). However, a heavier χ_0 can also accommodate Δa_μ without having any difficulties. Recall that setting $Y_{4\mu} = 0$ will automatically make vanishing contributions from Eqs. (45) and (46), which include M_{χ_0} . Thus, because of the choice of our parameters, χ_0 can affect Δa_μ only through Eq. (44), which can only lead to insignificant contribution. A further confirmation can be made through Fig. 4(b), where we show variations of Δa_μ as a function of M_{χ_0} for $M_\eta = 300$ GeV and $M_S = 130$ GeV. Neutral and charged vector leptons are fixed at masses $M_{\chi_1} = 800$ and $M_{L_2} = 190$ GeV. Here we varied the couplings ($Y_{1\mu} : [0.0001 - 1]$, $Y_{3\mu} : [0.0001 - 2]$) and M_{χ_0} randomly. The resultant Δa_μ can be seen to be consistent over the entire χ_0 range. We note here that, in Fig. 4(a) and Fig. 4(b), we refrain from considering LHC bounds based on with two leptons and missing transverse energy (see Sec.III D) on the parameter space. This helps us to study the dependence of different parameters on the Δa_μ numerically and to choose a valid parameter space which is consistent with the LHC searches. For instance, a light L_2 accompanied with a light scalar S may easily accommodate Δa_μ with a perturbative value of $Y_{3\mu} \sim 2$. We have checked that $Y_{3\mu}$ remains perturbative upto TeV scale even when one includes dominant radiative corrections while at and above TeV scale beta function of $Y_{3\mu}$ may include new gauge interactions. This is in particular true if our low energy model is embedded in a TeV scale LR model. However, as discussed

earlier, the LHC limits can be managed if one assumes a light χ_0 as well. Thus in the following sections, particularly, in the computation of cLFV and DM observables, we would fix a few parameters at values $M_{L_2} = 190$ GeV, $M_S = 130$ GeV and $M_{\chi_0} = 120$ GeV.

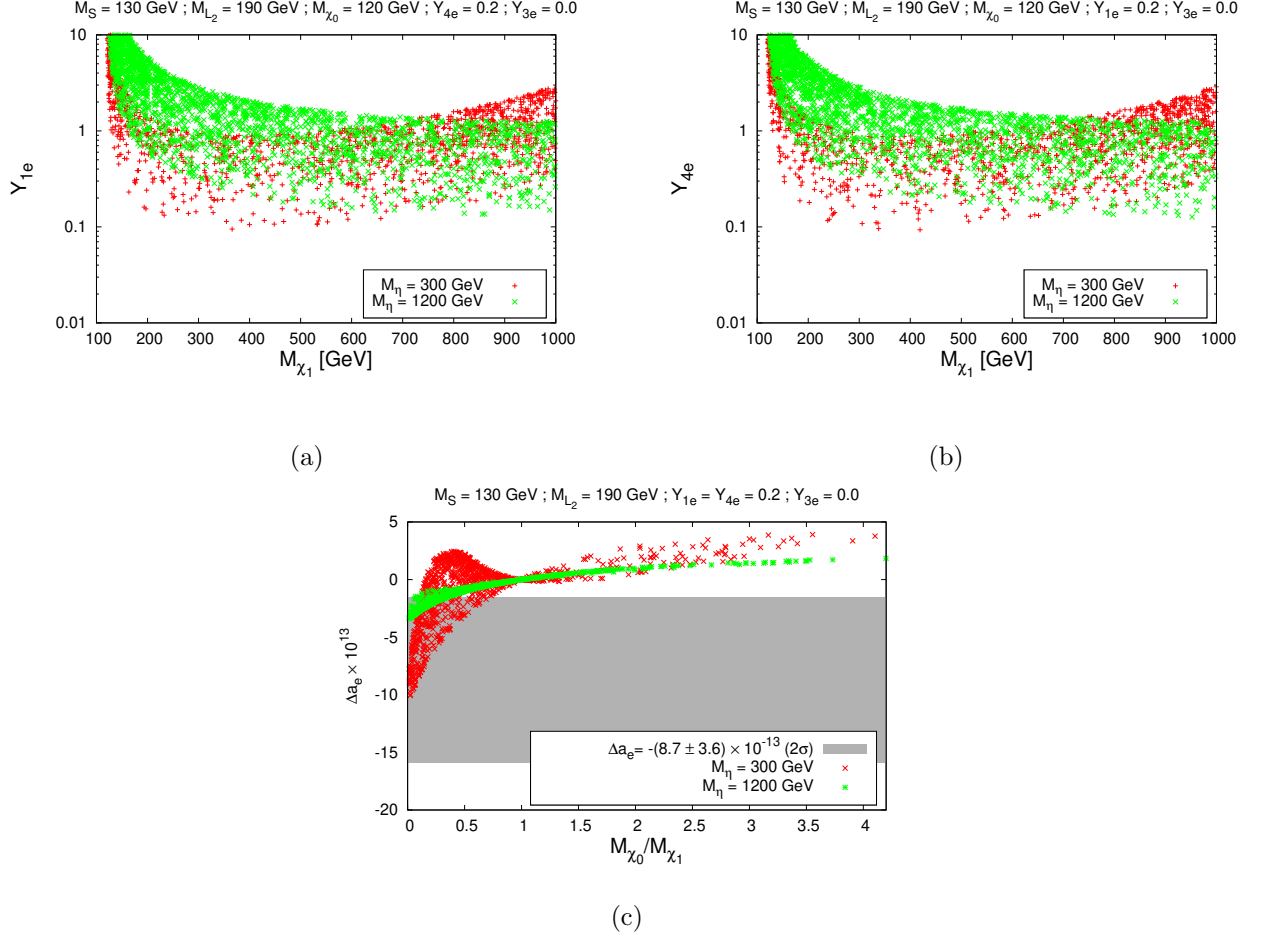


FIG. 5. Allowed parameter space satisfying Δa_e within 2σ bound. As before $\sin \theta = 0.01$ is taken. Here, red and green dots represent the scenarios corresponding to $M_\eta = 300$ GeV and 1200 GeV respectively.

In our next precision calculation, we will now see the role of different parameters in obtaining a correct value for Δa_e . Note that, here, for practical purposes, one finds $\Delta a_e \simeq \Delta a_e^{Y_{4(e)}Y_{1(e)}}$. The reasons are as follows. $\Delta a_e^{Y_{1(e)}}$ becomes insignificant due to cancellation between different terms. Moreover, $\Delta a_e^{Y_{1(e)}}$ and $\Delta a_e^{Y_{4(e)}}$ are $\propto m_e^2$, thus, are much suppressed and can be neglected for the parameter space, we are interested in. Additionally, we choose $Y_{3e} = 0$ to forbid the positive part in Eq. (43). So we may re-express Δa_e as follows:

$$\Delta a_e \simeq -\frac{(Y_{1e})(Y_{4e}) \sin 2\theta m_e}{16\pi^2 M_\eta^2} \left[M_{\chi_1} F_1 \left(\frac{M_{\chi_1}^2}{M_\eta^2} \right) - M_{\chi_0} F_1 \left(\frac{M_{\chi_0}^2}{M_\eta^2} \right) \right]. \quad (47)$$

As before, in the numerical analysis, we fixed $M_S = 130$ GeV, $M_\eta = 300$ and 1200 GeV, $M_{L_2} = 190$ GeV and $M_{\chi_0} = 120$ GeV. Fig. 5(a) depicts the variation of Y_{1e} as a function of M_{χ_1} , when Y_{4e} is fixed at 0.2. And similarly for the Fig. 5(b), where Y_{4e} appears as the variable and Y_{1e} is fixed at 0.2. In both of these plots red and green dots represent the scenarios corresponding to $M_\eta = 300$ GeV and 1200 GeV respectively. Note that, for the smaller values of M_{χ_1} , there is a difference between the allowed regions corresponding to $M_\eta = 300$ GeV and 1200 GeV, while at the higher values both the red and green dots merge [see Fig. 5(a) and (b)]. In the lighter χ_1 regime, where $M_{\chi_1} \sim M_{\chi_0}$, a partial cancellation in the bracketed part of Eq. (47) can be observed. The suppression is more for a heavier η , thus, a larger coupling can be helpful to tune Δa_e . On the other hand, for larger values of M_{χ_1} , the term $M_{\chi_1} F_1 \left(\frac{M_{\chi_1}^2}{M_\eta^2} \right)$ may appear to have the leading contribution. At this large M_{χ_1} region, for a fixed value of M_{χ_1} , $F_1 \left(\frac{M_{\chi_1}^2}{M_\eta^2} \right)$ increases with the increasing value of M_η . However, the overall term $\frac{1}{M_\eta^2} F_1 \left(\frac{M_{\chi_1}^2}{M_\eta^2} \right)$ becomes somewhat insensitive to the variation in M_η and hence only a slight increment in Yukawa coupling can be observed for the lighter M_η value.

Fig. 5(c) shows the scaled variation of Δa_e as a function of M_{χ_0}/M_{χ_1} where we have again relaxed the potential constraints coming from LHC. All the other masses and couplings are fixed as before. The grey patch represents the 2σ range of the Δa_e . One can easily see that, a small mass ratio (< 0.25 , < 0.75) for $M_\eta = 1200, 300$ GeV respectively, can lead to the desired negative contribution. For larger M_η , to compensate the suppression, a lighter χ_0 is desired to produce the correct value for Δa_e . On the other hand, with increasing M_{χ_0}/M_{χ_1} the positive contribution starts to increase for a fixed M_η [see Eq. (47)] and hence a correct value of Δa_e would be difficult to obtain.

As a final remark, it is now evident that the presence of the two VL states L_1 and L_2 are necessary to accommodate the both Δa_μ and Δa_e . The second doublet L_2 may provide the sole contribution to muon magnetic moment, while the other one can be used to tune the magnitude and sign of the e magnetic moment. Moreover, we will find that, satisfying different cLFV processes may become much easier in this scenario.

B. cLFV constraints

In this model framework, in computing the cLFV observables we closely follow Refs. [135, 136]. One-loop effective vertices, relevant for the different two and three body processes $\ell_\alpha \rightarrow \ell_\beta \gamma$ or $\ell_\alpha \rightarrow 3\ell_\beta$ are generated through the interactions among BSM fermions (χ_a, L_a^\pm), scalars η and S and the SM leptons.

1. $\ell_\alpha \rightarrow \ell_\beta \gamma$

We start with the form factors for $\ell_\alpha \rightarrow \ell_\beta \gamma$, where the relevant diagrams have been depicted in Fig. 3. The details of the calculation are presented in Appendix C. Here we recast the form factors $A_2^{(n)L,R}$ and $A_2^{(c)L,R}$ related to neutral and charged fermions in terms of our model parameters respectively.

$$A_2^{(n)L} = \frac{1}{32\pi^2 M_\eta^2} \left[Y_{1\beta}^\dagger Y_{4\alpha}^\dagger \sin \theta \cos \theta \left\{ \frac{2M_{\chi_1}}{m_{\ell_\alpha}} F_1 \left(\frac{M_{\chi_1}^2}{M_\eta^2} \right) - \frac{2M_{\chi_0}}{m_{\ell_\alpha}} F_1 \left(\frac{M_{\chi_0}^2}{M_\eta^2} \right) \right\} \right. \\ \left. + Y_{1\beta}^\dagger Y_{1\alpha} \cos^2 \theta F_2 \left(\frac{M_{\chi_1}^2}{M_\eta^2} \right) + Y_{4\beta} Y_{4\alpha}^\dagger \cos^2 \theta \frac{m_{\ell_\beta}}{m_{\ell_\alpha}} F_2 \left(\frac{M_{\chi_0}^2}{M_\eta^2} \right) \right], \quad (48)$$

$$A_2^{(c)L} = \frac{1}{32\pi^2 M_S^2} Y_{3\beta} Y_{3\alpha}^\dagger \frac{m_{\ell_\beta}}{m_{\ell_\alpha}} F_3 \left(\frac{M_{L_2}^2}{M_S^2} \right) + \frac{1}{32\pi^2 M_\eta^2} Y_{1\beta}^\dagger Y_{1\alpha} F_3 \left(\frac{M_{L_1}^2}{M_\eta^2} \right), \\ A_2^{(n)R} = A_2^{(n)L} \Big|_{Y_4 \leftrightarrow Y_1^\dagger, F_2 \left(\frac{M_{\chi_1}^2}{M_\eta^2} \right) \leftrightarrow F_2 \left(\frac{M_{\chi_0}^2}{M_\eta^2} \right)}, \quad A_2^{(c)R} = A_2^{(c)L} \Big|_{Y_3 \leftrightarrow Y_1^\dagger}. \quad (49)$$

Finally, the coefficients in the above can be clubbed to get the total contributions.

$$A_2^{L,R} = A_2^{(n)L,R} + A_2^{(c)L,R}, \quad (50)$$

The decay width is given by [135, 136]

$$\Gamma(\ell_\alpha \rightarrow \ell_\beta \gamma) = \frac{\alpha_{em} m_{\ell_\alpha}^5}{4} (|A_2^L|^2 + |A_2^R|^2), \\ \text{Br}(\ell_\alpha \rightarrow \ell_\beta \gamma) = \tau_\alpha \frac{\alpha_{em} m_{\ell_\alpha}^5}{4} (|A_2^L|^2 + |A_2^R|^2). \quad (51)$$

where α_{em} is the electromagnetic fine structure constant and τ_α is the lifetime of ℓ_α .

2. $\ell_\alpha \rightarrow 3\ell_\beta$

Here we calculate the decay width for the processes where a heavier SM lepton decays into three lighter leptons of the same flavor, i.e., $\ell_\alpha^- \rightarrow \ell_\beta^- \ell_\beta^- \ell_\beta^+$. We present the relevant γ -penguin, Z -penguin and Box diagrams contributions to get the complete decay width and hence the branching ratio for $\ell_\alpha \rightarrow 3\ell_\beta$ processes. The details of the calculation can be found in Appendix C.



FIG. 6. γ -penguin diagrams contributing to the $\ell_\alpha^- \rightarrow \ell_\beta^- \ell_\beta^- \ell_\beta^+$ decay. The index a reads 0, 1 for neutral and 1, 2 for charged fermions and $s_1 = \eta^0$, $s_2 = S$ for the charged lepton loops. The corresponding leg-corrections (not shown) are also taken into account.

- Photon penguin contribution: As shown in Fig. 6, the monopole contributions can be recast in terms of our model parameters,

$$A_1^{(n)L} = \frac{1}{576\pi^2 M_\eta^2} \left[Y_{4\beta} Y_{4\alpha}^\dagger \cos^2 \theta F_4 \left(\frac{M_{\chi_0}^2}{M_\eta^2} \right) \right], \quad A_1^{(n)R} = A_1^{(n)L} |_{Y_4 \rightarrow Y_1^\dagger, M_{\chi_0} \rightarrow M_{\chi_1}}, \quad (52)$$

$$A_1^{(c)L} = -\frac{1}{576\pi^2 M_S^2} \left[Y_{3\beta} Y_{3\alpha}^\dagger F_5 \left(\frac{M_{L_2}^2}{M_S^2} \right) \right], \quad A_1^{(c)R} = A_1^{(c)L} |_{Y_3 \rightarrow Y_1^\dagger, M_{L_2} \rightarrow M_{L_1}, M_S \rightarrow M_\eta}. \quad (53)$$

The dipole contributions can be read from Eq. (48) and Eq. (49).

- Z penguin contribution: Dominant Feynman diagrams are shown in Fig. 7. We have calculated the coefficients as follows:

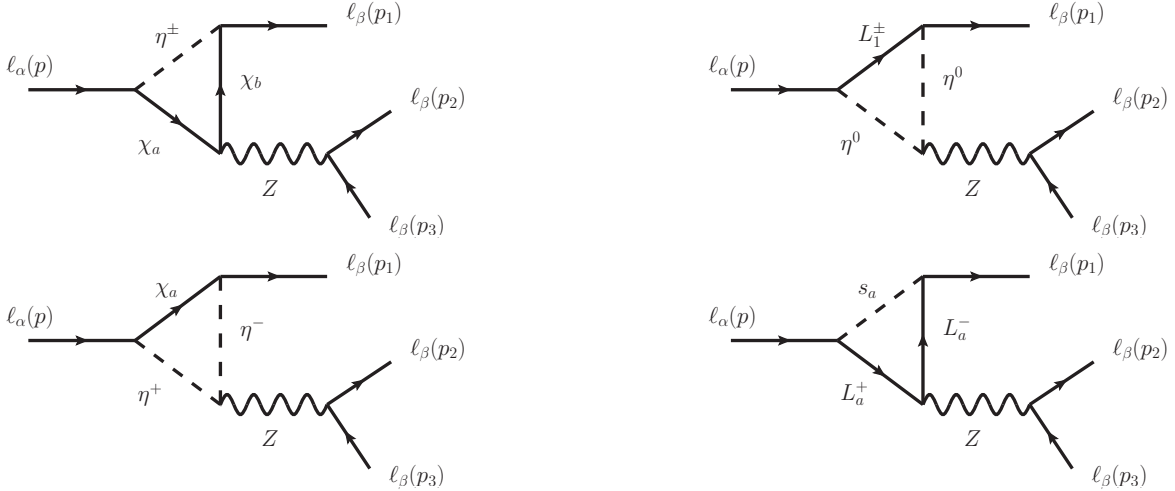


FIG. 7. Leading Z penguin diagrams contributing to the $\ell_\alpha^- \rightarrow \ell_\beta^- \ell_\beta^- \ell_\beta^+$ decay. Leg corrections are also considered (not shown). Indices $a, b = 1, 2$ (for $L_{a,b}^\pm$), 0, 1 (for $\chi_{a,b}$) and $s_1 = \eta^0$, $s_2 = S$ as before.

The expressions for the form factors are given below [137–139]:

$$F_L^{(n)} = -\frac{1}{16\pi^2} \sum_{a,b=0,1} \left[Y_{4\beta} Y_{4\alpha}^\dagger U_b U_a \left\{ E_{ba}^{R(n)} \left(2C_{24}(M_\eta^2, M_{\chi_a}^2, M_{\chi_b}^2) - \frac{1}{2} \right) - E_{ba}^{L(n)} M_{\chi_a} M_{\chi_b} C_0(M_\eta^2, M_{\chi_a}^2, M_{\chi_b}^2) \right\} \right. \\ \left. + Y_{4\beta} Y_{4\alpha}^\dagger U_a^2 \{ 2Q_{\eta\eta} C_{24}(M_{\chi_a}^2, M_\eta^2, M_\eta^2) \} + Y_{4\beta} Y_{4\alpha}^\dagger U_a^2 \{ g_L^{(\ell)} B_1(M_{\chi_a}^2, M_\eta^2) \} \right], \quad (54)$$

$$F_L^{(c)} = -\frac{1}{16\pi^2} \left[Y_{3\beta} Y_{3\alpha}^\dagger \left\{ E_{22}^{R(c)} \left(2C_{24}(M_S^2, M_{L_2}^2, M_{L_2}^2) - \frac{1}{2} \right) - E_{22}^{L(c)} M_{L_2} M_{L_2} C_0(M_S^2, M_{L_2}^2, M_{L_2}^2) \right\} \right. \\ \left. + Y_{3\beta} Y_{3\alpha}^\dagger \{ 2Q_{22} C_{24}(M_{L_2}^2, M_S^2, M_S^2) \} + Y_{3\beta} Y_{3\alpha}^\dagger \{ g_L^{(\ell)} B_1(M_{L_2}^2, M_S^2) \} \right], \quad (55)$$

$$F_R^{(n)} = F_L^{(n)}|_{Y_4 \rightarrow Y_1^\dagger, U \rightarrow U', g_L^{(\ell)} \rightarrow g_R^{(\ell)}}, F_R^{(c)} = F_L^{(c)}|_{Y_3 \rightarrow Y_1^\dagger, M_{L_2} \rightarrow M_{L_1}, M_S \rightarrow M_\eta, Q_{22} \rightarrow Q_{11}, g_L^{(\ell)} \rightarrow g_R^{(\ell)}}. \quad (56)$$

As before, $F_{L,R} = F_{L,R}^{(n)} + F_{L,R}^{(c)}$. The generic forms of C_{24} , C_0 and B_1 functions are listed in Appendix B.

- Box diagram contributions: Leading contributions are shown in Fig. 8.

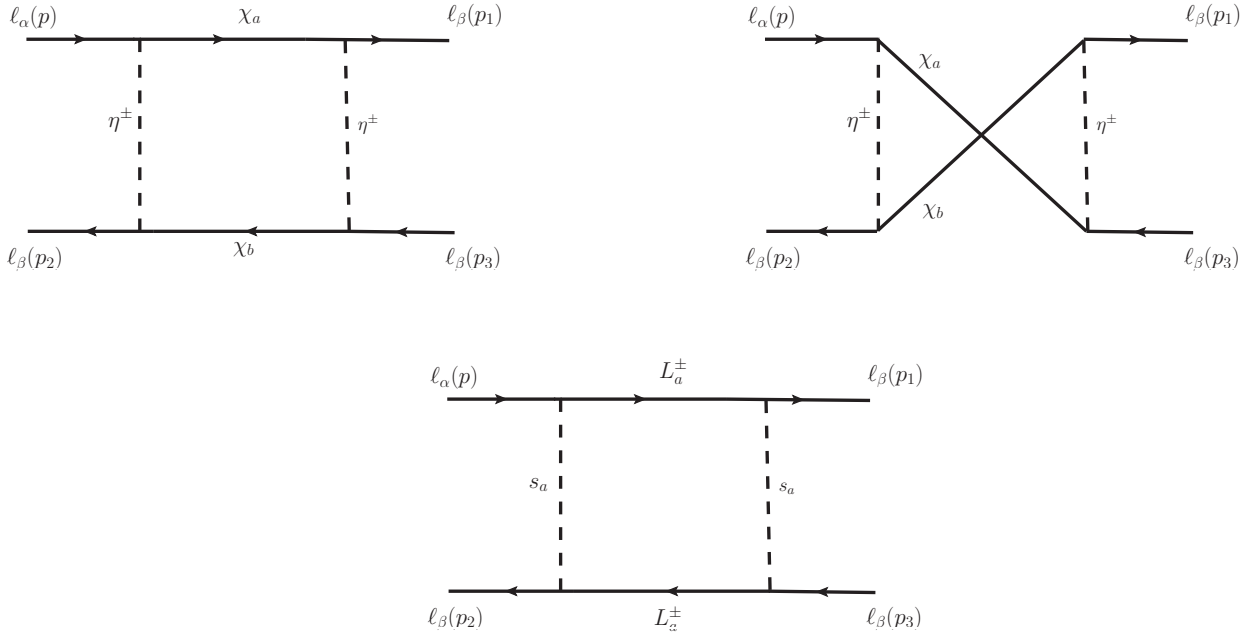


FIG. 8. Box diagrams contributing to the $\ell_\alpha^- \rightarrow \ell_\beta^- \ell_\beta^- \ell_\beta^+$ decay. As before, $a, b = 1, 2$ (for $L_{a,b}^\pm$), $0, 1$ (for $\chi_{a,b}$) and $s_1 = \eta^0$, $s_2 = S$.

The dominant B -factors can be calculated as,

$$e^2 B_1^{(n)L} = \frac{1}{16\pi^2} \left[\frac{\tilde{D}_0}{2} Y_{4\beta} Y_{4\alpha}^\dagger Y_{4\beta} Y_{4\beta}^\dagger |U_a|^2 |U_b|^2 + D_0 M_{\chi_a} M_{\chi_b} Y_{4\beta} Y_{4\beta} Y_{4\alpha}^\dagger Y_{4\beta}^\dagger U_b^2 U_a^{\dagger 2} \right], \quad (57)$$

$$e^2 B_2^{(n)L} = \frac{1}{16\pi^2} \left[\frac{\tilde{D}_0}{4} Y_{4\beta} Y_{4\alpha}^\dagger Y_{1\beta}^\dagger Y_{1\beta} |U_a|^2 |U_b'|^2 - \frac{D_0}{2} M_{\chi_a} M_{\chi_b} Y_{1\beta}^\dagger Y_{4\alpha}^\dagger Y_{4\beta} Y_{1\beta} U_a' U_a^\dagger U_b U_b'^\dagger \right. \\ \left. - \frac{\tilde{D}_0}{4} Y_{1\beta}^\dagger Y_{4\beta} Y_{4\alpha}^\dagger Y_{1\beta} U_b' U_b U_a^\dagger U_a'^\dagger + \frac{\tilde{D}_0}{4} Y_{4\beta} Y_{1\beta}^\dagger Y_{4\alpha}^\dagger Y_{1\beta} U_b U_b' U_a^\dagger U_a'^\dagger \right], \quad (58)$$

$$e^2 B_1^{(n)R} = e^2 B_1^{(n)L} |_{Y_4 \rightarrow Y_1^\dagger, U \rightarrow U'} , \quad e^2 B_2^{(n)R} = e^2 B_2^{(n)L} |_{Y_4 \leftrightarrow Y_1^\dagger, U \leftrightarrow U'} . \quad (59)$$

$$e^2 B_1^{(c)L} = \frac{1}{16\pi^2} \left[\frac{\tilde{D}_0}{2} Y_{3\beta} Y_{3\alpha}^\dagger Y_{3\beta} Y_{3\beta}^\dagger \right], \quad (60)$$

$$e^2 B_2^{(c)L} = \frac{1}{16\pi^2} \left[\frac{\tilde{D}_0}{4} Y_{3\beta} Y_{3\alpha}^\dagger Y_{1\beta}^\dagger Y_{1\beta} - \frac{D_0}{2} M_{L_a} M_{L_a} Y_{1\beta}^\dagger Y_{3\alpha}^\dagger Y_{3\beta} Y_{1\beta} \right], \quad (61)$$

$$e^2 B_1^{(c)R} = e^2 B_1^{(c)L} |_{Y_3 \rightarrow Y_1^\dagger} , \quad e^2 B_2^{(c)R} = e^2 B_2^{(c)L} |_{Y_3 \leftrightarrow Y_1^\dagger} . \quad (62)$$

The generic functional forms for these D_0 and \tilde{D}_0 are again available at Appendix B. Though only the dominant terms are mentioned, for numerical purposes, we calculated all $B_i^{L,R}$ [$i = 1, 2, 3, 4$]. Finally, there may be Higgs penguin diagrams as well, but the Higgs couplings to the SM leptons are much suppressed ($\sim \mathcal{O}(\leq 10^{-2})$) compared to that of γ and Z , and hence we can ignore them³.

3. Numerical Results

Here, we will particularly identify the allowed regions of parameter space associated with free parameters and masses as introduced in Eq. (36), in regard to different cLFV decays. Some of the free parameters, as already tuned by Δa_i ($i \in e, \mu$), collider or the electroweak precision searches would be set within their allowed domains. In Figs. 9 and 10, the variation of branching ratios for the different cLFV processes with respect to the relevant couplings have been shown for $M_\eta = 300$ GeV and 1200 GeV respectively. We have followed a particular color code for all these plots, i.e., the red signifies $\text{Br}(\ell_\alpha \rightarrow \ell_\beta \gamma)$ while blue stands for $\text{Br}(\ell_\alpha \rightarrow 3\ell_\beta)$. The horizontal lines specify the present experimental bounds [see Table III] on the

³ In some specific models, Higgs penguin may lead to significant contributions [140–142].

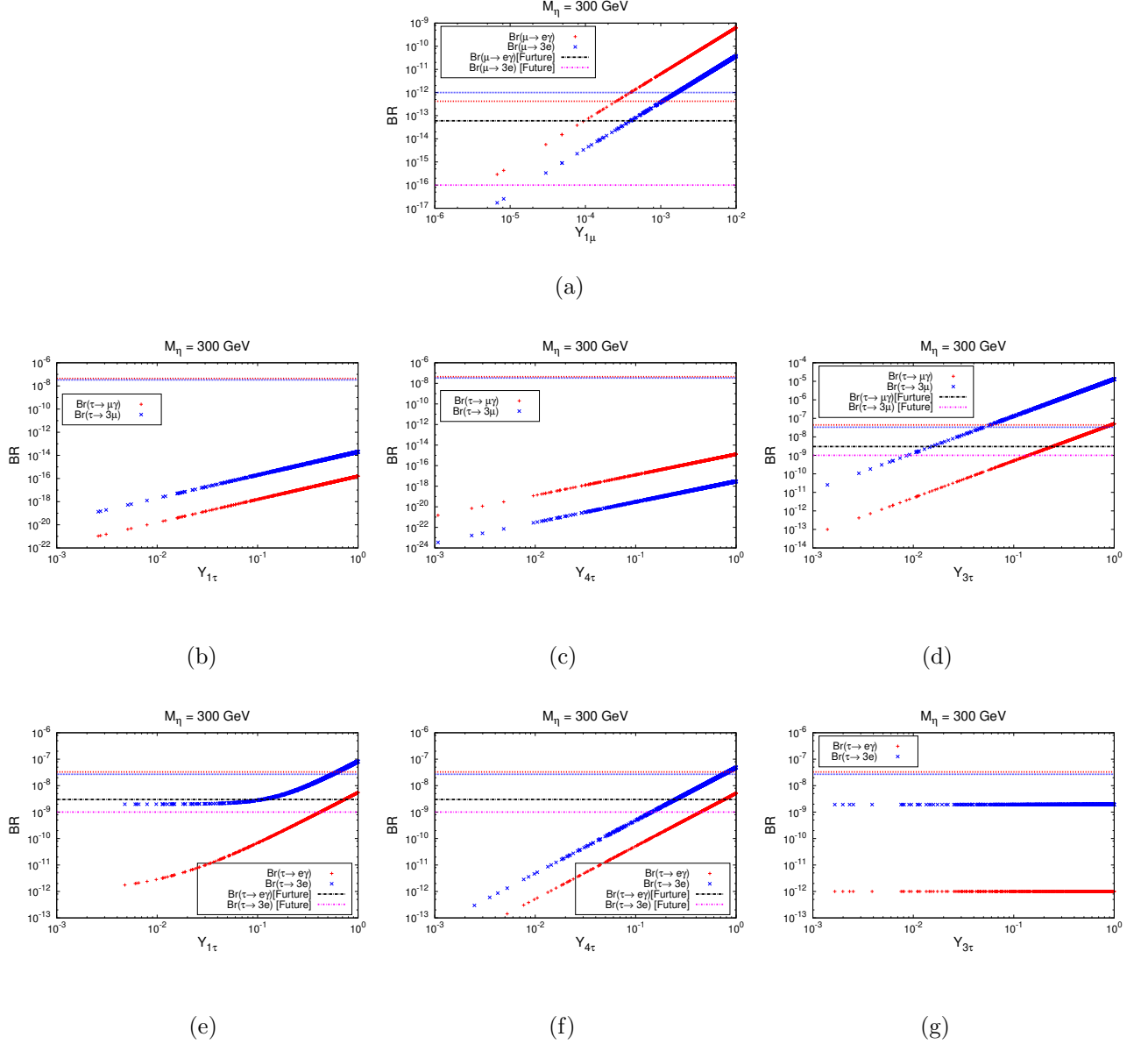


FIG. 9. Variation of $\text{Br}(\ell_\alpha \rightarrow \ell_\beta \gamma)$ (Red) and $\text{Br}(\ell_\alpha \rightarrow 3\ell_\beta)$ (Blue) as a function of $Y_{i\ell}$ [$i = 1, 3, 4$]. Input parameters are set as $M_\eta = 300$ GeV, $M_S = 130$ GeV, $M_{\chi_1} = 800$ GeV, $M_{L_2} = 190$ GeV and $M_{\chi_0} = 120$ GeV. In the μ -sector, i.e., for plot (a) the e and μ -specific couplings are fixed at those values which are mentioned in the text. In the τ -sector, we choose for the plot (b) $Y_{4\tau} = Y_{3\tau} = 0$, (c) $Y_{1\tau} = Y_{3\tau} = 0$, (d) $Y_{1\tau} = 0$ & $Y_{4\tau} = 0.01$, (e) $Y_{4\tau} = 0.01$ & $Y_{3\tau} = 0$, (f) $Y_{1\tau} = Y_{3\tau} = 0$ and (g) $Y_{1\tau} = 0$ & $Y_{4\tau} = 0.01$. In the plots (a), (d), (e), (f) the projected future bounds corresponding to $\text{Br}(\ell_\alpha \rightarrow \ell_\beta \gamma)$ and $\text{Br}(\ell_\alpha \rightarrow 3\ell_\beta)$ have been marked with the black and magenta horizontal lines respectively.

respective cLFV processes as indicated by the color code. Moreover, to have an idea of the future prospects of our results, in the plots (a), (d), (e), (f) [of Figs. 9 and 10], the projected future bounds corresponding to

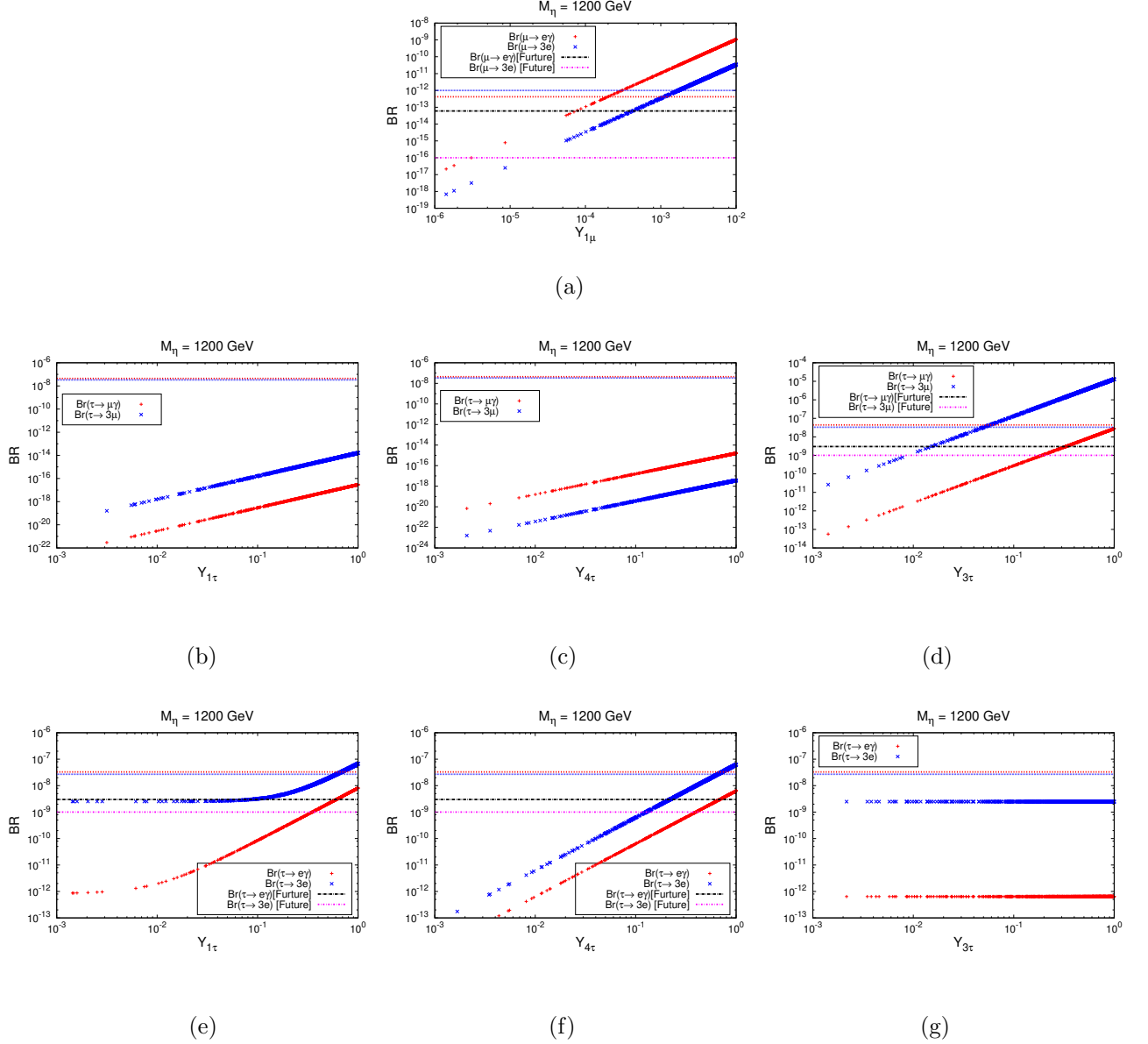


FIG. 10. Variation of $\text{Br}(\ell_\alpha \rightarrow \ell_\beta \gamma)$ (Red) and $\text{Br}(\ell_\alpha \rightarrow 3\ell_\beta)$ (Blue) as a function of $Y_{i\ell}$ [$i = 1, 3, 4$]. Input parameters are set as $M_\eta = 1200$ GeV, $M_S = 130$ GeV, $M_{\chi_1} = 800$ GeV, $M_{L_2} = 190$ GeV and $M_{\chi_0} = 120$ GeV. In the μ -sector, i.e., for plot (a) the e and μ -specific couplings are fixed at those values which are mentioned in the text. In the τ -sector, we chose for the plot (b) $Y_{4\tau} = Y_{3\tau} = 0$, (c) $Y_{1\tau} = Y_{3\tau} = 0$, (d) $Y_{1\tau} = 0$ & $Y_{4\tau} = 0.01$, (e) $Y_{4\tau} = 0.01$ & $Y_{3\tau} = 0$, (f) $Y_{1\tau} = Y_{3\tau} = 0$ and (g) $Y_{1\tau} = 0$ & $Y_{4\tau} = 0.01$. In the plots (a), (d), (e), (f) the projected future bounds corresponding to $\text{Br}(\ell_\alpha \rightarrow \ell_\beta \gamma)$ and $\text{Br}(\ell_\alpha \rightarrow 3\ell_\beta)$ have been marked with the black and magenta horizontal lines respectively.

$\text{Br}(\ell_\alpha \rightarrow \ell_\beta \gamma)$ and $\text{Br}(\ell_\alpha \rightarrow 3\ell_\beta)$ have been marked with the black and magenta horizontal lines respectively.

For the numerical set-up we have fixed,

- Scalar masses: $M_\eta = 300$ GeV and 1200 GeV, $M_S = 130$ GeV. Here, Fig. 9 considers $M_\eta = 300$ GeV and Fig. 10 assumes $M_\eta = 1200$ GeV.
- Vector lepton masses and mixings: $M_{\chi_1} = 800$ GeV, $M_{L_2} = 190$ GeV, $M_{\chi_0} = 120$ GeV, and $\sin \theta = 0.01$.
- μ -specific flavor dependent couplings: $Y_{4\mu} = 0.0$ and $Y_{3\mu} = 2.3$.
- e -specific flavor dependent couplings: $Y_{1e} = 0.2$, $Y_{4e} = 0.2$ and $Y_{3e} = 0.0$.

So, at this point, we are left with only four flavor specific free parameters, i.e., $Y_{1\mu}, Y_{1\tau}, Y_{3\tau}$ and $Y_{4\tau}$. Our aim would be to constrain these free couplings using the present and future limits of the cLFV branching ratios for $\ell_\alpha \rightarrow \ell_\beta \gamma$ and $\ell_\alpha \rightarrow 3\ell_\beta$ processes (where $\alpha, \beta = e, \mu, \tau$). Thus, we have varied the free couplings randomly, and calculated the corresponding values for $\text{Br}(\ell_\alpha \rightarrow \ell_\beta \gamma)$ and $\text{Br}(\ell_\alpha \rightarrow 3\ell_\beta)$. Focusing on a particular flavor at a time, in the following, we present the possible 2-body and 3-body decays.

- $\text{Br}(\mu \rightarrow e\gamma)$ and $\text{Br}(\mu \rightarrow 3e)$: The first rows of the Figs. 9 and 10 depict the variation of $\mu \rightarrow e$ branching fractions. Here the relevant couplings can be read as $Y_{(1,3,4)i} \sim (i = e, \mu)$. However, only $Y_{1\mu}$ can be regarded as the free parameter since all the other couplings have already been fixed by the precision measurements of μ and e anomalous magnetic moments. As can be evident from the plot, for $Y_{1\mu} \leq 10^{-4}$ both the $\text{Br}(\mu \rightarrow e\gamma)$ and $\text{Br}(\mu \rightarrow 3e)$ can be made satisfied. This explains our choice for $Y_{1\mu}$ in the earlier $(g-2)_\mu$ analysis. Thus, to have a simultaneous validation of the $(g-2)_\mu$ and cLFV constraints (i.e. $\text{Br}(\mu \rightarrow e\gamma)$ and $\text{Br}(\mu \rightarrow 3e)$) one certainly needs a much smaller value of $Y_{1\mu}$ ($\sim 10^{-4}$).
- $\text{Br}(\tau \rightarrow \mu\gamma)$ and $\text{Br}(\tau \rightarrow 3\mu)$: The second rows of Figs. 9 and 10 correspond to these processes. All the μ specific couplings are already fixed: $Y_{3\mu}$ and $Y_{4\mu}$ have been set to their earlier values and $Y_{1\mu} = 10^{-4}$ is considered (in accordance with Figs. 9(a) and 10(a)). Thus we have varied the τ specific free parameters $Y_{j\tau}$ ($j = 1, 4, 3$) and calculated the branching ratios. The allowed ranges of these couplings where $\text{Br}(\tau \rightarrow \mu\gamma)$ and $\text{Br}(\tau \rightarrow 3\mu)$ are satisfied, can be seen from Figs. 9 (b), (c), (d) and 10 (b), (c), (d) respectively. Clearly, only meaningful constraint can be derived for $Y_{3\tau}$ which reads as $Y_{3\tau} \leq 0.04$. The bound can be placed using $\text{Br}(\tau \rightarrow 3\mu)$ which seems to be much stringent compared to $\text{Br}(\tau \rightarrow \mu\gamma)$. This is a result of the Z -penguin dominance in that region of the parameter space.

To illustrate it further, we focus on the dominant parts of γ penguin contributions. In case of photon initiated 2-body $\text{Br}(\ell_\alpha \rightarrow \ell_\beta \gamma)$, or 3-body $\text{Br}(\ell_\alpha \rightarrow 3\ell_\beta)$ decays, dipole terms become more important, and specially the most significant parts read as:

$$A_2^{(n)} \supset \sin \theta \cos \theta \left[Y_{1\beta}^\dagger Y_{4\alpha}^\dagger \left\{ \frac{2M_{\chi_1}}{m_{\ell_\alpha}} F_1 \left(\frac{M_{\chi_1}^2}{M_\eta^2} \right) - \frac{2M_{\chi_0}}{m_{\ell_\alpha}} F_1 \left(\frac{M_{\chi_0}^2}{M_\eta^2} \right) \right\} \right. \\ \left. + Y_{4\beta} Y_{1\alpha} \left\{ \frac{2M_{\chi_1}}{m_{\ell_\alpha}} F_1 \left(\frac{M_{\chi_1}^2}{M_\eta^2} \right) - \frac{2M_{\chi_0}}{m_{\ell_\alpha}} F_1 \left(\frac{M_{\chi_0}^2}{M_\eta^2} \right) \right\} \right]. \quad (63)$$

The other terms related to dipole or monopole terms are proportional to the products of the other flavor specific couplings $Y_{1\beta}Y_{1\alpha}, Y_{4\beta}Y_{4\alpha}, Y_{3\beta}Y_{3\alpha}$. However, generically, considering the couplings for any α, β are of the same size, these terms are few orders of magnitude smaller compared to $A_2^{(n)}$. For $\tau - \mu$ cLFV processes, $A_2^{(n)} \propto \sin \theta \cos \theta (Y_{1\mu}Y_{4\tau} + Y_{1\tau}Y_{4\mu})$, thus extremely suppressed, unless $Y_{4\tau}$ is reasonably large. This suppression can be attributed to the tinyness of $\sin \theta$ and our choice of Yukawa couplings. In fact $A_2^{(n)}$ may become large if $Y_{4\tau}$ is reasonably large or moderate. This can be verified from Figs. 9 (c) and 10 (c) where due to the choice of $Y_{1\tau} = Y_{3\tau} = 0$, the 2-body process dominates over the entire range of $Y_{4\tau}$. Similarly, based on the relative choice of Yukawa couplings the Z -penguin diagrams may become more important or comparable to the γ initiated ones in some cases. For illustration, we choose a particular set of τ -specific couplings as mentioned in the captions of Figs. 9 and 10. For example, in Figs. 9 (b), (d) and 10 (b), (d), $Y_{4\tau} = 0, 0.01$ have been chosen respectively, thus, γ penguin is always suppressed which results in the dominance of $\text{Br}(\tau \rightarrow 3\mu)$ over $\text{Br}(\tau \rightarrow \mu\gamma)$. We may note here that, in the $\mu - e$ processes, the choice of parameters (particularly $Y_{4\mu} = Y_{3e} = 0$ and $Y_{1\mu} = 10^{-4}$) makes the 3-body BR always suppressed in comparison to that of 2-body (see the first row of the Figs. 9 and 10).

- $\text{Br}(\tau \rightarrow e\gamma)$ and $\text{Br}(\tau \rightarrow 3e)$: Third rows of Figs. 9 and 10 show the plots for these two processes. Here the only free parameters are $Y_{j\tau}$ ($j = 1, 4, 3$), as the electronic couplings are fixed by the $(g-2)_e$ results. Indeed, the τ specific parameters are same as in the $\tau \rightarrow \mu$ analysis. The ranges of $Y_{j\tau}$ couplings where $\text{Br}(\tau \rightarrow e\gamma)$ and $\text{Br}(\tau \rightarrow 3e)$ can be simultaneously satisfied, have been shown in Figs. 9 (e), (f) and (g) and 10 (e), (f) and (g) respectively. We may observe that Z -penguin diagrams become dominant over photon penguins in Figs. 9, 10 (f) since $Y_{4\tau}Y_{4e}$ can now contribute significantly. From these plots (Figs. 9 (e), (f) and 10 (e), (f)), we are able to constrain the two τ -specific couplings as: $Y_{1\tau} \leq 0.5$ and $Y_{4\tau} \leq 0.7$. Note that, the variation of BRs with respect to $Y_{3\tau}$ has been appearing as two horizontal lines, implying that the BRs are apparently independent of this coupling. This result is a sole outcome of the choice $Y_{3e} = 0$. Since in both $\text{Br}(\tau \rightarrow e\gamma)$ and

$\text{Br}(\tau \rightarrow 3e)$, the coupling structure appears as $Y_{3e}Y_{3\tau}$, putting $Y_{3e} = 0$ automatically ensures the invariance of the BRs with respect to $Y_{3\tau}$.

So finally, collecting all the constraints, i.e., from the anomalous magnetic moment data and non observation of the cLFV processes, we find that all the flavor specific couplings $Y_{1,3,4}$ may assume $\sim \mathcal{O}(1 - 10^{-4})$ values, some of which may be tested in the near future.

C. Z and h observables

- 1) Invisible decays $Z, h \rightarrow \chi_0\chi_0$: In this model, a light DM is natural and the parameter space associated with it can be observed to be consistent with the all low energy data. It is well known that for a light DM, invisible decays of Z and h which lead to $Z, h \rightarrow \chi_0\chi_0$ can be substantial to constrain the parameter space. The corresponding decay widths are given by,

$$\begin{aligned}\Gamma(Z \rightarrow \chi_0\chi_0) &= \frac{1}{48\pi} M_Z \left(\frac{g^2 \sin^4 \theta}{\cos^2 \theta_W} \right) \left(1 + \frac{2M_{\chi_0}^2}{M_Z^2} \right) \left(1 - \frac{4M_{\chi_0}^2}{M_Z^2} \right)^{1/2}, \\ \Gamma(h \rightarrow \chi_0\chi_0) &= \frac{(Y_5 \sin 2\theta)^2}{16\pi} m_h \left(1 - \frac{4M_{\chi_0}^2}{m_h^2} \right)^{3/2},\end{aligned}\tag{64}$$

where, $Y_5 = -\frac{(M_{\chi_1} - M_{\chi_0})}{v\sqrt{2}} \sin 2\theta$, with M_{χ_1} fixed at 800 GeV. We also plot the valid regions in $\sin \theta - M_{\chi_0}$ plane. For depicting our results, we use (i) the observed invisible partial width of Z boson, $\Gamma_Z^{inv} = 499 \pm 1.5$ MeV which is below the SM prediction $\Gamma_{SM}^{inv} = 501.44 \pm 0.04$ MeV at 1.5σ C.L. [143] and (ii) the experimental bound on invisible h decay reads as $\text{Br}^{inv} < 0.26$ [144]. Note also that, $\Gamma_h^{\text{SM}} = 4.07$ MeV, has been taken [143].

Clearly, a more stringent bound on the model parameters comes from the invisible h decay, compared to that of the Z decay, but for $\sin \theta \simeq 0.01$ the entire parameter space is allowed.

- 2) $Z \rightarrow \ell_i^\pm \ell_i^\mp, \ell_i^\pm \ell_j^\mp$: The new fermions $f = \chi_0, \chi_1, L_1, L_2$ and the scalars $s = \eta, S$ can lead to $Z \rightarrow \ell_i \ell_j$ decays. Rare charged lepton flavour violating (cLFV) Z decays also inherit a possible complementarity test with low-energy cLFV searches. The current LHC limits put stringent bounds compared to the old limits obtained by the LEP experiments on the three flavor violating decay modes of Z boson. Similarly, future sensitivity can be estimated from [145] which considers the future e^+e^- colliders CEPC/FCC-ee [146, 147] experiments assuming 3×10^{12} visible Z decays. The present limits and the future bounds can be read as,

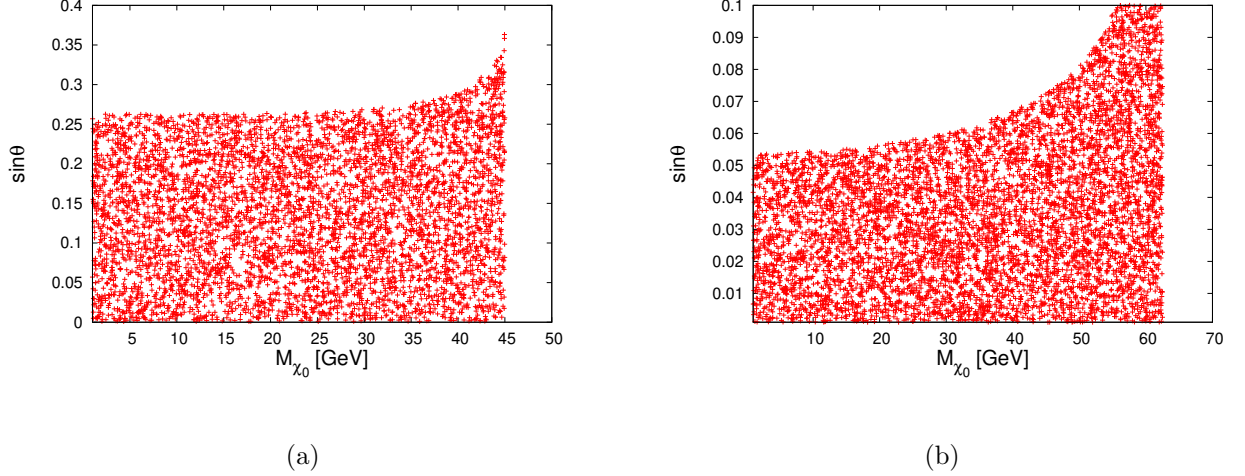


FIG. 11. (a) The allowed values of $\sin \theta$ for different DM masses ($\leq M_Z/2 \simeq 45$ GeV) from the invisible Z decay constraints and (b) from the invisible h ($\leq M_h/2 \simeq 62$ GeV) decay constraints.

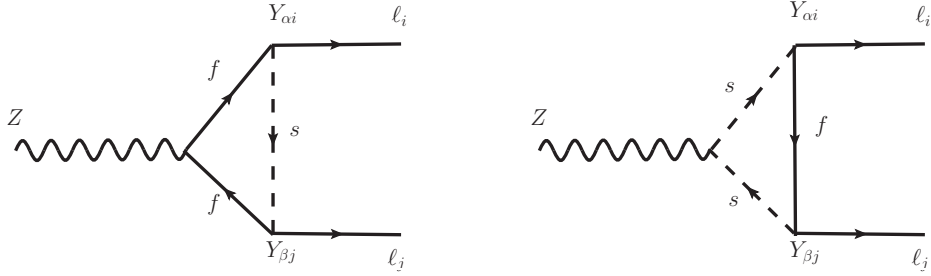


FIG. 12. Representative diagram for $Z \rightarrow \ell_i \ell_j$ processes. Here $f = \chi_0, \chi_1, L_1, L_2$ and $s \in \eta, S$. The indices stand for $i, j = e, \mu, \tau$ and $\alpha, \beta = 1, 3, 4$ (see Eq. (14)).

- a) $\text{Br}(Z \rightarrow e^\pm \mu^\mp) \leq 7.5 \times 10^{-7}$ [148] ; $10^{-8} - 10^{-10}$ [145]
- b) $\text{Br}(Z \rightarrow e^\pm \tau^\mp) \leq 5 \times 10^{-6}$ [149, 150] ; 10^{-9} [145]
- c) $\text{Br}(Z \rightarrow \mu^\pm \tau^\mp) \leq 6.5 \times 10^{-6}$ [149, 150] ; 10^{-9} [145]

The branching ratio can be expressed as [151, 152],

$$\text{Br}(Z \rightarrow \ell_i^\pm \ell_j^\mp) = \frac{\alpha}{3 \sin^2 2\theta_W} \left(\frac{M_Z}{\Gamma_Z} \right) (|F_L|^2 + |F_R|^2), \quad (65)$$

where, $\sin 2\theta_W = 2 \sin \theta_W \cos \theta_W$, F_L and F_R are defined via Eqs. (54)–(56) and (89). Here, considering the on-shell decay of Z , M_Z dependence has been incorporated in the definitions of F_L and F_R . The form factors F_L and F_R control the loop induced couplings for $Z \ell_i^\pm \ell_j^\mp$; its numerical values ($|F_L| = |F_R| \sim 10^{-5}$) can be found to be orders of magnitudes suppressed compared to the tree level

couplings, specially in the parameter space where cLFV constraints are satisfied. The total width Γ_Z includes the contributions from all the new BSM modes in addition to the contributions from SM. For numerical evaluations of the branching fractions, we consider the parts of the parameter space where all $(g-2)_\ell$, cLFV, and DM abundance are simultaneously satisfied. Thus we fix $M_\eta = 300$ GeV, $M_S = 130$ GeV, $M_{\chi_1} = 800$ GeV, $M_{\chi_0} = 120$ GeV and $M_{L_2} = 190$ GeV, as chosen in the previous sections. All the Yukawa couplings are fixed at values, as given in following Table VI which will subsequently be helpful to obtain a correct relic density for the DM. Substituting these values

| Y_{1e} | Y_{3e} | Y_{4e} | $Y_{1\mu}$ | $Y_{3\mu}$ | $Y_{4\mu}$ | $Y_{1\tau}$ | $Y_{3\tau}$ | $Y_{4\tau}$ |
|----------|----------|----------|------------|------------|------------|-------------|-------------|-------------|
| 0.2 | 0.0 | 0.2 | 10^{-4} | 2.3 | 0.0 | 0.0 | 0.01 | 0.6 |

TABLE VI. Values of the Yukawa couplings for the evaluation of $Z \rightarrow \ell_i \ell_j$.

in Eq. (65), we get the following branching ratios:

- $\text{Br}(Z \rightarrow e^\pm \mu^\mp) = 4.16 \times 10^{-16}$
- $\text{Br}(Z \rightarrow e^\pm \tau^\mp) = 7.48 \times 10^{-10}$
- $\text{Br}(Z \rightarrow \mu^\pm \tau^\mp) = 5.67 \times 10^{-11}$.

The first branching fraction is much suppressed due to the choice of the Yukawa couplings. Thus, the chances of observing the LFV decays of Z bosons even in the future are not quite attractive. Similarly, we have observed that BSM loop contributions to $\text{Br}(Z \rightarrow \ell^\pm \ell^\mp)$ ($\ell \in e, \mu, \tau$), arising in our framework are lying below the present limits [143].

3) $h \rightarrow \ell^\pm \ell^\mp$: The radiative corrections to Yukawa couplings of SM leptons (y_ℓ) can also be generated

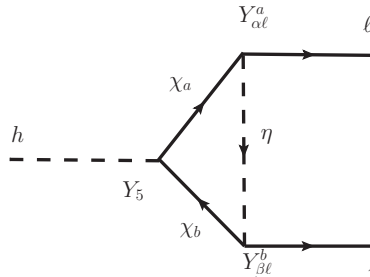


FIG. 13. Representative diagram for $h \rightarrow \ell \ell$ processes. Here $a, b = 0, 1$ and α, β stand for the flavor specific new couplings = 1, 4 (see Eq. (14)). Leg corrections are also considered (not shown).

through the new neutral fermions χ_0, χ_1 in the loop (see Fig. 13). The new physics contributions at

one loop can be calculated as,

$$\tilde{Y}_\ell^h \equiv \frac{Y_5}{16\pi^2} \sum_{a,b=0,1} \left[Y_{\alpha\ell}^a Y_{\beta\ell}^b \left\{ M_\eta^2 C_0(0, 0, m_h^2, M_{\chi_a}^2, M_\eta^2, M_{\chi_b}^2) + B_0(m_h^2, M_{\chi_a}^2, M_{\chi_b}^2) \right. \right. \\ \left. \left. + M_{\chi_a} M_{\chi_b} C_0(0, 0, m_h^2, M_{\chi_a}^2, M_\eta^2, M_{\chi_b}^2) \right\} - (Y_{\alpha\ell}^a)^2 B_0(0, M_{\chi_a}^2, M_\eta^2) \right], \quad (66)$$

where, in terms of our definitions of Yukawa couplings, we define $Y_{\alpha\ell}^0 = Y_{4\ell}$ and $Y_{\alpha\ell}^1 = Y_{1\ell}$ for $\ell \in e, \mu, \tau$. Similarly, Y_5 has been recast via Eq. (13) with $\sin \theta = 0.01$. The corresponding decay width is [143],

$$\Gamma(h \rightarrow \ell\ell) = \frac{1}{8\pi m_h^2} |Y_{\text{eff}}^h|^2 (m_h^2 - 4m_\ell^2)^{3/2}, \quad (67)$$

where, $Y_{\text{eff}}^h = Y_\ell^{SM} + \tilde{Y}_\ell^h$. Now, for the same masses and Yukawa couplings as discussed for the flavor violating Z decays (also see Table VI), $\Gamma(h \rightarrow ee/\mu\mu)$ has been found to be practically unchanged to the corresponding SM value.

- 4) Contribution to $W^\pm \ell^\mp \nu_\ell$ vertex: The one-loop correction to $W \rightarrow \ell \nu_\ell$ process as shown in Fig. 14,

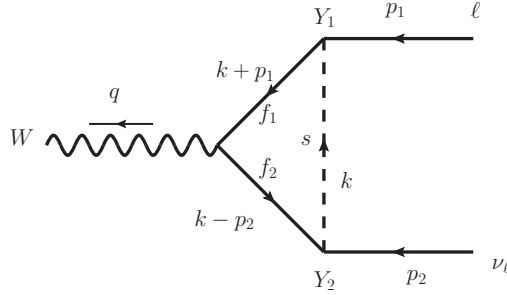


FIG. 14. Representative diagram for one-loop correction to the $W \rightarrow \ell \nu_\ell$ vertex.

results in,

$$\tilde{V}^{l\nu} = \frac{Y_1 Y_2 g}{16\sqrt{2}\pi^2} m_\ell \left[M_{f_2} C_0(0, 0, M_W^2, M_s^2, M_{f_1}^2, M_{f_2}^2) + \right. \\ \left. \frac{(M_{f_2} + M_{f_1})}{M_W^2} \left\{ (M_S^2 - M_{f_2}^2) C_0(0, 0, M_W^2, M_s^2, M_{f_1}^2, M_{f_2}^2) + B_0(M_W^2, M_{f_2}^2, M_{f_1}^2) - B_0(0, M_{f_1}^2, M_S^2) \right\} \right], \quad (68)$$

where, C_0, B_0 are the standard PV integrals. M_{f_1} and M_{f_2} correspond to the masses of VL leptons f_1 and f_2 respectively, while m_ℓ stands for the mass of SM lepton. We are assuming the neutrinos to be massless.

Clearly, $\tilde{V}^{l\nu}$ will include the desired corrections at one loop to $W^\pm \ell^\mp \nu_\ell$ vertex due to presence of the BSM states. However, we find the total contribution to be much suppressed. For having an estimate about the most significant part in it, we consider $f_1 = L_2^\pm$, $f_2 = L_2^0$, $\ell = \mu$ and $s = S$. In this case, the general couplings in Eq. (68) can be read as, $Y_1 = Y_2 = Y_{3\mu}$. We set the masses and couplings in accordance with our previous discussion i.e., $M_{L_2} = 190$ GeV, $M_S = 130$ GeV and $Y_{3\mu} = 2.3$. With these choice of parameters, one can directly get, $\tilde{V}^{l\nu} \sim 10^{-6}$, thus smaller than its tree level values.

As evident from the discussion, in our model, gauge boson-leptonic vertex does not receive any meaningful contribution at all. In fact, both $Z\ell^\pm\ell^\mp$ and $W^\pm\ell^\mp\nu_\ell$ can be considered at their SM values, thus, processes involving leptonic or semileptonic decays of mesons, e.g., $K_L \rightarrow \mu\mu$, $K_L \rightarrow \pi\nu\nu$, or $B_s \rightarrow \mu\mu$, or precisely measured CKM elements can be completely determined by the SM physics.

VI. DARK MATTER PHENOMENOLOGY

This model may offer a singlet-doublet dark matter; phenomenology of such scenarios have been studied in detail [42–50]. Here we would simply check that if all the couplings which are already constrained by the different precision and collider bounds, can provide us with an acceptable DM relic density, consistent with SI DM-nucleon elastic cross section bounds. After EWSB, χ_0 — a dominantly singlet-like state, odd under $\mathcal{Z}_2 \times \mathcal{Z}'_2$ symmetry can be considered to be the lightest particle — thus a valid DM candidate while the other neutral state χ_1 carries a strong doublet-like nature for a small mixing angle θ . In general, the singlet-doublet mixing parameter θ is completely controlled by the SI direct detection bounds (much stronger than the EWPO constraints); usually, only a very tiny θ is allowed. We have fixed all other BSM particles (L_1^\pm , $L_2^{\pm,0}$, η , S) at a heavier mass scale, discussed as in our previous exercises. Since a small M_{χ_0} is preferred from cLFV and Δa_ℓ , we may focus on the parameter space with a light DM.

The relic abundance of DM in the universe as obtained from the PLANCK data is $\Omega_{DM}h^2 = 0.1198 \pm 0.0012$ [153]. The singlet-like fermionic DM χ_0 , being the lightest odd particle and stable under the imposed $\mathcal{Z}_2 \times \mathcal{Z}'_2$ symmetry, was in thermal equilibrium in the early universe through its interaction with the SM particles. But at a point of time (or temperature: $T \leq T_{freezeout}$) it gets decoupled from the thermal bath when the interaction rate fell shorter than the expansion rate of the universe. The relic density of the DM can be obtained by solving the Boltzmann equation, given by,

$$\frac{dn}{dt} + 3\mathcal{H}n = -\langle\sigma_{eff}v\rangle(n^2 - n_{eq}^2) \quad (69)$$

where \mathcal{H} is the Hubble constant, $\langle\sigma_{eff} v\rangle$ is the thermal averaged cross section of the DM annihilating to the SM particles and n signifies the number of interacting particles, with the subscript ‘eq’ designating its equilibrium value. Though, for doing the numerical analysis we have used micrOMEGAs [154, 155]. After implementing the model parameters in LanHEP [156], the output files have been used as the input for micrOMEGAs, to solve the Boltzmann equation numerically and for calculating the relic density. Here, the mass parameters have been fixed at the same values as was done in Sec. V, with M_η assuming the lower value, i.e. 300 GeV. For the flavor dependent Yukawa couplings, which are restricted by the cLFV and $(g-2)_\ell$ bounds, we choose them at the representative values, shown in Table VI. We also note here that though the choices for $Y_{4\tau}$ or $Y_{3\tau}$ are somewhat different than the values in Fig. 9 and in Fig. 10, we have checked that the cLFV constraints are completely unaffected.

The other meaningful coupling for DM phenomenology is Y_{6i} ($=Y_{6(1i)}$, as in Eq. (14)) — the interaction between DM, singlet scalar S and the right handed neutrinos ν_{Ri} . The same coupling controls the calculation of neutrino masses [see Sec. IV]. Here we set Y_6 without affecting the neutrino masses and mixings, e.g., $Y_{6\tau} = 0.13$ is taken.

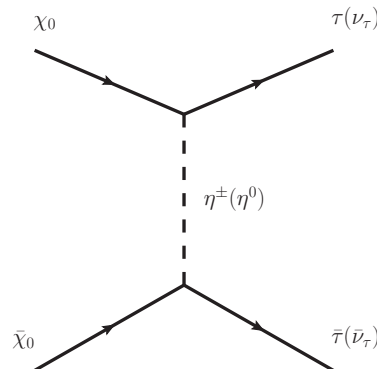


FIG. 15. The most dominant annihilation channels contributing to the relic density. This is particularly true when the other input parameters are fixed at the values shown in Table VI.

In this model, there may be a number of annihilation channels which can contribute to the relic density calculation. The order of dominance of these channels changes with the choice of the other input parameters. Here, Fig. 15 shows the most dominant annihilation channel for the chosen parameter space. We have listed the annihilation channels at $M_{\chi_0} = 120$ GeV in Table VII.

| Parameters | $M_{\chi_0} = 120 \text{ GeV}$ |
|---|--|
| $M_{\chi_1} = 800 \text{ GeV}$ | $\chi_0 \bar{\chi}_0 \rightarrow \tau \bar{\tau} \text{ (49\%)}$ |
| $M_\eta = 300 \text{ GeV}$ | $\chi_0 \bar{\chi}_0 \rightarrow \nu_\tau \bar{\nu}_\tau \text{ (49\%)}$ |
| $M_S = 130 \text{ GeV}$ | $\chi_0 \bar{\chi}_0 \rightarrow \nu_R \nu_R \text{ (2\%)}$ |
| $M_{L_2} = 190 \text{ GeV}$ $\sin \theta = 0.01$ | |
| $\Omega_{\chi_0} h^2 \Rightarrow$ | 0.103 |

TABLE VII. Dominant ($\geq 1\%$) annihilation channels relevant in determining the relic density at $M_{\chi_0} = 120 \text{ GeV}$.

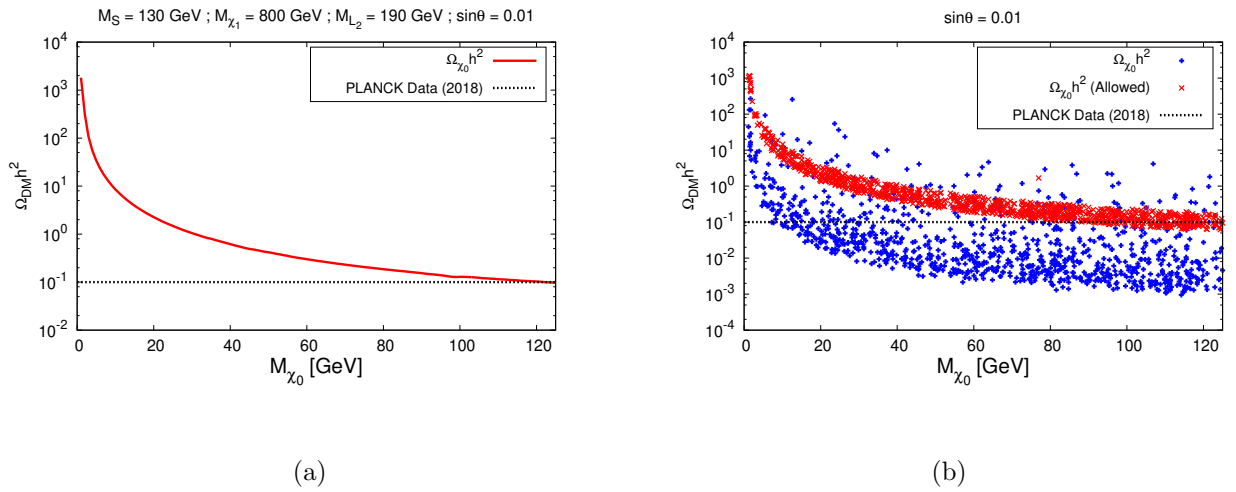


FIG. 16. (a) Variation of Relic density as a function of DM mass M_{χ_0} , when $M_\eta = 300 \text{ GeV}$. (b) Allowed parameter space projected over the relic density plane.

Fig. 16 (a) depicts the variation of relic density with respect to M_{χ_0} for $\sin \theta = 0.01$. The horizontal straight line at $\Omega h^2 \sim 0.12$ is the central value for the acceptable DM relic abundance, while the red line signifies the calculated relic density in this model as one varies M_{χ_0} in the range of $[1 - 125] \text{ GeV}$. Fig. 16 (b) represents the allowed parameter space projected over the relic density plane. Here, the blue dotted region corresponds to the complete parameter space which has been obtained by varying all the parameters randomly, while the red patch stands for the region which is simultaneously allowed from the $(g-2)_\ell$, cLFV, EWPO and neutrino mass constraints. The parameters have been varied within the range of $M_{\chi_0} \rightarrow [1 : 125]$, $M_{\chi_1} \rightarrow [700 : 2000]$, $Y_{1\mu} \rightarrow [10^{-6} : 10^{-1}]$, $Y_{1\tau} \rightarrow [10^{-3} : 2]$, $Y_{4\tau} \rightarrow [10^{-3} : 2]$, $Y_{6i} \rightarrow [0.01 : 1]$, $Y_{1e} \rightarrow [0.01 : 5]$, $Y_{4e} \rightarrow [0.01 : 5]$, $Y_{4\tau} \rightarrow [0 : 1]$.

In our model $\chi_0 - \text{nucleon}$ SI scattering processes, mediated by the Higgs and Z bosons are shown in

Fig. 17. The SI scattering cross sections per nucleon corresponding to the Z -mediated diagram of Fig. 17

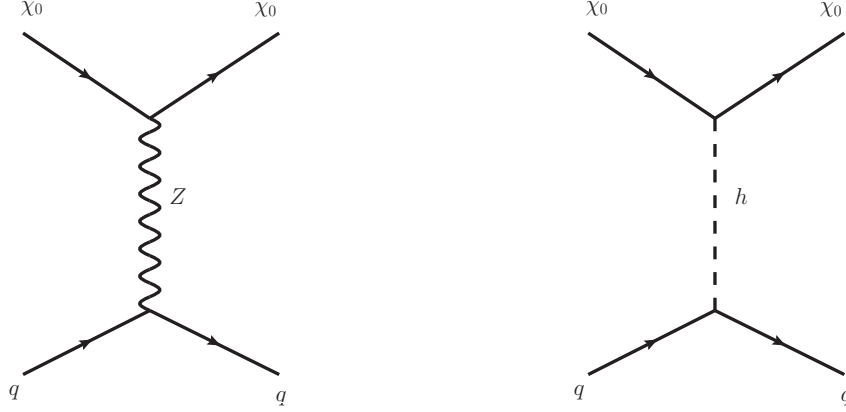


FIG. 17. Feynman diagrams contributing to the SI direct detection cross section.

is given by [157–159],

$$\sigma_Z^{SI} = \frac{G_F^2 \mu_r^2}{2\pi A^2} \left[(1 - 4 \sin^2 \theta_W) Z - (A - Z) \right]^2 \sin^4 \theta, \quad (70)$$

where, ‘ A ’ and ‘ Z ’ represent the mass number and atomic number of the target nucleus respectively, G_F is the Fermi’s constant, $\mu_r = \left(\frac{M_{\chi_0} m_N}{M_{\chi_0} + m_N} \right) \approx m_N$ defines the reduced mass, m_N being the mass of nucleon (proton or neutron). The second contribution in direct detection comes from the h -mediated diagram and the corresponding SI cross section per nucleon is given as,

$$\sigma_h^{SI} = \frac{\mu_r^2}{\pi A^2} \left[Z f_p + (A - Z) f_n \right]^2, \quad (71)$$

where the DM-nucleon effective interaction strength can be parameterized as,

$$f_N = \sum_{q=u,d,s} f_{Tq}^{(N)} \alpha_q \frac{m_N}{m_q} + \frac{2}{27} f_{TG}^{(N)} \sum_{q=c,t,b} \alpha_q \frac{m_N}{m_q}. \quad (72)$$

Where $N = n, p$ and $\alpha_q = \frac{Y_5 \sin 2\theta}{\sqrt{2} m_h^2} \left(\frac{m_q}{v} \right) = -\frac{(M_{\chi_1} - M_{\chi_0}) \sin^2 2\theta}{2v m_h^2} \left(\frac{m_q}{v} \right)$. $f_{Tq}^{(N)}$ is the nuclear matrix element as determined in the chiral perturbation theory from the pion-nucleon scattering sigma term, and the gluonic part $f_{TG}^{(N)}$ is given by,

$$f_{TG}^{(N)} = 1 - \sum_{q=u,d,s} f_{Tq}^{(N)}. \quad (73)$$

Thus for a fixed M_{χ_1} , the above equation becomes only a function of M_{χ_0} (DM mass) and the mixing angle θ . Here we note that, Higgs contribution to SI scattering can be completely evaded if one considers the

light-quark Yukawa couplings to assume non-Standard Model (non-SM)-like values [160]⁴. For generating the numerical results we have used the code “micrOMEGAs”, as was done for studying the relic density, and analysed the variation of SI scattering cross section as a function of DM mass for $\sin\theta = 0.01$. In

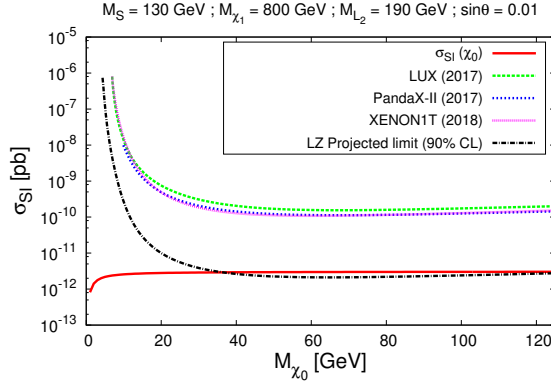


FIG. 18. Variation of SI scattering cross section as a function of DM mass M_{χ_0} when $M_\eta = 300$ GeV.

Fig. 18 the variation of SI cross section with respect to M_{χ_0} is shown by the red line. All the other mass and coupling parameters are fixed at the same values as was done for the relic density analysis [see Table VI]. Mostly, for the entire parameter space, the σ_{SI} becomes effectively independent of the DM mass, since the Z -mediated scattering process (shown in Fig. 17) appears as the dominant contributor to the total SI cross section over this mass regime. From the observational side we have mainly considered the LUX [52], PandaX-II [162] and XENON 1T [51] limits, which show that the calculated SI cross section, proportional to $\sin^4\theta$, lies much below the present bounds for the entire mass range. However, the future projected limit coming from LZ collaboration [163] may probe only a parts of the parameter space [see Fig. 18]. Further, due to Z -mediation there is a small amount of SD cross section as well, but it is observed to be far below the existing limits. Moreover, note that, the direct detection cross section has no dependence on the Y_{1i} , Y_{3i} and Y_{4i} couplings, which directly govern the $(g-2)_\ell$ and cLFV phenomenology. Therefore, under the variation of different Yukawa couplings (as was done in Fig. 16 (b)), the σ_{SI} remains mostly unchanged.

VII. CONCLUSION

In this paper, we have studied a simple extension where SM is augmented with a pair of vector like lepton doublets L_1 and L_2 , a $SU(2)$ doublet scalar η in particular. Similarly, singlet-like states including a scalar S and a singlet fermion ψ are also considered for specific purposes. An additional $\mathcal{Z}_2 \times \mathcal{Z}'_2$

⁴ See Ref. [161] for radiative generation of such non-SM-like Yukawa couplings.

symmetry has been imposed under which all the SM fields are even while the new fields may be odd under the transformation. Adopting a bottom-up approach, in this paper, we systematically scrutinize the parameter space in terms of the allowed couplings and masses to obtain: (i) the Dirac masses for the SM neutrinos and mixings through a radiative mechanism, (ii) electron and muon $(g-2)$ discrepancy simultaneously while considering the cLFV and EWPO constraints and finally (iii) a viable DM candidate, consistent with direct detection observations so far.

We start with our proposed model where the new interactions have been introduced. Subsequently we discuss about the relevant constraints on the new parameters by reviewing the different experimental constraints related to the lepton $(g-2)$ observations, cLFV bounds, vacuum stability conditions, electroweak precision constraints and collider observables. In our model, L_1 and ψ may mix to produce the physical states, and the lightest state χ_0 can be regarded as the dark matter. Electroweak precision parameters and, more importantly, the null results from the dark matter direct detection experiments require a small mixing between L_1 and ψ ; thus we choose $\sin \theta = 0.01$.

We have shown that in the absence of a tree-level neutrino mass (being forbidden due to the imposed symmetry), one can generate the correct neutrino mass matrix at one-loop level if the \mathcal{Z}'_2 is allowed to break softly. The masses and mixings may be controlled by two free parameters $Y_{2(1i)}$ and $Y_{6(1i)}$ which do not have any effect on the charged lepton flavor processes, e.g., $(g-2)_{\mu/e}$ or different cLFV processes like $\ell_\alpha \rightarrow \ell_\beta \gamma$ and $\ell_\alpha \rightarrow 3\ell_\beta$. We have performed a comprehensive study to show the interplay between different charged and neutral vector like leptons for satisfying $(g-2)_e$ and $(g-2)_\mu$ bounds simultaneously. A moderately large coupling $Y_{3\mu}$ is required to tune $(g-2)_\mu$ while Δa_e can easily be controlled with other $\mathcal{O}(1)$ couplings. Further, the same diagrams are able to generate $\ell_\alpha \rightarrow \ell_\beta \gamma$ processes when $\alpha \neq \beta$. For the 3-body processes like $\ell_\alpha \rightarrow 3\ell_\beta$, we have considered all the Z and photon penguin diagrams along with the box contributions. Numerically, we have calculated $\text{Br}(\ell_\alpha \rightarrow \ell_\beta \gamma)$ and $\text{Br}(\ell_\alpha \rightarrow 3\ell_\beta)$ for different lepton generations and shown their variations as functions of the relevant couplings for two sets of doublet scalar masses ($M_\eta \sim 300$ GeV and 1200 GeV), along with their respective experimental bounds. These cLFV constraints, in addition to the lepton $(g-2)$ results set an important exclusion limit or upper bound for the different Yukawa couplings present in this model. Here, we note that, larger mass value of η is not at all disfavoured in the context of tuning the charged lepton flavor conserving or violating processes. However, the vector like leptons, especially L_2 has to be light (≤ 200 GeV), otherwise, the relevant coupling $Y_{3\mu}$ may have to be raised to accommodate $(g-2)_\mu$. Moreover, in the parts of the parameter space, Z -dominance over the γ -penguin in the computation of the 3-body charged lepton processes may be observed. Finally, the dark matter phenomenology of the singlet-doublet χ_0 DM has been presented. As shown, a light DM

can comply with $(g - 2)_\mu$ bound, though in general TeV scale values of DM are allowed in our model. This minimal model can be tested at the LHC. Presently a stringent bound can be realized on the mass of vector like leptons L_1 and L_2 , though the mass difference between the VLs and the inert doublet η can be tuned to evade the strong bounds on them. The mass splitting does not have any role on the lepton phenomenology which we have exhaustively studied here.

ACKNOWLEDGEMENTS

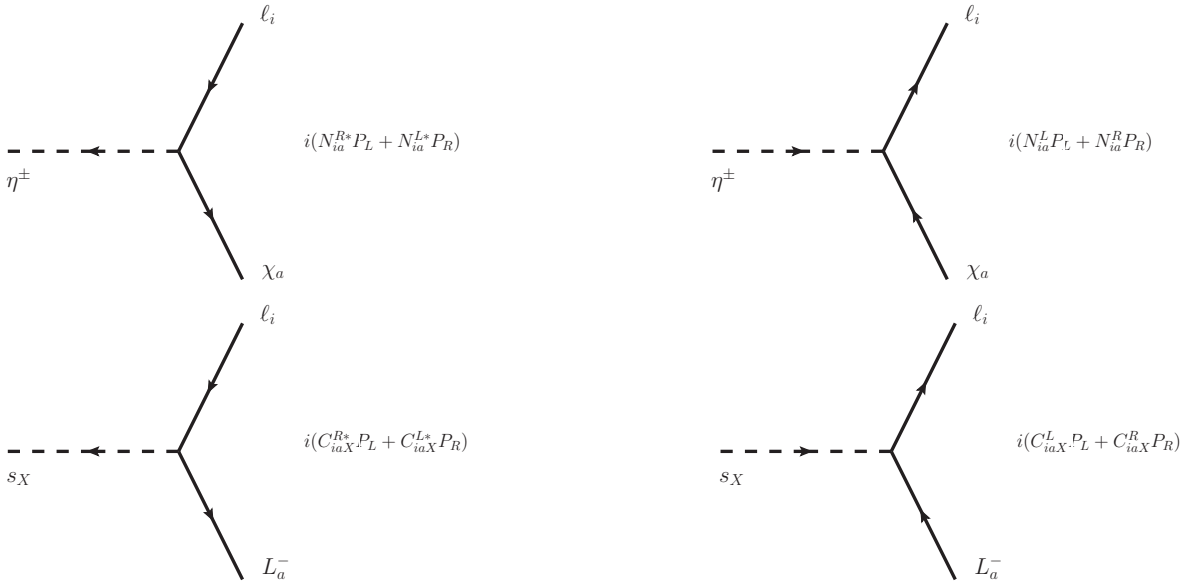
Our computations were supported in part by SAMKHYA: the High Performance Computing Facility provided by the Institute of Physics (IoP), Bhubaneswar, India. DD likes to thank Subhadeep Mondal for some valuable discussions. NS likes to thank Dr. Prafulla Kumar Panda, Utkal University, for his valuable suggestions. NS acknowledges RUSA 2.0 project, Ministry of Human Resource Development, India.

APPENDIX A

In this appendix we list all the Feynman rules required for our calculation. These rules have been expressed in physical eigen basis for particles: Neutral scalar $s_X = (\eta^0, S)$, charged scalar η^\pm , neutral VL fermions χ_a ($a = 1, 0$) and charged VL fermions L_a^- ($a = 1, 2$).

Scalar interactions

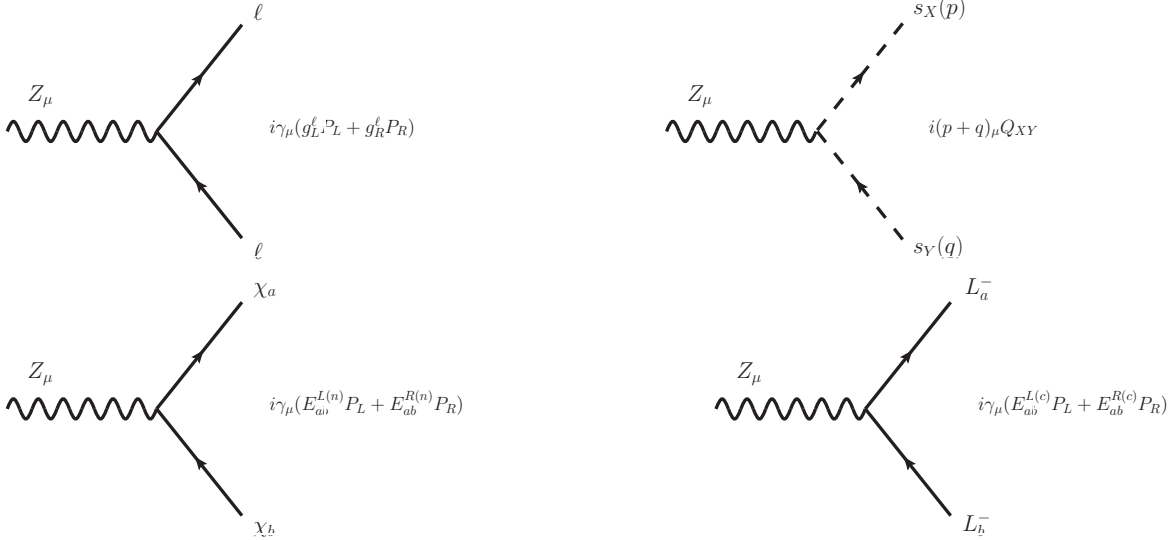
The Feynman rules for scalar interactions are given by,



Where, $N_{ia}^R = Y_{4i}U_a$, with $U_1 = \sin \theta$, $U_0 = -\cos \theta$; $N_{ia}^L = Y_{1i}^\dagger U'_a$, with $U'_1 = \cos \theta$, $U'_0 = \sin \theta$ and $C_{i11}^L = Y_{1i}^\dagger$, $C_{i11}^R = 0$, $C_{i22}^L = 0$, $C_{i22}^R = Y_{3i}$.

Z boson interactions

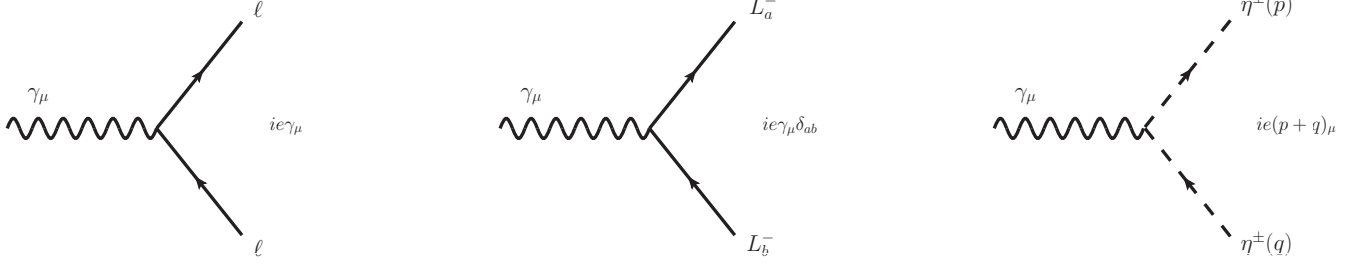
The Feynman rules governing the Z boson interactions are given by,



- $g_L^{(\ell)} = -\frac{g}{\cos \theta_W} \left(-\frac{1}{2} + \sin^2 \theta_W\right)$, $g_R^{(\ell)} = -\frac{g}{\cos \theta_W} \sin^2 \theta_W$ are the left and right chiral couplings among two SM leptons and Z boson respectively, g being the $SU(2)_L$ coupling constant.
- $Q_{11} = Q_{\eta^0 \eta^0} = -\frac{g}{2 \cos \theta_W}$ & $Q_{\eta^+ \eta^+} = -\frac{g \cos 2\theta_W}{2 \cos \theta_W}$, $Q_{22} = Q_{SS} = 0$ and $Q_{12} = Q_{21} = 0$ are the Z -scalar-scalar couplings.
- For neutral VL fermions: $E_{11}^{L,R(n)} = -\frac{g}{2 \cos \theta_W} \cos^2 \theta$, $E_{00}^{L,R(n)} = -\frac{g}{2 \cos \theta_W} \sin^2 \theta$, $E_{10}^{L,R(n)} = E_{01}^{L,R(n)} = -\frac{g}{2 \cos \theta_W} \sin \theta \cos \theta$ and for charged VL fermions: $E_{11}^{L,R(c)} = E_{22}^{L,R(c)} = -\frac{g}{\cos \theta_W} \left(-\frac{1}{2} + \sin^2 \theta_W\right)$, $E_{12}^{L,R(c)} = E_{21}^{L,R(c)} = 0$ are the Z -fermion-fermion couplings.

Photon interactions

The Feynman rules for γ interactions are given by,



APPENDIX B

In this appendix, we have listed the explicit forms of all the mass functions. The two point and three functions are defined as,

$$B_1(m_1^2, m_2^2) = -\frac{1}{2} + \frac{1}{2} \ln m_2^2 - \frac{m_1^2 - m_2^2 + 2m_1^2 \ln \left(\frac{m_2^2}{m_1^2} \right)}{4(m_1^2 - m_2^2)^2}, \quad (74)$$

$$C_0(m_1^2, m_2^2, m_3^2) = -\frac{1}{m_2^2 - m_3^2} \left[\frac{m_1^2 \ln m_1^2 - m_2^2 \ln m_2^2}{m_1^2 - m_2^2} - \frac{m_1^2 \ln m_1^2 - m_3^2 \ln m_3^2}{m_1^2 - m_3^2} \right], \quad (75)$$

$$4C_{24}(m_1^2, m_2^2, m_3^2) = \tilde{C}_0(m_1^2, m_2^2, m_3^2) + \frac{1}{2} = \frac{3}{2} - \frac{1}{m_2^2 - m_3^2} \left[\frac{m_1^4 \ln m_1^2 - m_2^4 \ln m_2^2}{m_1^2 - m_2^2} - \frac{m_1^4 \ln m_1^2 - m_3^4 \ln m_3^2}{m_1^2 - m_3^2} \right]. \quad (76)$$

The functional forms for the four point functions relevant in case of Box diagrams are given by,

$$D_0(m_1^2, m_2^2, m_3^2, m_4^2) = -\frac{m_1^2 \ln m_1^2}{(m_1^2 - m_2^2)(m_1^2 - m_3^2)(m_1^2 - m_4^2)} + \frac{m_2^2 \ln m_2^2}{(m_1^2 - m_2^2)(m_2^2 - m_3^2)(m_2^2 - m_4^2)} \\ - \frac{m_3^2 \ln m_3^2}{(m_1^2 - m_3^2)(m_2^2 - m_3^2)(m_3^2 - m_4^2)} + \frac{m_4^2 \ln m_4^2}{(m_1^2 - m_4^2)(m_2^2 - m_4^2)(m_3^2 - m_4^2)}, \quad (77)$$

$$\tilde{D}_0(m_1^2, m_2^2, m_3^2, m_4^2) = -\frac{m_1^4 \ln m_1^2}{(m_1^2 - m_2^2)(m_1^2 - m_3^2)(m_1^2 - m_4^2)} + \frac{m_2^4 \ln m_2^2}{(m_1^2 - m_2^2)(m_2^2 - m_3^2)(m_2^2 - m_4^2)} \\ - \frac{m_3^4 \ln m_3^2}{(m_1^2 - m_3^2)(m_2^2 - m_3^2)(m_3^2 - m_4^2)} + \frac{m_4^4 \ln m_4^2}{(m_1^2 - m_4^2)(m_2^2 - m_4^2)(m_3^2 - m_4^2)}. \quad (78)$$

The other functions appearing in the expressions of the dipole and monopole terms of the γ -penguin are defined as:

$$\begin{aligned}
F_1(r) &= \frac{1 - r^2 + 2r \ln r}{2(1 - r)^3}, \\
F_2(r) &= \frac{1 - 6r + 3r^2 + 2r^3 - 6r^2 \ln r}{6(1 - r)^4}, \\
F_3(r) &= \frac{2 + 3r - 6r^2 + r^3 + 6r \ln r}{6(1 - r)^4}, \\
F_4(r) &= \frac{2 - 9r + 18r^2 - 11r^3 + 6r^3 \ln r}{(1 - r)^4}, \\
F_5(r) &= \frac{16 - 45r + 36r^2 - 7r^3 + 6(2 - 3r) \ln r}{(1 - r)^4}.
\end{aligned} \tag{79}$$

APPENDIX C

In this section, we present the general and explicit results for the on-shell and off-shell decays of the charged leptons.

A. $\ell_\alpha \rightarrow \ell_\beta \gamma$

The on-shell amplitude, mediated by the dipole operators, can be expressed as,

$$\mathcal{L}_{\ell\ell\gamma} \supset e \bar{u}_\beta [i m_{\ell_\alpha} \sigma^{\mu\nu} q_\nu (A_2^L P_L + A_2^R P_R)] u_\alpha A_\mu + h.c. \tag{80}$$

Here e is the electric charge, q is the photon momentum, $P_{L,R} = \frac{1}{2}(1 \mp \gamma_5)$ are the usual chirality projectors and the lepton spinors are denoted by $u_{\alpha,\beta}$, where α, β stand for the flavor indices. The coefficients in Eq. (80) can be written as, $A_2^{L,R} = A_2^{(n)L,R} + A_2^{(c)L,R}$, where ‘ n ’ and ‘ c ’ indicate the dipole contributions from neutral and charged fermion loops [shown in Fig. 3] respectively. The general forms for $A_2^{(n)L,R}$ and $A_2^{(c)L,R}$ are given below:

$$\begin{aligned}
A_2^{(n)L} = \frac{1}{32\pi^2 M_\eta^2} & \left[N_{\beta a}^L N_{\alpha a}^{R*} \left(\frac{2M_{\chi_a}}{m_{\ell_\alpha}} \right) F_1 \left(\frac{M_{\chi_a}^2}{M_\eta^2} \right) + N_{\beta a}^L N_{\alpha a}^{L*} F_2 \left(\frac{M_{\chi_a}^2}{M_\eta^2} \right) \right. \\
& \left. + N_{\beta a}^R N_{\alpha a}^{R*} \left(\frac{m_{\ell_\beta}}{m_{\ell_\alpha}} \right) F_2 \left(\frac{M_{\chi_a}^2}{M_\eta^2} \right) \right],
\end{aligned} \tag{81}$$

$$A_2^{(n)R} = A_2^{(n)L}|_{L \leftrightarrow R}, \tag{82}$$

$$A_2^{(c)L} = \frac{1}{32\pi^2 M_S^2} C_{\beta 22}^R C_{\alpha 22}^{R*} \frac{m_{\ell_\beta}}{m_{\ell_\alpha}} F_3 \left(\frac{M_{L_2}^2}{M_S^2} \right) + \frac{1}{32\pi^2 M_\eta^2} C_{\beta 11}^L C_{\alpha 11}^{L*} F_3 \left(\frac{M_{L_1}^2}{M_\eta^2} \right), \quad (83)$$

$$A_2^{(c)R} = \frac{1}{32\pi^2 M_\eta^2} C_{\beta 11}^L C_{\alpha 11}^{L*} \frac{m_{\ell_\beta}}{m_{\ell_\alpha}} F_3 \left(\frac{M_{L_1}^2}{M_\eta^2} \right) + \frac{1}{32\pi^2 M_S^2} C_{\beta 22}^R C_{\alpha 22}^{R*} F_3 \left(\frac{M_{L_2}^2}{M_S^2} \right). \quad (84)$$

B. $\ell_\alpha \rightarrow 3\ell_\beta$

The amplitude for such a process like $\ell_\alpha^-(p) \rightarrow \ell_\beta^-(p_1)\ell_\beta^-(p_2)\ell_\beta^+(p_3)$ can be decomposed into three major contributions given by,

$$\mathcal{M}(\ell_\alpha^- \rightarrow \ell_\beta^- \ell_\beta^- \ell_\beta^+) \simeq \mathcal{M}_\gamma + \mathcal{M}_Z + \mathcal{M}_{\text{Box}}. \quad (85)$$

In general there should be a contribution from Higgs penguin diagrams (i.e. \mathcal{M}_H) as well, but one can neglect it in most cases, in comparison to the other three contributions of Eq. (85). Different contributions can be expressed as follows:

- Photon penguin contribution: The monopole and dipole contributions can be calculated from,

$$\begin{aligned} \mathcal{M}_\gamma = & \bar{u}_\beta(p_1) \left[q^2 \gamma^\mu (A_1^L P_L + A_1^R P_R) + i m_{\ell_\alpha} \sigma^{\mu\nu} q_\nu (A_2^L P_L + A_2^R P_R) \right] u_\alpha(p) \\ & \times \frac{e^2}{q^2} \bar{u}_\beta(p_2) \gamma_\mu v_\beta(p_3) - (p_1 \leftrightarrow p_2). \end{aligned} \quad (86)$$

The explicit form of the Wilson coefficients A_2^L and A_2^R are already described in Eqs. (81)–(84). The coefficients associated with the monopole operator can be calculated as,

$$A_1^{(n)L} = \frac{1}{576\pi^2 M_\eta^2} \left[N_{\beta a}^R N_{\alpha a}^{R*} F_4 \left(\frac{M_{\chi_a}^2}{M_\eta^2} \right) \right], \quad A_1^{(n)R} = A_1^{(n)L}|_{L \leftrightarrow R}, \quad (87)$$

$$A_1^{(c)L} = -\frac{1}{576\pi^2 M_S^2} \left[C_{\beta 22}^R C_{\alpha 22}^{R*} F_5 \left(\frac{M_{L_2}^2}{M_S^2} \right) \right], \quad A_1^{(c)R} = -\frac{1}{576\pi^2 M_\eta^2} \left[C_{\beta 11}^L C_{\alpha 11}^{L*} F_5 \left(\frac{M_{L_1}^2}{M_\eta^2} \right) \right]. \quad (88)$$

- Z penguin contribution: Feynman diagrams are shown in Fig. 7. We have calculated the coefficients as follows:

$$\mathcal{M}_Z = \frac{1}{M_Z^2} \bar{u}_\beta(p_1) \left[\gamma^\mu (F_L P_L + F_R P_R) \right] u_\alpha(p) \bar{u}_\beta(p_2) \left[\gamma_\mu (g_L^{(\ell)} P_L + g_R^{(\ell)} P_R) \right] v_\beta(p_3) - (p_1 \leftrightarrow p_2), \quad (89)$$

where, as before, $F_{L,R} = F_{L,R}^{(n)} + F_{L,R}^{(c)}$. The expressions for these form factors are given below:

$$F_L^{(n)} = -\frac{1}{16\pi^2} \left[N_{\beta b}^R N_{\alpha a}^{R*} \left\{ E_{ba}^{R(n)} \left(2C_{24}(M_\eta^2, M_{\chi_a}^2, M_{\chi_b}^2) - \frac{1}{2} \right) - E_{ba}^{L(n)} M_{\chi_a} M_{\chi_b} C_0(M_\eta^2, M_{\chi_a}^2, M_{\chi_b}^2) \right\} \right. \\ \left. + N_{\beta a}^R N_{\alpha a}^{R*} \left\{ 2Q_{\eta\eta} C_{24}(M_{\chi_a}^2, M_\eta^2, M_\eta^2) \right\} + N_{\beta a}^R N_{\alpha a}^{R*} \left\{ g_L^{(\ell)} B_1(M_{\chi_a}^2, M_\eta^2) \right\} \right], \quad (90)$$

$$F_L^{(c)} = -\frac{1}{16\pi^2} \left[C_{\beta a X}^R C_{\alpha a X}^{R*} \left\{ E_{aa}^{R(c)} \left(2C_{24}(M_X^2, M_{L_a}^2, M_{L_a}^2) - \frac{1}{2} \right) - E_{aa}^{L(c)} M_{L_a} M_{L_a} C_0(M_X^2, M_{L_a}^2, M_{L_a}^2) \right\} \right. \\ \left. + C_{\beta a X}^R C_{\alpha a X}^{R*} \left\{ 2Q_{XX} C_{24}(M_{L_a}^2, M_X^2, M_X^2) \right\} + C_{\beta a X}^R C_{\alpha a X}^{R*} \left\{ g_L^{(\ell)} B_1(M_{L_a}^2, M_X^2) \right\} \right], \quad (91)$$

$$F_R^{(n)} = F_L^{(n)}|_{L \leftrightarrow R}, \quad F_R^{(c)} = F_L^{(c)}|_{L \leftrightarrow R}. \quad (92)$$

- Box diagram contribution: Leading contributions are shown in Fig. 8.

$$\mathcal{M}_{\text{Box}} \simeq e^2 B_1^L [\bar{u}_\beta(p_1)(\gamma^\mu P_L)u_\alpha(p)][\bar{u}_\beta(p_2)(\gamma_\mu P_L)v_\beta(p_3)] \\ + e^2 B_1^R [\bar{u}_\beta(p_1)(\gamma^\mu P_R)u_\alpha(p)][\bar{u}_\beta(p_2)(\gamma_\mu P_R)v_\beta(p_3)] \\ + e^2 B_2^L \{ [\bar{u}_\beta(p_1)(\gamma^\mu P_L)u_\alpha(p)][\bar{u}_\beta(p_2)(\gamma_\mu P_R)v_\beta(p_3)] - (p_1 \leftrightarrow p_2) \} \\ + e^2 B_2^R \{ [\bar{u}_\beta(p_1)(\gamma^\mu P_R)u_\alpha(p)][\bar{u}_\beta(p_2)(\gamma_\mu P_L)v_\beta(p_3)] - (p_1 \leftrightarrow p_2) \} \\ + e^2 B_3^L \{ [\bar{u}_\beta(p_1)(P_L)u_\alpha(p)][\bar{u}_\beta(p_2)(P_L)v_\beta(p_3)] - (p_1 \leftrightarrow p_2) \} \\ + e^2 B_3^R \{ [\bar{u}_\beta(p_1)(P_R)u_\alpha(p)][\bar{u}_\beta(p_2)(P_R)v_\beta(p_3)] - (p_1 \leftrightarrow p_2) \} \\ + e^2 B_4^L \{ [\bar{u}_\beta(p_1)(\sigma^{\mu\nu} P_L)u_\alpha(p)][\bar{u}_\beta(p_2)(\sigma_{\mu\nu} P_L)v_\beta(p_3)] - (p_1 \leftrightarrow p_2) \} \\ + e^2 B_4^R \{ [\bar{u}_\beta(p_1)(\sigma^{\mu\nu} P_R)u_\alpha(p)][\bar{u}_\beta(p_2)(\sigma_{\mu\nu} P_R)v_\beta(p_3)] - (p_1 \leftrightarrow p_2) \}, \quad (93)$$

where, $B_i^{L,R} = B_i^{(n)L,R} + B_i^{(c)L,R}$ [$i = 1, 2, 3, 4$]. The B -factors for the neutral fermions (χ_1, χ_0) can be calculated as,

$$e^2 B_1^{(n)L} = \frac{1}{16\pi^2} \left[\frac{\tilde{D}_0}{2} N_{\beta a}^R N_{\alpha a}^{R*} N_{\beta b}^R N_{\beta b}^{R*} + D_0 M_{\chi_a} M_{\chi_b} N_{\beta b}^R N_{\beta b}^R N_{\alpha a}^{R*} N_{\beta a}^{R*} \right], \quad (94)$$

$$e^2 B_2^{(n)L} = \frac{1}{16\pi^2} \left[\frac{\tilde{D}_0}{4} N_{\beta a}^R N_{\alpha a}^{R*} N_{\beta b}^L N_{\beta b}^{L*} - \frac{D_0}{2} M_{\chi_a} M_{\chi_b} N_{\beta a}^L N_{\alpha a}^{R*} N_{\beta b}^R N_{\beta b}^{L*} \right. \\ \left. - \frac{\tilde{D}_0}{4} N_{\beta b}^L N_{\beta b}^R N_{\alpha a}^{R*} N_{\beta a}^{L*} + \frac{\tilde{D}_0}{4} N_{\beta b}^R N_{\beta b}^L N_{\alpha a}^{R*} N_{\beta a}^{L*} \right], \quad (95)$$

$$e^2 B_3^{(n)L} = \frac{1}{16\pi^2} \left[D_0 M_{\chi_a} M_{\chi_b} N_{\beta a}^L N_{\alpha a}^{R*} N_{\beta b}^L N_{\beta b}^{R*} + \frac{D_0}{2} M_{\chi_a} M_{\chi_b} N_{\beta b}^L N_{\beta b}^L N_{\alpha a}^{R*} N_{\beta a}^{R*} \right], \quad (96)$$

$$e^2 B_4^{(n)L} = \frac{1}{16\pi^2} \left[\frac{D_0}{8} M_{\chi_a} M_{\chi_b} N_{\alpha a}^{R*} N_{\beta a}^{R*} N_{\beta b}^L N_{\beta b}^L \right], \quad (97)$$

$$B_i^{(n)R} = B_i^{(n)L}|_{L \leftrightarrow R}, \quad (98)$$

where,

$$D_0 = D_0(M_{\chi_a}^2, M_{\chi_b}^2, M_\eta^2, M_\eta^2), \quad \tilde{D}_0 = \tilde{D}_0(M_{\chi_a}^2, M_{\chi_b}^2, M_\eta^2, M_\eta^2). \quad (99)$$

And for the charged fermions (L_1^\pm, L_2^\pm) ,

$$e^2 B_1^{(c)L} = \frac{1}{16\pi^2} \left[\frac{\tilde{D}_0}{2} C_{\beta a X}^R C_{\alpha a X}^{R*} C_{\beta a X}^R C_{\beta a X}^{R*} \right], \quad (100)$$

$$e^2 B_2^{(c)L} = \frac{1}{16\pi^2} \left[\frac{\tilde{D}_0}{4} C_{\beta a X}^R C_{\alpha a X}^{R*} C_{\beta a X}^L C_{\beta a X}^{L*} - \frac{D_0}{2} M_{L_a} M_{L_a} C_{\beta a X}^L C_{\alpha a X}^{R*} C_{\beta a X}^R C_{\beta a X}^{L*} \right], \quad (101)$$

$$e^2 B_3^{(c)L} = \frac{1}{16\pi^2} \left[D_0 M_{L_a} M_{L_a} C_{\beta a X}^L C_{\alpha a X}^{R*} C_{\beta a X}^L C_{\beta a X}^{R*} \right], \quad (102)$$

$$e^2 B_4^{(c)L} = 0, \quad (103)$$

$$B_i^{(c)R} = B_i^{(c)L}|_{L \leftrightarrow R}, \quad (104)$$

where,

$$D_0 = D_0(M_{L_a}^2, M_{L_a}^2, M_X^2, M_X^2), \quad \tilde{D}_0 = \tilde{D}_0(M_{L_a}^2, M_{L_a}^2, M_X^2, M_X^2), \quad (105)$$

with $M_1 = M_\eta$ and $M_2 = M_S$. The generic functional forms for these D_0 and \tilde{D}_0 are again available in Appendix B.

The decay width for $\ell_\alpha^- \rightarrow \ell_\beta^- \ell_\beta^- \ell_\beta^+$ can be obtained by considering all the possible contributions coming from photon and Z penguins in addition to the box diagrams and can be expressed as [135,

136],

$$\begin{aligned}
\Gamma(\ell_\alpha^- \rightarrow \ell_\beta^- \ell_\beta^- \ell_\beta^+) &= \frac{e^4 m_{\ell_\alpha}^5}{512\pi^3} \left[|A_1^L|^2 + |A_1^R|^2 - 2 \left(A_1^L A_2^{R*} + A_2^L A_1^{R*} + h.c. \right) + (|A_2^L|^2 + |A_2^R|^2) \times \right. \\
&\quad \left\{ \frac{16}{3} \ln \left(\frac{m_{\ell_\alpha}}{m_{\ell_\beta}} \right) - \frac{22}{3} \right\} + \frac{1}{6} (|B_1^L|^2 + |B_1^R|^2) + \frac{1}{3} (|B_2^L|^2 + |B_2^R|^2) \\
&\quad + \frac{1}{24} (|B_3^L|^2 + |B_3^R|^2) + 6 (|B_4^L|^2 + |B_4^R|^2) - \frac{1}{2} (B_3^L B_4^{L*} + B_3^R B_4^{R*} + h.c.) \\
&\quad + \frac{1}{3} (A_1^L B_1^{L*} + A_1^R B_1^{R*} + A_1^L B_2^{L*} + A_1^R B_2^{R*} + h.c.) \\
&\quad - \frac{2}{3} (A_2^R B_1^{L*} + A_2^L B_1^{R*} + A_2^L B_2^{R*} + A_2^R B_2^{L*} + h.c.) \\
&\quad + \frac{1}{3} \left\{ 2 (|F_{LL}|^2 + |F_{RR}|^2) + |F_{LR}|^2 + |F_{RL}|^2 \right. \\
&\quad + (B_1^L F_{LL}^* + B_1^R F_{RR}^* + B_2^L F_{LR}^* + B_2^R F_{RL}^* + h.c.) \\
&\quad + 2 (A_1^L F_{LL}^* + A_1^R F_{RR}^* + h.c.) + (A_1^L F_{LR}^* + A_1^R F_{RL}^* + h.c.) \\
&\quad \left. \left. - 4 (A_2^R F_{LL}^* + A_2^L F_{RR}^* + h.c.) - 2 (A_2^L F_{RL}^* + A_2^R F_{LR}^* + h.c.) \right\} \right], \quad (106)
\end{aligned}$$

where,

$$\begin{aligned}
F_{LL} &= \frac{F_L g_L^{(\ell)}}{g^2 \sin^2 \theta_W M_Z^2}, & F_{RR} &= F_{LL}|_{L \leftrightarrow R}, \\
F_{LR} &= \frac{F_L g_R^{(\ell)}}{g^2 \sin^2 \theta_W M_Z^2}, & F_{RL} &= F_{LR}|_{L \leftrightarrow R}.
\end{aligned} \quad (107)$$

The corresponding branching ratio can be directly calculated as $\text{Br}(\ell_\alpha^- \rightarrow \ell_\beta^- \ell_\beta^- \ell_\beta^+) = \tau_\alpha \Gamma(\ell_\alpha^- \rightarrow \ell_\beta^- \ell_\beta^- \ell_\beta^+)$, τ_α being the lifetime of ℓ_α .

-
- [1] PARTICLE DATA GROUP collaboration, J. e. a. Beringer, *Review of particle physics*, *Phys. Rev. D* **86** (Jul, 2012) 010001.
 - [2] ATLAS collaboration, G. Aad et al., *Observation of a new particle in the search for the Standard Model Higgs boson with the ATLAS detector at the LHC*, *Phys. Lett.* **B716** (2012) 1–29, [1207.7214].
 - [3] CMS collaboration, S. Chatrchyan et al., *Observation of a New Boson at a Mass of 125 GeV with the CMS Experiment at the LHC*, *Phys. Lett.* **B716** (2012) 30–61, [1207.7235].
 - [4] ATLAS, CMS collaboration, G. Aad et al., *Measurements of the Higgs boson production and decay rates and constraints on its couplings from a combined ATLAS and CMS analysis of the LHC pp collision data at $\sqrt{s} = 7$ and 8 TeV*, *JHEP* **08** (2016) 045, [1606.02266].

- [5] ATLAS collaboration, G. Aad et al., *Combined measurements of Higgs boson production and decay using up to 80 fb⁻¹ of proton-proton collision data at $\sqrt{s} = 13$ TeV collected with the ATLAS experiment*, *Phys. Rev. D* **101** (2020) 012002, [1909.02845].
- [6] PLANCK collaboration, N. Aghanim et al., *Planck 2015 results. XI. CMB power spectra, likelihoods, and robustness of parameters*, *Astron. Astrophys.* **594** (2016) A11, [1507.02704].
- [7] WMAP collaboration, G. Hinshaw et al., *Nine-Year Wilkinson Microwave Anisotropy Probe (WMAP) Observations: Cosmological Parameter Results*, *Astrophys. J. Suppl.* **208** (2013) 19, [1212.5226].
- [8] P. Minkowski, $\mu \rightarrow e\gamma$ at a rate of one out of 10^9 muon decays, *Phys. Lett.* **67B** (1977) .
- [9] T. Yanagida, *Horizontal gauge symmetry and masses of neutrinos*, *Conf. Proc.* **C7902131** (1979) 95–99.
- [10] M. Gell-Mann, P. Ramond and R. Slansky, *Complex Spinors and Unified Theories*, *Conf. Proc.* **C790927** (1979) 315–321, [1306.4669].
- [11] S. Kanemura, T. Nabeshima and H. Sugiyama, *Neutrino Masses from Loop-Induced Dirac Yukawa Couplings*, *Phys. Lett.* **B703** (2011) 66–70, [1106.2480].
- [12] S. Kanemura, T. Nabeshima and H. Sugiyama, *TeV-Scale Seesaw with Loop-Induced Dirac Mass Term and Dark Matter from $U(1)_{B-L}$ Gauge Symmetry Breaking*, *Phys. Rev.* **D85** (2012) 033004, [1111.0599].
- [13] Y. Farzan and E. Ma, *Dirac neutrino mass generation from dark matter*, *Phys. Rev.* **D86** (2012) 033007, [1204.4890].
- [14] E. Ma and O. Popov, *Pathways to Naturally Small Dirac Neutrino Masses*, *Phys. Lett.* **B764** (2017) 142–144, [1609.02538].
- [15] S. Kanemura, K. Sakurai and H. Sugiyama, *Probing Models of Dirac Neutrino Masses via the Flavor Structure of the Mass Matrix*, *Phys. Lett.* **B758** (2016) 465–472, [1603.08679].
- [16] C.-Y. Yao and G.-J. Ding, *Systematic Study of One-Loop Dirac Neutrino Masses and Viable Dark Matter Candidates*, *Phys. Rev.* **D96** (2017) 095004, [1707.09786]. [Erratum: *Phys. Rev.* D98,no.3,039901(2018)].
- [17] E. Ma and U. Sarkar, *Radiative Left-Right Dirac Neutrino Mass*, *Phys. Lett.* **B776** (2018) 54–57, [1707.07698].
- [18] S. Singirala, R. Mohanta and S. Patra, *Singlet scalar Dark matter in $U(1)_{B-L}$ models without right-handed neutrinos*, *Eur. Phys. J. Plus* **133** (2018) 477, [1704.01107].
- [19] J. Calle, D. Restrepo, C. E. Yaguna and . Zapata, *Minimal radiative Dirac neutrino mass models*, *Phys. Rev.* **D99** (2019) 075008, [1812.05523].
- [20] C.-Y. Yao and G.-J. Ding, *Systematic analysis of Dirac neutrino masses from a dimension five operator*, *Phys. Rev.* **D97** (2018) 095042, [1802.05231].
- [21] D. Borah, B. Karmakar and D. Nanda, *Common Origin of Dirac Neutrino Mass and Freeze-in Massive Particle Dark Matter*, *JCAP* **1807** (2018) 039, [1805.11115].
- [22] E. Ma, *Scotogenic $U(1)_X$ Dirac neutrinos*, *Phys. Lett.* **B793** (2019) 411–414, [1901.09091].
- [23] A. Dasgupta, S. K. Kang and O. Popov, *Radiative Dirac Neutrino Mass with Dark Matter and it's implication to $0\nu 4\beta$ in the $U(1)_{B-L}$ extension of the Standard Model*, 1903.12558.

- [24] A. Das, T. Nomura, H. Okada and S. Roy, *Generation of a radiative neutrino mass in the linear seesaw framework, charged lepton flavor violation, and dark matter*, *Phys. Rev. D* **96** (2017) 075001, [1704.02078].
- [25] Y. Cai, J. Herrero-Garcia, M. A. Schmidt, A. Vicente and R. R. Volkas, *From the trees to the forest: a review of radiative neutrino mass models*, *Front.in Phys.* **5** (2017) 63, [1706.08524].
- [26] E. Ma, *Verifiable radiative seesaw mechanism of neutrino mass and dark matter*, *Phys. Rev.* **D73** (2006) 077301, [hep-ph/0601225].
- [27] J. Calle, D. Restrepo and . Zapata, *Dirac neutrino mass generation from a Majorana messenger*, *Phys. Rev. D* **101** (2020) 035004, [1909.09574].
- [28] S. Jana, P. Vishnu and S. Saad, *Minimal realizations of Dirac neutrino mass from generic one-loop and two-loop topologies at $d = 5$* , *JCAP* **04** (2020) 018, [1910.09537].
- [29] D. Nanda and D. Borah, *Connecting Light Dirac Neutrinos to a Multi-component Dark Matter Scenario in Gauged $B - L$ Model*, *Eur. Phys. J. C* **80** (2020) 557, [1911.04703].
- [30] J. Leite, A. Morales, J. W. Valle and C. A. Vaquera-Araujo, *Scotogenic dark matter and Dirac neutrinos from unbroken gauged $B - L$ symmetry*, *Phys. Lett. B* **807** (2020) 135537, [2003.02950].
- [31] P. Escribano, M. Reig and A. Vicente, *Generalizing the Scotogenic model*, *JHEP* **07** (2020) 097, [2004.05172].
- [32] S.-Y. Guo and Z.-L. Han, *Observable Signatures of Scotogenic Dirac Model*, 2005.08287.
- [33] E. Ma and M. Raidal, *Neutrino mass, muon anomalous magnetic moment, and lepton flavor nonconservation*, *Phys. Rev. Lett.* **87** (2001) 011802, [hep-ph/0102255]. [Erratum: *Phys. Rev. Lett.* 87,159901(2001)].
- [34] F. S. Queiroz and W. Shepherd, *New Physics Contributions to the Muon Anomalous Magnetic Moment: A Numerical Code*, *Phys. Rev. D* **89** (2014) 095024, [1403.2309].
- [35] M. Lindner, M. Platscher and F. S. Queiroz, *A Call for New Physics : The Muon Anomalous Magnetic Moment and Lepton Flavor Violation*, *Phys. Rept.* **731** (2018) 1–82, [1610.06587].
- [36] K. Kowalska and E. M. Sessolo, *Expectations for the muon $g-2$ in simplified models with dark matter*, *JHEP* **09** (2017) 112, [1707.00753].
- [37] R. Dermisek and A. Raval, *Explanation of the Muon $g-2$ Anomaly with Vectorlike Leptons and its Implications for Higgs Decays*, *Phys. Rev. D* **88** (2013) 013017, [1305.3522].
- [38] Z. Poh and S. Raby, *Vectorlike leptons: Muon $g-2$ anomaly, lepton flavor violation, Higgs boson decays, and lepton nonuniversality*, *Phys. Rev. D* **96** (2017) 015032, [1705.07007].
- [39] B. Barman, D. Borah, L. Mukherjee and S. Nandi, *Correlating the anomalous results in $b \rightarrow s$ decays with inert Higgs doublet dark matter and muon $(g - 2)$* , *Phys. Rev. D* **100** (2019) 115010, [1808.06639].
- [40] C.-H. Chen and T. Nomura, *Influence of an inert charged Higgs boson on the muon $g - 2$ and radiative neutrino masses in a scotogenic model*, *Phys. Rev. D* **100** (2019) 015024, [1903.03380].
- [41] A. De Jesus, S. Kovalenko, F. Queiroz, K. Sinha and C. Siqueira, *Vector-Like Leptons and Inert Scalar Triplet: Lepton Flavor Violation, $g - 2$ and Collider Searches*, 2004.01200.
- [42] T. Cohen, J. Kearney, A. Pierce and D. Tucker-Smith, *Singlet-Doublet Dark Matter*, *Phys. Rev. D* **85** (2012) 075003, [1109.2604].

- [43] C. Cheung and D. Sanford, *Simplified Models of Mixed Dark Matter*, *JCAP* **02** (2014) 011, [1311.5896].
- [44] A. Vicente and C. E. Yaguna, *Probing the scotogenic model with lepton flavor violating processes*, *JHEP* **02** (2015) 144, [1412.2545].
- [45] D. Restrepo, A. Rivera, M. Snchez-Pelez, O. Zapata and W. Tangarife, *Radiative Neutrino Masses in the Singlet-Doublet Fermion Dark Matter Model with Scalar Singlets*, *Phys. Rev. D* **92** (2015) 013005, [1504.07892].
- [46] L. Calibbi, A. Mariotti and P. Tziveloglou, *Singlet-Doublet Model: Dark matter searches and LHC constraints*, *JHEP* **10** (2015) 116, [1505.03867].
- [47] S. Bhattacharya, N. Sahoo and N. Sahu, *Minimal vectorlike leptonic dark matter and signatures at the LHC*, *Phys. Rev. D* **93** (2016) 115040, [1510.02760].
- [48] C. E. Yaguna, *Singlet-Doublet Dirac Dark Matter*, *Phys. Rev. D* **92** (2015) 115002, [1510.06151].
- [49] G. Arcadi, *2HDM portal for Singlet-Doublet Dark Matter*, *Eur. Phys. J. C* **78** (2018) 864, [1804.04930].
- [50] P. Konar, A. Mukherjee, A. K. Saha and S. Show, *Linking the pseudo-Dirac dark matter and radiative neutrino mass in a singlet doublet scenario*, 2001.11325.
- [51] XENON collaboration, E. Aprile et al., *Dark Matter Search Results from a One Ton-Year Exposure of XENON1T*, *Phys. Rev. Lett.* **121** (2018) 111302, [1805.12562].
- [52] LUX collaboration, D. S. Akerib et al., *Limits on spin-dependent WIMP-nucleon cross section obtained from the complete LUX exposure*, *Phys. Rev. Lett.* **118** (2017) 251302, [1705.03380].
- [53] J. C. Pati and A. Salam, *Lepton Number as the Fourth Color*, *Phys. Rev. D* **10** (1974) 275–289. [Erratum: *Phys.Rev.D* **11**, 703–703 (1975)].
- [54] R. N. Mohapatra and J. C. Pati, *A Natural Left-Right Symmetry*, *Phys. Rev. D* **11** (1975) 2558.
- [55] G. Senjanovic and R. N. Mohapatra, *Exact Left-Right Symmetry and Spontaneous Violation of Parity*, *Phys. Rev. D* **12** (1975) 1502.
- [56] C. S. Aulakh, K. Benakli and G. Senjanovic, *Reconciling supersymmetry and left-right symmetry*, *Phys. Rev. Lett.* **79** (1997) 2188–2191, [hep-ph/9703434].
- [57] P. Duka, J. Gluza and M. Zralek, *Quantization and renormalization of the manifest left-right symmetric model of electroweak interactions*, *Annals Phys.* **280** (2000) 336–408, [hep-ph/9910279].
- [58] C. Arbeláez, M. Hirsch, M. Malinský and J. C. Romão, *LHC-scale left-right symmetry and unification*, *Phys. Rev. D* **89** (2014) 035002, [1311.3228].
- [59] S. Antusch, C. Hohl, S. F. King and V. Susic, *Non-universal Z' from $SO(10)$ GUTs with vector-like family and the origin of neutrino masses*, *Nucl. Phys. B* **934** (2018) 578–605, [1712.05366].
- [60] MUON G-2 collaboration, G. Bennett et al., *Final Report of the Muon E821 Anomalous Magnetic Moment Measurement at BNL*, *Phys. Rev. D* **73** (2006) 072003, [hep-ex/0602035].
- [61] A. Keshavarzi, D. Nomura and T. Teubner, *Muon $g - 2$ and $\alpha(M_Z^2)$: a new data-based analysis*, *Phys. Rev. D* **97** (2018) 114025, [1802.02995].
- [62] PARTICLE DATA GROUP collaboration, M. Tanabashi et al., *Review of Particle Physics*, *Phys. Rev. D* **98**

- (2018) 030001.
- [63] T. Aoyama et al., *The anomalous magnetic moment of the muon in the Standard Model*, *Phys. Rept.* **887** (2020) 1–166, [2006.04822].
 - [64] S. Borsanyi et al., *Leading-order hadronic vacuum polarization contribution to the muon magnetic moment from lattice QCD*, 2002.12347.
 - [65] M. Passera, W. J. Marciano and A. Sirlin, *The Muon $g-2$ and the bounds on the Higgs boson mass*, *Phys. Rev. D* **78** (2008) 013009, [0804.1142].
 - [66] M. Davier, A. Hoecker, B. Malaescu and Z. Zhang, *Reevaluation of the hadronic vacuum polarisation contributions to the Standard Model predictions of the muon $g-2$ and $\alpha(m_Z^2)$ using newest hadronic cross-section data*, *Eur. Phys. J. C* **77** (2017) 827, [1706.09436].
 - [67] M. Davier, A. Hoecker, B. Malaescu and Z. Zhang, *A new evaluation of the hadronic vacuum polarisation contributions to the muon anomalous magnetic moment and to $\alpha(m_Z^2)$* , *Eur. Phys. J. C* **80** (2020) 241, [1908.00921]. [Erratum: *Eur.Phys.J.C* 80, 410 (2020)].
 - [68] G. Colangelo, M. Hoferichter and P. Stoffer, *Constraints on the two-pion contribution to hadronic vacuum polarization*, *Phys. Lett. B* **814** (2021) 136073, [2010.07943].
 - [69] A. Crivellin, M. Hoferichter, C. A. Manzari and M. Montull, *Hadronic vacuum polarization: $(g-2)_\mu$ versus global electroweak fits*, 2003.04886.
 - [70] A. Keshavarzi, W. J. Marciano, M. Passera and A. Sirlin, *Muon $g-2$ and $\Delta\alpha$ connection*, *Phys. Rev. D* **102** (2020) 033002, [2006.12666].
 - [71] B. Malaescu and M. Schott, *Impact of correlations between a_μ and α_{QED} on the EW fit*, *Eur. Phys. J. C* **81** (2021) 46, [2008.08107].
 - [72] MUON $G-2$ collaboration, B. Abi et al., *Measurement of the Positive Muon Anomalous Magnetic Moment to 0.46 ppm*, *Phys. Rev. Lett.* **126** (2021) 141801, [2104.03281].
 - [73] MUON $G-2$ collaboration, T. Albahri et al., *Measurement of the anomalous precession frequency of the muon in the Fermilab Muon $g-2$ experiment*, *Phys. Rev. D* **103** (2021) 072002, [2104.03247].
 - [74] M. Chakraborti, S. Heinemeyer and I. Saha, *The new "MUON $G-2$ " Result and Supersymmetry*, 2104.03287.
 - [75] M. Chakraborti, L. Roszkowski and S. Trojanowski, *GUT-constrained supersymmetry and dark matter in light of the new $(g-2)_\mu$ determination*, 2104.04458.
 - [76] G. Arcadi, L. Calibbi, M. Fedele and F. Mescia, *Muon $g-2$ and B -anomalies from Dark Matter*, 2104.03228.
 - [77] J. C. Criado, A. Djouadi, N. Koivunen, K. M  rsepp, M. Raidal and H. Veerm  e, *Confronting spin-3/2 and other new fermions with the muon $g-2$ measurement*, 2104.03231.
 - [78] F. Wang, L. Wu, Y. Xiao, J. M. Yang and Y. Zhang, *GUT-scale constrained SUSY in light of E989 muon $g-2$ measurement*, 2104.03262.
 - [79] M. Ibe, S. Kobayashi, Y. Nakayama and S. Shirai, *Muon $g-2$ in Gauge Mediation without SUSY CP Problem*, 2104.03289.
 - [80] K. S. Babu, S. Jana, M. Lindner and V. P. K., *Muon $g-2$ Anomaly and Neutrino Magnetic Moments*,

2104.03291.

- [81] Y. Bai and J. Berger, *Muon $g - 2$ in Lepton Portal Dark Matter*, 2104.03301.
- [82] W.-Y. Keung, D. Marfatia and P.-Y. Tseng, *Axion-like particles, two-Higgs-doublet models, leptiquarks, and the electron and muon $g - 2$* , 2104.03341.
- [83] P. Athron, C. Balázs, D. H. Jacob, W. Kotlarski, D. Stöckinger and H. Stöckinger-Kim, *New physics explanations of a_μ in light of the FNAL muon $g - 2$ measurement*, 2104.03691.
- [84] A. Aboubrahim, M. Klasen and P. Nath, *What Fermilab $(g - 2)_\mu$ experiment tells us about discovering SUSY at HL-LHC and HE-LHC*, 2104.03839.
- [85] P. Escribano, J. Terol-Calvo and A. Vicente, *$(g - 2)_{e,\mu}$ in an extended inverse type-III seesaw*, 2104.03705.
- [86] M. Endo, K. Hamaguchi, S. Iwamoto and T. Kitahara, *Supersymmetric Interpretation of the Muon $g - 2$ Anomaly*, 2104.03217.
- [87] A. Crivellin and M. Hoferichter, *Consequences of chirally enhanced explanations of $(g - 2)_\mu$ for $h \rightarrow \mu\mu$ and $Z \rightarrow \mu\mu$* , 2104.03202.
- [88] D. Zhang, *Radiative neutrino masses, lepton flavor mixing and muon $g - 2$ in a leptiquark model*, 2105.08670.
- [89] W. Yin, *Muon $g - 2$ anomaly in anomaly mediation*, *JHEP* **06** (2021) 029, [2104.03259].
- [90] T. Aoyama, T. Kinoshita and M. Nio, *Revised and Improved Value of the QED Tenth-Order Electron Anomalous Magnetic Moment*, *Phys. Rev. D* **97** (2018) 036001, [1712.06060].
- [91] R. H. Parker, C. Yu, W. Zhong, B. Estey and H. Mller, *Measurement of the fine-structure constant as a test of the standard model*, *Science* **360** (Apr, 2018) 191195.
- [92] G. F. Giudice, P. Paradisi and M. Passera, *Testing new physics with the electron $g-2$* , *JHEP* **11** (2012) 113, [1208.6583].
- [93] A. Crivellin, M. Hoferichter and P. Schmidt-Wellenburg, *Combined explanations of $(g - 2)_{\mu,e}$ and implications for a large muon EDM*, *Phys. Rev. D* **98** (2018) 113002, [1807.11484].
- [94] J. Liu, C. E. Wagner and X.-P. Wang, *A light complex scalar for the electron and muon anomalous magnetic moments*, *JHEP* **03** (2019) 008, [1810.11028].
- [95] B. Dutta and Y. Mimura, *Electron $g - 2$ with flavor violation in MSSM*, *Phys. Lett. B* **790** (2019) 563–567, [1811.10209].
- [96] A. Crcamo Hernndez, S. King, H. Lee and S. Rowley, *Is it possible to explain the muon and electron $g - 2$ in a Z model?*, *Phys. Rev. D* **101** (2020) 11, [1910.10734].
- [97] M. Bauer, M. Neubert, S. Renner, M. Schnubel and A. Thamm, *Axion-like particles, lepton-flavor violation and a new explanation of a_μ and a_e* , *Phys. Rev. Lett.* **124** (2020) 211803, [1908.00008].
- [98] C. Cornella, P. Paradisi and O. Sumensari, *Hunting for ALPs with Lepton Flavor Violation*, *JHEP* **01** (2020) 158, [1911.06279].
- [99] G. Hiller, C. Hormigos-Feliu, D. F. Litim and T. Steudtner, *Anomalous magnetic moments from asymptotic safety*, 1910.14062.

- [100] I. Doršner, S. Fajfer and S. Saad, $\mu \rightarrow e\gamma$ selecting scalar leptoquark solutions for the $(g-2)_{e,\mu}$ puzzles, 2006.11624.
- [101] A. Crcamo Hernndez, Y. Hidalgo Velsquez, S. Kovalenko, H. Long, N. A. Prez-Julve and V. Vien, *Fermion spectrum and $g-2$ anomalies in a low scale 3-3-1 model*, 2002.07347.
- [102] L. Calibbi, M. Lpez-Ibez, A. Melis and O. Vives, *Muon and electron $g2$ and lepton masses in flavor models*, *JHEP* **06** (2020) 087, [2003.06633].
- [103] F. J. Botella, F. Cornet-Gomez and M. Nebot, *Electron and muon $g-2$ anomalies in general flavour conserving two Higgs doublets models*, 2006.01934.
- [104] S. Jana, V. P. K. and S. Saad, *Resolving electron and muon $g-2$ within the 2HDM*, *Phys. Rev. D* **101** (2020) 115037, [2003.03386].
- [105] C. Hati, J. Kriewald, J. Orloff and A. Teixeira, *Anomalies in ^8Be nuclear transitions and $(g-2)_{e,\mu}$: towards a minimal combined explanation*, 2005.00028.
- [106] B. Dutta, S. Ghosh and T. Li, *Explaining $(g-2)_{\mu,e}$, KOTO anomaly and MiniBooNE excess in an extended Higgs model with sterile neutrinos*, 2006.01319.
- [107] C. Arbeláez, R. Cepedello, R. M. Fonseca and M. Hirsch, *$(g-2)$ anomalies and neutrino mass*, *Phys. Rev. D* **102** (2020) 075005, [2007.11007].
- [108] M. Endo and W. Yin, *Explaining electron and muon $g-2$ anomaly in SUSY without lepton-flavor mixings*, *JHEP* **08** (2019) 122, [1906.08768].
- [109] M. Badziak and K. Sakurai, *Explanation of electron and muon $g-2$ anomalies in the MSSM*, *JHEP* **10** (2019) 024, [1908.03607].
- [110] L. Morel, Z. Yao, P. Cladé and S. Guellati-Khélifa, *Determination of the fine-structure constant with an accuracy of 81 parts per trillion*, *Nature* **588** (2020) 61–65.
- [111] A. Baldini et al., *MEG Upgrade Proposal*, 1301.7225.
- [112] A. Blondel et al., *Research Proposal for an Experiment to Search for the Decay $\mu \rightarrow eee$* , 1301.6113.
- [113] Mu3E collaboration, A.-K. Perrevoort, *Status of the Mu3E Experiment at PSI*, *EPJ Web Conf.* **118** (2016) 01028, [1605.02906].
- [114] SINDRUM collaboration, U. Bellgardt et al., *Search for the Decay $\mu^+ \rightarrow e^+ e^+ e^-$* , *Nucl. Phys. B* **299** (1988) 1–6.
- [115] T. Aushev et al., *Physics at Super B Factory*, 1002.5012.
- [116] BABAR, BELLE collaboration, A. Bevan et al., *The Physics of the B Factories*, *Eur. Phys. J. C* **74** (2014) 3026, [1406.6311].
- [117] MEG collaboration, A. Baldini et al., *Search for the lepton flavour violating decay $\mu^+ \rightarrow e^+ \gamma$ with the full dataset of the MEG experiment*, *Eur. Phys. J. C* **76** (2016) 434, [1605.05081].
- [118] BABAR collaboration, B. Aubert et al., *Searches for Lepton Flavor Violation in the Decays $\tau^{\pm} \rightarrow e^{\pm} \gamma$ and $\tau^{\pm} \rightarrow \mu^{\pm} \gamma$* , *Phys. Rev. Lett.* **104** (2010) 021802, [0908.2381].
- [119] K. Hayasaka et al., *Search for Lepton Flavor Violating Tau Decays into Three Leptons with 719 Million*

- Produced Tau+Tau- Pairs*, *Phys. Lett. B* **687** (2010) 139–143, [1001.3221].
- [120] K. Kannike, *Vacuum Stability Conditions From Copositivity Criteria*, *Eur. Phys. J. C* **72** (2012) 2093, [1205.3781].
 - [121] A. Datta, N. Ganguly, N. Khan and S. Rakshit, *Exploring collider signatures of the inert Higgs doublet model*, *Phys. Rev. D* **95** (2017) 015017, [1610.00648].
 - [122] M. E. Peskin and T. Takeuchi, *Estimation of oblique electroweak corrections*, *Phys. Rev. D* **46** (1992) 381–409.
 - [123] R. Barbieri, A. Pomarol, R. Rattazzi and A. Strumia, *Electroweak symmetry breaking after LEP-1 and LEP-2*, *Nucl. Phys. B* **703** (2004) 127–146, [hep-ph/0405040].
 - [124] G. Cynolter and E. Lendvai, *Electroweak Precision Constraints on Vector-like Fermions*, *Eur. Phys. J. C* **58** (2008) 463–469, [0804.4080].
 - [125] R. Barbieri, L. J. Hall and V. S. Rychkov, *Improved naturalness with a heavy Higgs: An Alternative road to LHC physics*, *Phys. Rev. D* **74** (2006) 015007, [hep-ph/0603188].
 - [126] B. Barman, D. Borah, P. Ghosh and A. K. Saha, *Flavoured gauge extension of singlet-doublet fermionic dark matter: neutrino mass, high scale validity and collider signatures*, *JHEP* **10** (2019) 275, [1907.10071].
 - [127] ATLAS collaboration, G. Aad et al., *Search for heavy lepton resonances decaying to a Z boson and a lepton in pp collisions at $\sqrt{s} = 8$ TeV with the ATLAS detector*, *JHEP* **09** (2015) 108, [1506.01291].
 - [128] CMS collaboration, *Search for vector-like leptons in multilepton final states in pp collisions at $\sqrt{s} = 13$ TeV*, CMS-PAS-EXO-18-005.
 - [129] CMS collaboration, A. M. Sirunyan et al., *Search for vector-like leptons in multilepton final states in proton-proton collisions at $\sqrt{s} = 13$ TeV*, *Phys. Rev. D* **100** (2019) 052003, [1905.10853].
 - [130] S. Bißmann, G. Hiller, C. Hormigos-Feliu and D. F. Litim, *Multi-lepton signatures of vector-like leptons with flavor*, *Eur. Phys. J. C* **81** (2021) 101, [2011.12964].
 - [131] ATLAS collaboration, G. Aad et al., *Search for electroweak production of charginos and sleptons decaying into final states with two leptons and missing transverse momentum in $\sqrt{s} = 13$ TeV pp collisions using the ATLAS detector*, *Eur. Phys. J. C* **80** (2020) 123, [1908.08215].
 - [132] G. Bélanger, B. Dumont, A. Goudelis, B. Herrmann, S. Kraml and D. Sengupta, *Dilepton constraints in the inert doublet model from run 1 of the LHC*, *Phys. Rev. D* **91** (Jun, 2015) 115011.
 - [133] ALEPH, DELPHI, L3, OPAL, LEP collaboration, G. Abbiendi et al., *Search for Charged Higgs bosons: Combined Results Using LEP Data*, *Eur. Phys. J. C* **73** (2013) 2463, [1301.6065].
 - [134] P. de Salas, D. Forero, C. Ternes, M. Tortola and J. Valle, *Status of neutrino oscillations 2018: 3σ hint for normal mass ordering and improved CP sensitivity*, *Phys. Lett. B* **782** (2018) 633–640, [1708.01186].
 - [135] J. Hisano, T. Moroi, K. Tobe and M. Yamaguchi, *Lepton-flavor violation via right-handed neutrino Yukawa couplings in the supersymmetric standard model*, *Physical Review D* **53** (Mar, 1996) 24422459.
 - [136] E. Arganda and M. J. Herrero, *Testing supersymmetry with lepton flavor violating tau and mu decays*, *Phys. Rev. D* **73** (2006) 055003, [hep-ph/0510405].
 - [137] M. E. Krauss, W. Porod, F. Staub, A. Abada, A. Vicente and C. Weiland, *Decoupling of heavy sneutrinos in*

- low-scale seesaw models*, *Phys. Rev. D* **90** (2014) 013008, [1312.5318].
- [138] M. Hirsch, F. Staub and A. Vicente, *Erratum: Enhancing $l_i \rightarrow 3l_j$ with the Z^0 -penguin [phys. rev. d 85, 113013 (2012)]*, *Phys. Rev. D* **91** (Mar, 2015) 059902.
- [139] E. Arganda and M. J. Herrero, *Remark on the one-loop Z form factors for LFV Z -penguin diagrams in SUSY*, 1403.6161.
- [140] A. Abada, D. Das and C. Weiland, *Enhanced Higgs Mediated Lepton Flavour Violating Processes in the Supersymmetric Inverse Seesaw Model*, *JHEP* **03** (2012) 100, [1111.5836].
- [141] K. S. Babu and C. Kolda, *Higgs mediated $\tau \rightarrow 3\mu$ in the supersymmetric seesaw model*, *Phys. Rev. Lett.* **89** (2002) 241802, [hep-ph/0206310].
- [142] A. Dedes, J. R. Ellis and M. Raidal, *Higgs mediated $B_{s,d}^0 \rightarrow \mu\tau$, $e\tau$ and $\tau \rightarrow 3\mu$, $e\mu\mu$ decays in supersymmetric seesaw models*, *Phys. Lett. B* **549** (2002) 159–169, [hep-ph/0209207].
- [143] PARTICLE DATA GROUP collaboration, M. Tanabashi et al., *Review of particle physics*, *Phys. Rev. D* **98** (2018) 030001.
- [144] ATLAS collaboration, M. Aaboud et al., *Combination of searches for invisible Higgs boson decays with the ATLAS experiment*, *Phys. Rev. Lett.* **122** (2019) 231801, [1904.05105].
- [145] M. Dam, *Tau-lepton Physics at the FCC-ee circular e^+e^- Collider*, *SciPost Phys. Proc.* **1** (2019) 041, [1811.09408].
- [146] CEPC STUDY GROUP collaboration, M. Dong et al., *CEPC Conceptual Design Report: Volume 2 - Physics & Detector*, 1811.10545.
- [147] FCC collaboration, A. Abada et al., *FCC-ee: The Lepton Collider: Future Circular Collider Conceptual Design Report Volume 2*, *Eur. Phys. J. ST* **228** (2019) 261–623.
- [148] ATLAS collaboration, G. Aad et al., *Search for the lepton flavor violating decay $Z \rightarrow e\mu$ in pp collisions at \sqrt{s} TeV with the ATLAS detector*, *Phys. Rev. D* **90** (2014) 072010, [1408.5774].
- [149] ATLAS collaboration, G. Aad et al., *Charged-lepton-flavour violation at the LHC: a search for $Z \rightarrow e\tau/\mu\tau$ decays with the ATLAS detector*, 2010.02566.
- [150] ATLAS collaboration, G. Aad et al., *Search for charged-lepton-flavour violation in Z -boson decays with the ATLAS detector*, *Nature Phys.* **17** (2021) 819–825, [2105.12491].
- [151] D. Delepine and F. Vissani, *Indirect bounds on $Z \rightarrow \mu e$ and lepton flavor violation at future colliders*, *Phys. Lett. B* **522** (2001) 95–101, [hep-ph/0106287].
- [152] A. Flores-Tlalpa, J. M. Hernandez, G. Tavares-Velasco and J. J. Toscano, *Effective Lagrangian description of the lepton flavor violating decays $Z \rightarrow l^+ (i) l^- (j)$* , *Phys. Rev. D* **65** (2002) 073010, [hep-ph/0112065].
- [153] PLANCK collaboration, N. Aghanim et al., *Planck 2018 results. VI. Cosmological parameters*, 1807.06209.
- [154] G. Belanger, F. Boudjema, A. Pukhov and A. Semenov, *MicrOMEGAs 2.0: A Program to calculate the relic density of dark matter in a generic model*, *Comput. Phys. Commun.* **176** (2007) 367–382, [hep-ph/0607059].
- [155] G. Belanger, F. Boudjema, A. Pukhov and A. Semenov, *Dark matter direct detection rate in a generic model with micrOMEGAs 2.2*, *Comput. Phys. Commun.* **180** (2009) 747–767, [0803.2360].

- [156] A. Semenov, *Lanhep—a package for the automatic generation of feynman rules in field theory. version 3.0*, *Computer Physics Communications* **180** (Mar, 2009) 431454.
- [157] R. Essig, *Direct detection of nonchiral dark matter*, *Physical Review D* **78** (Jul, 2008) .
- [158] G. Arcadi, Y. Mambrini and F. Richard, *Z-portal dark matter*, *JCAP* **03** (2015) 018, [1411.2985].
- [159] K. Hamaguchi and K. Ishikawa, *Prospects for Higgs- and Z-resonant Neutralino Dark Matter*, *Phys. Rev. D* **93** (2016) 055009, [1510.05378].
- [160] D. Das, B. De and S. Mitra, *Cancellation in Dark Matter-Nucleon Interactions: the Role of Non-Standard-Model-like Yukawa Couplings*, *Phys. Lett. B* **815** (2021) 136159, [2011.13225].
- [161] A. Bhaskar, D. Das, B. De and S. Mitra, *Enhancing scalar productions with leptoquarks at the LHC*, *Phys. Rev. D* **102** (2020) 035002, [2002.12571].
- [162] PANDAX-II collaboration, X. Cui et al., *Dark Matter Results From 54-Ton-Day Exposure of PandaX-II Experiment*, *Phys. Rev. Lett.* **119** (2017) 181302, [1708.06917].
- [163] LUX-ZEPLIN collaboration, D. S. Akerib et al., *Projected WIMP Sensitivity of the LUX-ZEPLIN (LZ) Dark Matter Experiment*, 1802.06039.